Development of Electronics and Control for Servo Actuators in Robotic Applications

Diploma Thesis

Janis Wojtusch

TECHNISCHE
UNIVERSITÄT
DARMSTADT

Development of Electronics and Control for Servo Actuators in Robotic Applications
Diploma Thesis

Submitted by Janis Wojtusch
Submitted on January 1, 2011

Examiner: Prof. Dr. Oskar von Stryk
First Supervisor: Dipl.-Inf. Dorian Scholz (SIM)
Second Supervisor: Dipl.-Ing. Kim Listmann (RTR)

Technische Universität Darmstadt
Department of Computer Science

Simulation, Systems Optimization and Robotics
Prof. Dr. Oskar von Stryk

Abstract

Servo actuators are integrated mechatronic drives for applications with high demands in dynamic response and positioning accuracy. In robotic applications, servo actuators are applied for fast and precise positioning of joint axes, manipulators or senors. The drives have to be able to move to the desired positions without any overshoot and need to provide high stead-state accuracy despite fast changes in load torque and disturbances.

In the course of this thesis, improved electronics and advanced control for the widely used RX-28 and RX-64 servo actuators of the Dynamixel series produced by Robotis were developed and evaluated. The enhanced electronic setup improves the operating characteristics and eliminates design-related deficiencies of the original servo actuators. The essential improvements comprise increased measurement accuracy, computational capability and power efficiency. The advanced control concept introduces a tracking control with a highly adjustable desired trajectory for an individual control of the angular position and speed. The used trajectory generation allows to customize the desired actuator motion and the applied state observer provides an accurate estimation of relevant actuator values. For the implementation of the tracking control, a novel model predictive control strategy was proposed and compared to a loop-shaping control with a conditional anti-windup scheme. By applying the designed electronic setup and control concept, the enhanced DD-28 and DD-64 servo actuators become universal and capable drives for small and medium scaled robotic applications with an increased performance and durability.

Zusammenfassung

Servoantriebe sind integrierte, mechatronische Stellglieder für Anwendungen mit hohen Anforderungen an Stelldynamik und Positioniergenauigkeit. In der Robotik werden Servoantriebe zur schnellen und exakten Positionierung von Gelenkachsen, Manipulatoren oder Sensoren verwendet. Trotz der dabei auftretenden schnellen Lastwechsel und Störungen müssen die Stellglieder in der Lage sein, die gewünschten Positionen ohne Überschwingen und mit hoher stationärer Genauigkeit anzufahren.

Im Rahmen dieser Arbeit wurde eine verbesserte Servoelektronik und ein fortschrittliches Regelungskonzept für die weit verbreiteten Servoantriebe RX-28 und RX-64 aus der Dynamixel Serie der Firma Robotis entwickelt und evaluiert. Die entwickelte Servoelektronik verbessert das Betriebsverhalten und beseitigt konstruktionsbedingte Mängel der ursprünglichen Servoantriebe. Die grundlegenden Verbesserungen bestehen aus einer Erhöhung der Messgenauigkeit, Rechenleistung und Energieeffizienz. Das entwickelte Regelungskonzept sieht für die Regelung der Winkelposition und -geschwindigkeit eine Trajektorienfolgeregelung mit parametrierbarer Solltrajektorie vor. Die verwendete Trajektoriengenerierung ermöglicht eine individuelle Anpassung der Stellbewegung und der eingesetzte Zustandsbeobachter liefert eine präzise Schätzung aller relevanten Betriebsdaten des Stellglieds. Für die Implementierung der Trajektorienfolgeregelung wurde ein neuartiger Ansatz für eine modellbasierte prädiktive Regelung vorgestellt und mit einer Loopshaping-Regelung mit schaltendem Antiwindup-Element verglichen. Durch die Verwendung der entwickelten Servoelektronik und dem vorgestellten Regelungskonzept werden die verbesserten Servoantriebe DD-28 und DD-64 zu einen universell einsetzbaren Antrieb für kleine und mittlere Robotersysteme mit gesteigerter Leistungsfähigkeit und Lebensdauer.

Statement of Authorship

I hereby affirm having composed this diploma thesis without the help of third parties and only using the declared sources and utilities. All parts taken from the sources are marked as such. This diploma thesis has not been submitted to any examination office in the actual or any similar form.

Ehrenwörtliche Erklärung

Hiermit versichere ich, dass ich die vorliegende Diplomarbeit ohne Hilfe Dritter und nur mit den angegebenen Quellen und Hilfsmitteln angefertigt habe. Alle Stellen, die aus den Quellen entnommen wurden, sind als solche kenntlich gemacht. Diese Arbeit hat in gleicher oder ähnlicher Form noch keiner Prüfungsbehörde vorgelegen.

Darmstadt, January 1, 2011 Janis Wojtusch

Contents

List of Figures

List of Tables

List of Symbols

a_n	Process noise of the servo actuator.
b_n	Measurement noise of the servo actuator.
c_p	Correction factor of the power law.
d	Disturbance signal.
d_g	Diameter of the gear.
e	Control error.
f	Signal frequency.
h_g	Height of the gear.
i_m	Armature current of the servo motor.
i_s	Supply current of the servo actuator.
k	Sequence variable.
k_k	Kinetic friction constant of the servo actuator.
k_s	Static friction constant of the servo actuator.
k_v	Viscous friction constant of the servo actuator.
k_τ	Torque constant of the servo motor.
k_ω	Speed constant of the servo motor.
l_s	Luminance of the signal light.
m	Margin vector.
p_i	Input power of the voltage regulator.
p_d	Dissipation power of the voltage regulator.
p_o	Output power of the voltage regulator.
q	Constraint variable.
r	Trajectory variable.
r_g	Ratio of the gearbox.
r_{ij}	Ratio between gear i and gear j.
r_m	Resolution of the measurement.
r_s	Resolution of the position sensor.
s	Laplace transform variable.
s_s	Measuring signal of the position sensor.
t	Time variable.

u	Control signal.
u_b	Partial control signal of the feedback control.
u_f	Partial control signal of the feedforward control.
v_d	Control voltage of the servo motor driver.
v_e	Back electromotive force of the servo motor.
v_m	Armature voltage of the servo motor.
v_s	Supply voltage of the servo actuator.
v_t	Reference voltage of the temperature sensor.
w	Reference variable.
x	System state.
y	Control variable.
z	Z-Transform variable.
A	System matrix of the state space model.
A_t	Temperature parameter of the temperature sensor.
B	Input matrix of the state space model.
B_t	Temperature parameter of the temperature sensor.
C	Output matrix of the state space model.
D	Feedthrough matrix of the state space model.
F_T	Terminal cost of the finite optimization problem.
G_m	Gain margin of the loop-shaping control.
H	Transfer function.
K_f	Control gain of the feedforward control.
K_o	Kalman gain of the state observer.
K_D	Derivative control gain.
K_I	Integral control gain.
K_P	Proportional control gain.
L_m	Inductance of the servo motor.
M_c	Controllability matrix.
M_o	Observability matrix.
N_c	Prediction horizon of the model predictive control.
N_p	Duty cycle of the pulse width modulation.
P_c	Weight matrix of the model predictive control.
P_e	Covariance of the state observer error.

Q_c	Weight matrix of the model predictive control.
Q_n	Covariance of the process noise.
R_c	Weight matrix of the model predictive control.
R_i	Resistance of resistor i.
R_m	Resistance of the servo motor.
R_n	Covariance of the measurement noise.
R_p	Polyhedral region of the model predictive control.
R_t	Resistance of the thermistor.
T	Time constant.
T_s	Sampling time.
U_N	Optimization vector of the finite optimization problem.
U_∞	Optimization vector of the infinite optimization problem.
V	Disturbance matrix of the state space model.
V_N	Value function of the finite optimization problem.
V_∞	Value function of the infinite optimization problem.
α_0	Initial angular acceleration of the servo actuator.
α_a	Angular acceleration of the servo actuator.
α_d	Desired angular acceleration of the servo motor.
α_t	Angular acceleration of the trajectory.
ϵ_m	Relative error of the measurement.
η_v	Efficiency factor of the voltage regulator.
θ_c	Temperature of the microcontroller.
θ_m	Temperature of the servo motor.
θ_o	Temperature offset of the temperature sensor.
θ_t	Reference temperature of the temperature sensor.
ι_0	Initial angular jerk of the of the servo actuator.
ι_a	Angular jerk of the of the servo actuator.
ι_d	Desired angular jerk of the servo actuator.
ι_t	Angular jerk of the trajectory.
ρ	Mass density.
σ_n	Standard deviation of the sensor noise.
τ_a	Drive torque of the servo actuator.
τ_f	Friction torque of the servo actuator.

τ_l	Load torque of the servo actuator.
τ_m	Drive torque of the servo motor.
φ_0	Initial angular position of the servo actuator.
φ_a	Angular position of the servo actuator.
φ_b	Backlash of the gearbox.
φ_d	Desired angular position of the servo actuator.
φ_m	Angular position of the servo motor.
φ_n	Noise signal of the position sensor.
φ_t	Angular position of the trajectory.
ω	Angular frequency.
ω_0	Initial angular speed of the servo actuator.
ω_a	Angular speed of the servo actuator.
ω_d	Desired angular speed of the servo actuator.
ω_m	Angular speed of the servo motor.
ω_t	Angular speed of the trajectory.
ω_z	Angular cross-over frequency of the loop-shaping control.
ψ_e	Perception of the human eye.
Θ_a	Inertia of the servo actuator.
Θ_g	Inertia of the gearbox.
Θ_i	Inertia of gear i.
Θ_m	Inertia of the servo motor.
Φ_m	Phase margin of the loop-shaping control.

Notation

The applied symbols are selected in conformity with the usage and definition in current technical literature and are measured in base or derived units of the International System of units. Time-depended variables are represented by small symbols, while time-independent and transformed variables are denoted by large symbols. Regular typeface indicates scalar quantities. Matrices and vectors are printed in bold typeface. The subscript index labels identical symbols with different meaning and can be extended by comma separated abbreviations to allow a further distinction.

List of Abbreviations

ADC	Analog-digital-converter.
AS5045	Product name of a position sensor produced by austriamicrosystems.
AS5055	Product name of a position sensor produced by austriamicrosystems.
ASMT-QTB0	Product name of a light-emitting diode produced by Avago Technologies.
ATmega8	Product name of a microcontroller produced by Atmel.
AVR	Product name of a microcontroller family produced by Atmel.
CM	Compliance margin.
Cortex-M3	Name of a microcontroller architecture introduced by ARM.
CS	Compliance slope.
DA 22-12-4112	Product name of a servo actuator produced by Volz.
DD-28	Name of the enhanced servo actuator produced by Robotis and SIM.
DD-64	Name of the enhanced servo actuator produced by Robotis and SIM.
DMOSFET	Double-diffused metal–oxide semiconductor field-effect transistor.
DSP	Digital signal processing.
Dynamixel	Product name of a servo actuator family produced by Robotis.
EEPROM	Electrically erasable programmable read-only memory.
EIA-232	Name of a bus standard defined by the Electronic Industries Alliance.
EIA-422	Name of a bus standard defined by the Electronic Industries Alliance.
EIA-485	Name of a bus standard defined by the Electronic Industries Alliance.
FR-4	Grade designation of copper clad epoxy laminate.
ISP	In-system programming.
JTAG	Joint test action group.
L6201	Product name of a motor driver produced by STMicroelectronics.
L6201PS	Product name of a motor driver produced by STMicroelectronics.
LED	Light-emitting diode.
LGA	Land grid array package.
LM340MP-5.0	Product name of a voltage regulator produced by National Semiconductor.
LQFP	Low profile quad flat package.
LTM8020	Product name of a voltage regulator produced by Linear Technology.
MAX13431E	Product name of a transceiver produced by Maxim Integrated Products.

MAX14840E	Product name of a transceiver produced by Maxim Integrated Products.
MAX485	Product name of a transceiver produced by Maxim Integrated Products.
MCD EPOS	Product name of a servo actuator produced by Maxon Motor.
NB21J50103K	Product name of a thermistor produced by AVX.
PLCC	Plastic leaded chip carrier package.
PLL	Phase-locked loop.
Power-SO	Power small outline package.
PWM	Pulse width modulation.
QFN	Quad flat no leads package.
QFP	Quad flat package.
RE-max	Product name of a motor family produced by Maxon Motor.
RISC	Reduced instruction set computer.
RX-10	Product name of a servo actuator produced by Robotis.
RX-28	Product name of a servo actuator produced by Robotis.
RX-64	Product name of a servo actuator produced by Robotis.
S3050	Product name of a servo actuator produced by Futaba.
SMT	Surface mounted technology.
SO	Small outline package.
SOT	Small outline transistor package.
SRAM	Static random access memory.
SSOP	Shrink small outline package.
STM32F103CD	Product name of a microcontroller produced by STMicroelectronics.
SV01A103AEA01	Product name of a potentiometer produced by Murata.
SWD	Serial wired debug.
Thumb2	Name of an instruction set introduced by ARM.
TQFN	Thin quad flat no leads package.
TQFP	Thin quad flat package.
USART	Universal asynchronous and synchronous receiver transmitter.

1 Introduction

In everyday life, the human body performs a various number of complex motion sequences. The human legs are able to sprint after a leaving bus with high acceleration or can balance on slippery and icy roads in winter. For washing dishes, the human hands have the ability to handle fragile glasses or lift large and heavy pots. This wide functional range with versatile demands in performance and precision is made possible by the efficient and adaptive character of the human muscles.

For providing any form of motion in robotic systems, the function of the human muscles has to be reproduced by technical actuators. Generally, these robotic muscles are implemented as pneumatic, hydraulic or electrical drives for rotary or linear motion. The technically feasible performance characteristic and degree of accuracy depends on the applied drive technology. The various types of drives ensure an appropriate drive solution for a wide scope of applications. Due to battery-powered operation, the actuation of the majority of mobile robotic applications is restricted to electrical drives. The adaptable motion sequences in robotic systems result in high demands in dynamic response and positioning accuracy. Additional requirements in compact design and modular setup necessitate the usage of highly integrated drive solutions. These specifications suggest the application of capable servo actuators. Servo actuators are integrated drives that combine an electrical servo motor, power and control electronics as well as sensor elements into a functional unit. In order to cover a wide functional range and assure reliable operation, the applied servo actuators have to be universal and dependable drives.

To illustrate the requirements for servo actuators in mobile robotic applications, two recent research projects on autonomous and cooperative robotic systems are presented in the following section.

1.1 Motivation

The Simulation, Systems Optimization and Robotics Group of the Department of Computer Science at the Technische Universität Darmstadt has a focus on research into systems of autonomous, mobile robots. Teams of scientists and students analyze and optimize stable robotic locomotion in dynamic or unstructured environments as well as flexible software and control architectures for cooperating robotic systems. Results of this research are implemented on actual robots and tested at national and international robotics competitions [45].

The team Darmstadt Hector uses an enhanced remote controlled car, shown in figure 1.1a, for participation in the RoboCup Rescue League. Equipped with visual and thermal cameras, laser scanners and onboard computers the vehicle explores and maps an unknown, hostile disaster environment autonomously. Within this environment human victims are identified and located in order to initiate an immediate rescue [5,40]. The described scenario puts high demands on the drives of the robotic vehicle. For providing a reactive locomotion, the steering system has to apply a dynamic and powerful torque on the steering axle without any loss in accuracy. A detailed mapping of the environment requires high repeatability and accuracy of the positioning system of laser scanners and cameras with a smooth swiveling motion and an exactly known position at any time. Both functions are performed by the same type of highly integrated servo actuators.

The team Darmstadt Dribblers participates in the RoboCup Soccer Humanoid League with a team of small scaled, autonomous humanoid robots. A single robot, pictured in figure 1.1b, provides onboard computers, an articulated camera and an inertial measurement unit. The kinematic structure consists of twenty-one rotatory degrees of freedom, that are matched to human joint mobility. During the competition two opposing teams of three humanoid robots play a match of soccer on a scaled soccer field.

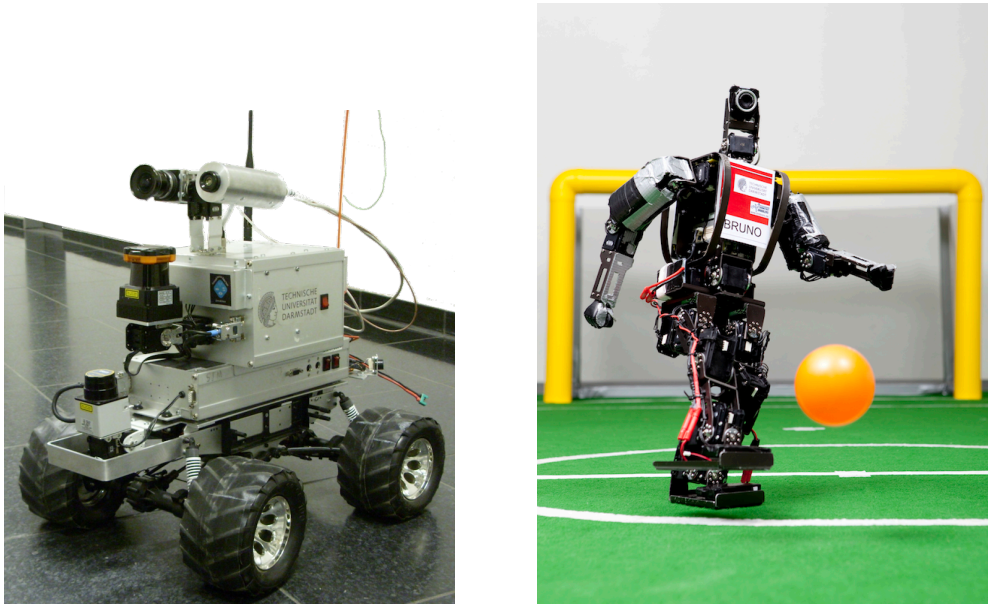

(a) Robotic vehicle of Darmstadt Hector. **(b)** Robot Bruno of Darmstadt Dribblers.

Figure 1.1.: Autonomous, mobile robots at Technische the Universität Darmstadt [14, 21].

Fixed landmarks and color markings help the robots to orientate and recognize the setting [17, 40]. An important feature in this competitive environment is fast and stable locomotion. The drives of the joint axes have to supply a fast changing dynamic torque in motion and a static holding torque in idle state. The load torque is amplified by the leverage effect of the rigid links, while the radius of action is limited to a small angular range. These conditions affect the durability and repeatability of the drives. Because of the restricted installation space, all joints of the humanoid robots are driven by highly integrated servo actuators.

Both applications show the importance and demonstrate the essential demands in servo actuators in advanced mobile robotic systems. Relevant performance features are high control rates and positioning accuracy paired with substantial driving power. Smooth motion sequences and credible timing require an adjustable actuator trajectory with a fine resolution in time. In the presented robotic applications, the actuators are continuously operated near the maximum capacity and are charged by fast changing load torques. These operational conditions stress the actuator structure and can decrease durability in existence of insufficiently designed or dimensioned components.

Currently available servo actuators for small or medium scaled robotic applications do not cover all desirable performance features. Due to design-related deficiencies or restricted control systems, the actuators are not able to take full advantage of the theoretically achievable operational capability. In order to utilize this unused potential, enhanced electronics and advanced control for two widely used servo actuators are introduced in the course of this thesis. The enhanced electronic setup improves the operating characteristics, while the advanced control concept provides a sophisticated angular position and speed control. By applying the introduced electronic setup and control concept, the enhanced servo actuators become universal drives with an increased performance and durability.

1.2 Requirements

The universal RX-28 servo actuator and the high power RX-64 servo actuator of the Dynamixel series produced by Robotis are the most widely used positioning drives in advanced mobile robotic applications.

This series of servo actuators is destined for research and development in small and medium scaled robotic systems. The objective of this thesis is the development of enhanced electronics and advanced control for RX-28 and RX-64 servo actuators. The performance in terms of increased control rates and control variable accuracy is to be improved and design-related deficiencies leading to damages or failures are to be eliminated or reduced. The enhanced DD-28 and DD-64 servo actuators are intended to be universal drives for different types of robotic applications and integrate into systems that are designed for the original RX-28 and RX-64 servo actuators.

The electronic design has to conform to specifications, dimensions and interfaces of the original servo actuators. The circuit boards need to provide a compact design and fit into the available installation space of the original enclosures without interfering the operation. The durability of the enhanced servo actuators is to be increased by reducing the wear of moving components and the introduction of reasonable measurements of essential actuator values. These measurements allow the definition of comprehensible safety margins and reduce failures and damages caused by exceeding mechanical or electronic limits. The intended use with battery power supplies subjected to changing battery voltages make a wide range of supported supply voltages necessary. For covering an extended field of application, the desired supply voltage ranges from 12 volts to 25 volts. This voltage range includes all relevant supply voltages for small and medium scaled robots. The communication interface of the original servo actuators allows a reliable networked operation of multiple actuators. In order to increase the network performance, the symbol rate of the communication interface is specified to cover the extended range from 9600 kilobits per second to 4 megabits per second with a supported operation of up to thirty networked devices. For assuring a safe and faultless operation of the servo actuators, the electromagnetic compatibility and the efficiency of the electronics need to be considered in the electronic design process. The following list summarizes the defined requirements for the electronic design:

- Backward compatibility
- Wearless setup
- Reasonable and high-resolution measurements
- Wide supply voltage range
- Fast communication interface

The control design of the enhanced servo actuators needs to provide a universal drive concept for different robotic applications including accurate angular positioning and continuous motion. The control concept has to cover an adjustable feedback control of angular position and speed that assures a high actuator performance without exceeding mechanical or electronic limits. Taking advantage of the full supply voltage range and high-resolution measurements of the control variable enable increased control rates paired with high steady-state accuracy and repeatability. The trajectory of the actuator needs to be adjustable in angular speed and acceleration for adapting the actuator motion. In order to ensure a continuous operation of the servo actuator, the implementation costs and efforts of the concept have to be considered in the control design process. The following list summarizes the defined requirements for the control design:

- Angular position and speed feedback control
- High control rate
- High steady-state accuracy
- High steady-state repeatability
- Adjustable actuator trajectory

1.3 Statement of Contribution

Servo actuators are universal drives for applications with high demands in dynamic response and positioning accuracy. The actuator motion is regulated by a feedback control system that ensures a stable and efficient operation. The performance of the control system is affected by interfering disturbances caused by static or dynamic load, initial deviations and noise signals. Present mechanical or electronic limits restrict the actuator motion and result in constrictive actuator states and input signal saturation.

This thesis introduces an advanced control concept for servo actuators that provides a tracking control with a highly adjustable desired trajectory for an individual control of the angular position and speed. The structure of the control concept is prepared for a rejection of noise signals and compensation of known disturbances and initial deviations. For the implementation of the tracking control, a novel model predictive control approach is proposed and compared to a competitive loop-shaping control approach. The control approach is a universal tracking control strategy for systems with variable input constraint. The finite optimization problem of standard model predictive control is modified to ensure optimal performance and exponential stability of the tracking control. By including the future progression of the desired trajectory into the constrained state space of the optimization problem, offset-free tracking is guaranteed for any type of trajectory. This characteristic generalizes offset-free tracking in model predictive control for the case of arbitrary motion.

1.4 Organization of the Thesis

The second chapter provides a brief overview on the actual state of technology of different servo actuator classes that are used in robotic applications. The third chapter describes and analyzes the specifications, setup and control concept of the original servo actuators. An analysis of the assets and deficiencies forms the basis for further design considerations. The design and development of the electronic setup applied in the enhanced servo actuators is presented in the forth chapter. The configuration and selection of components are related to the analysis of the original servo actuators and aligned to the defined requirements. The fifth chapter treats the control design of the enhanced servo actuators for angular position and speed control. With regard to the defined requirements, a novel model predictive control approach is proposed and compared to a competitive loop-shaping control approach. The conclusion in the sixth chapter summarizes the results and findings of this thesis and points to further development and improvements in control design.

2 State of Technology

Servo actuators are integrated mechatronic drives with an electric power input and a feedback controlled mechanical power output. The drive combines a servo motor, power and control electronics as well as sensor elements into a functional unit. An optional gear mechanism produces a mechanical advantage or translates rotatory to linear motion. Servo actuators are universal drives for applications with high demands in dynamic response and positioning accuracy. The field of application ranges from industrial production and packaging systems that require a high performance and an adaptive setup to hobby applications that need a simple control and a compact design. In robotic applications, servo actuators are applied for fast and precise positioning of joint axes, manipulators and senors. This wide range of application is covered by different performance classes of servo actuators.

2.1 Servo Actuators for Hobby Applications

Servo actuators for hobby applications are mostly used in battery-powered, remote-controlled models or lightweight robots. These actuators are affordable and highly integrated drives housing all functional components in a single enclosure. The intended use with battery power supplies limits the servo motor types to brushed or brushless, low power direct current motors. A plastic or metal gearbox is coupled to the servo motor and can be extended with variously shaped servo horns in order to translate the rotatory to linear motion. For measuring the actual angular position of the actuator, a potentiometer is mechanically linked to the output shaft and connected to the control electronics. All components of the power and control electronics are mounted on a shared circuit board. The design is improper for functional modifications or advancements of the actuator configuration and the abrasion of the potentiometer wiper or plastic gears affects the durability. Figure 2.1a shows an example of a compact hobby servo actuator.

The feedback control concept of hobby servo actuators is restricted to angular position control with a limited angular operating range. The actual angular position is measured as the output voltage of the potentiometer. The restricted measurement range of the potentiometer causes the limited angular range of the servo actuator. Modifications of the control parameters or algorithms are not provided by the control concept.

(a) Futaba S3050. **(b)** Maxon MCD EPOS. **(c)** Robotis RX-10.

Figure 2.1.: Examples of different performance classes of servo actuators [19, 35, 43].

Table 2.1 lists some technical specifications of the exemplary S3050 hobby servo actuator produced by Futaba. Characteristic features of this performance class of servo actuators are affordable costs, a compact design and a simple control.

2.2 Servo Actuators for Industrial Applications

In industrial applications servo actuators are universal drives for a broad spectrum of manufacturing facilities as well as production and packaging robots. These applications have high demands in positioning accuracy and perform with fast changing actuator speeds and load torques. The wide operational area results in a high diversity of different servo actuator configurations. Integrated drive setups consist of a single functional unit and provide a compact design and a simple installation. Modular drive setups allow uncomplicated service or modification of the actuator. Optional gearheads for mechanical advantage, brakes for holding a specific position or lead screws for translating rotatory to linear motion can be used to advance the configuration. According to the required driving power, the servo motor type is a synchronous or asynchronous alternating current motor or a direct current motor with a slimline armature design. The actual angular position is measured with high-resolution optical or magnetic sensors. Additional sensors for armature current, servo motor temperature or other relevant actuator values provide an overview of the operational drive state. Standardized industrial bus configurations are used for communicating with the actuators and allow a networked operation of multiple drives with a single control unit. The wearless sensors and high quality servo motors and gearboxes ensure a high actuator durability. Figure 2.1b shows an example of an integrated industrial servo actuator.

The universal application of servo actuators in industrial facilities requires a flexible and advanced feedback control concept. Depending on the application, the concept has to provide a stabilization or tracking control. The control law is implemented as a digital control algorithm and can be configured substantially through the communication interface. The applied optical or magnetic sensors do not limit the angular or linear position range of the actuator and allow a multiple turn operation.

Table 2.1.: Specifications of exemplary servo actuators for hobby and industrial applications [19, 25, 35].

	Unit	**S3050** (Futaba)	**MCD EPOS** (Maxon Motor)
Supply voltage range	V	4.8 - 6.0	12.0 - 50.0
Angular position accuracy	$mrad$	unknown	± 17.5
Angular position range	rad	± 0.8	$\pm\infty$
Angular speed limit	$\frac{rad}{s}$	6.5	2057.7
Torque limit	Nm	0.6	0.2
Control type		digital	digital
Communication interface		PWM	CAN/EIA-232
Enclosure dimensions	mm	40 x 20 x 38	120 x 33 x 53

Table 2.1 lists some technical specifications of the exemplary MCD EPOS industrial servo actuator produced by Maxon Motor. Characteristic features of this performance class of servo actuators are an adaptive setup, a standardized communication interface and an advanced control.

2.3 Servo Actuators for Mobile Robotic Applications

Servo actuators for mobile robotic or advanced hobby applications such as small scaled humanoid robots or remote-controlled helicopters combine essential features of hobby and industrial servo actuators. The limited installation space in mobile applications demands a compact, but also maintainable and durable design. High requirements in control rates, accuracy and repeatability necessitate the application of sensors with high resolution and an adjustable feedback control concept. The mechanical setup is based on high power hobby servo actuators with a direct current servo motor, an integrated metal gearbox and a potentiometer for measuring the angular position. The potentiometer has a limited measurement range, but is not restricted mechanically. This allows a multiple turn operation of the actuator. The electrical setup and communication interfaces originate from industrial servo actuators. A basic set of actual actuator values is provided by additional sensors or is derived from the measured angular position. Figure 2.1c shows an example of a servo actuator for mobile robotic applications.

In most cases, the feedback control concept implemented in this performance class of servo actuators is based on a digital proportional–integral–derivative control. The introduction of additional control parameters like a compliance margin or an increased gain for small control errors reduces the influence of disturbances and friction effects on the control action. Adjustable desired or maximum values for actuator speed permit rudimentary modifications of the actuator motion. Despite these control parameters, the fundamental control action and the progression of the actuator trajectory cannot be adapted to specific requirements. All modifiable control and configuration parameters can be set through the communication interface.

Table 2.2.: Specifications of exemplary servo actuators for robotic applications [43, 56].

	Unit	**Dynamixel RX-10** (Robotis)	**DA 22-12-4112** (Volz)
Supply voltage range	V	10.0 - 12.0	12.0
Angular position accuracy	$mrad$	± 2.5	unknown
Angular position range	rad	± 2.6 / $\pm\infty$	± 2.9
Angular speed limit	$\frac{rad}{s}$	5.7	4.4
Torque limit	Nm	1.3	3.5
Control type		digital	digital
Communication interface		EIA-485	PWM/EIA-422/EIA-485
Enclosure dimensions	mm	36 x 51 x 42	42 x 66 x 22

A different approach to obtain servo actuators for robotic applications is the upgrade of hobby servo actuators with enhanced electronics and control concepts. The open source project OpenServo provides a replacement circuit board with an eight bit microcontroller, power electronics and servo motor temperature, armature current and supply voltage sensors fitted for a wide range of low power hobby servo actuators. A sensor for the back electromotive force of the servo motor included in the power electronics gives an estimate of the actual angular speed. The original potentiometer is connected to the circuit board and is used to measure the actual angular position of the actuator. The feedback control concept is restricted to angular position control and is implemented as a digital proportional–derivative control [15]. The open source project SuperModified offers a modular setup of replacement circuit boards. A circuit board with an eight bit microcontroller, a power electronics circuit board and a high-resolution magnetic encoder circuit board can be stacked and allow an installation in low to medium power hobby servo actuators with minimum space requirements. The actual angular position of the actuator is measured by the magnetic encoder, that replaces the original potentiometer. The feedback control concept applies a digital proportional–integral–derivative control and supports profiled angular position and speed control [1].

Table 2.2 lists some technical specifications of two exemplary servo actuators for mobile robotic applications. Characteristic features of this performance class of servo actuators are a compact design, a standardized communication interface and an advanced control.

2.4 Evaluation

The great diversity of commercially available servo actuators demonstrates the universal character of this type of drive. While hobby servo actuators are designed for compact installation and preset operation with affordable costs, industrial servo actuators provide a maximum of adjustability in structure and control. Servo actuators intended for mobile robotic applications combine the basic and compact setup of high power hobby servo actuators with an extended communication and control concept based on advanced control systems of industrial servo actuators.

This configuration is subject to two restrictions. By retaining the application of a potentiometer for measuring the actual angular position, the measurement accuracy is limited and the actuator is prone to wear-related failures. The provided control parameters of the extended control concept do not have a qualitative influence on the control action and do not provide a significant customization of the actuator motion. These properties affect the durability and applicability of the servo actuators and constrain the operation to preset characteristics.

An indication of the demand in advanced adaptability of the control action such as adjustable acceleration and deceleration characteristics is the existence of noncommercial projects that provide enhanced electronics and control concepts for hobby servo actuators. The introduction of comprehensive control parameters and the possibility to access and modify the implementation of the control law allow to adapt the control action to specific needs and applications. The focus on hobby servo actuators limits the relevance for advanced mobile robotic applications.

3 Original System

The upcoming chapter describes the specifications, setup and control concept of the original servo actuators for mobile robotic applications. An analysis of the assets and deficiencies of the original system forms the basis for the further design considerations.

3.1 Specifications

The original RX-28 and RX-64 servo actuators of the Dynamixel series produced by Robotis are designed for research and development in small and medium scaled robotic applications. The supply voltage range for both actuators is rated from 12 volts to 18.5 volts. For the adjustment of configuration parameters, setting desired values and reading measurement values, both actuators provide a communication interface based on the EIA-485 bus standard. This communication interface allows the control and networked operation of multiple actuators with an adjustable symbol rate from 7343 bits per second to 1 megabits per second. The RX-28 type, pictured in figure 3.1a, is a universal servo actuator with a compact design and an even balance of maximum angular speed of 8.9 radians per second and maximum torque of 3.6 newton meters. The enclosure with the overall dimensions of 36 by 51 by 42 millimeters enables an installation with minimum space requirements. The designated operating temperature covers a range from 5 degrees Celsius to 85 degrees Celsius. The RX-64 type, shown in figure 3.1b, is a high power servo actuator with a high maximum torque of 5.1 newton meters and a moderate maximum angular speed of 6.7 radians per second. The overall enclosure dimensions measure 40 by 61 by 46 millimeters [41, 42, 43]. Both actuator enclosures provide a base for mounting frames in order to simplify assembly. A list of the technical specifications of the RX-28 and RX-64 servo actuators is presented in table 3.1.

The servo actuators support two different modes of operation. In joint mode the actuator drives with an adjustable angular speed to a desired angular position. The angular position is limited to a range of ± 2.6 radians around the neutral position and can be defined as an integer multiple of 5.1 milliradians. An adjustable upper limit value for each rotating direction allows to further reduce the angular range. The absolute value of the angular speed can be defined as an integer multiple of 11.6 milliradians per second. In wheel mode the actuator moves with a desired angular speed in endless turn operation. The

(a) Robotis Dynamixel RX-28. **(b)** Robotis Dynamixel RX-64.

Figure 3.1.: RX-28 and RX-64 servo actuators of the Dynamixel series [43].

Table 3.1.: Technical specifications of the RX-28 and RX-64 servo actuators of the Dynamixel series [43].

	Unit	**Dynamixel RX-28** (Robotis)	**Dynamixel RX-64** (Robotis)
Supply voltage range	V	12.0 - 18.5	12.0 - 18.5
Angular position accuracy	$mrad$	±2.5	±2.5
Angular position range	rad	±2.6 / ±∞	±2.6 / ±∞
Angular speed limit	$\frac{rad}{s}$	8.9	6.7
Torque limit	Nm	3.6	5.1
Armature current limit	A	1.9	2.6
Quiescent current	mA	50.0	50.0
Gearbox ratio		193.0	200.0
Control type		digital	digital
Communication interface		EIA-485	EIA-485
Symbol rate range	$\frac{kbit}{s}$	7.343 - 1000.0	7.343 - 1000.0
Temperature range	$°C$	+5.0 - +85.0	+5.0 - +85.0
Enclosure dimensions	mm	36 x 51 x 42	40 x 61 x 46

angular speed can be defined as a percentage of the maximum value as an integer multiple of 0.1 percent depending on the applied supply voltage. In both operation modes the actual angular position and actual angular speed are measured with the same accuracy as the corresponding desired values. Additionally, the actual values of the load torque, servo motor temperature and supply voltage are captured. The actual load torque is not measured directly, but is approximated as a related load value. This load value represents a percentage of the maximum actuator torque as an integer multiple of 0.1 percent depending on the applied supply voltage. The actual temperature of the servo motor is measured as an integer multiple of 1 degree Celsius. In order to prevent an overload of the actuator an upper limit value for the actual torque value and servo motor temperature can be defined. The actual supply voltage is measured in volts as an integer multiple of 0.1 volts. An upper and lower limit value for the supply voltage can be configured for ensuring a specific performance and avoiding an overvoltage. If any of the defined limit values is exceeded, the actuators can be configured to perform an emergency shutdown or activate a signal light in each case [43].

All configuration parameters and actual and desired values of the servo actuator are organized in an allocated memory structure. Configuration parameters are stored in a non-volatile memory area. During the initialization process after activating the actuator, copies of some of the configuration parameters, measured actual values and predefined desired values are saved in a volatile memory area. The predefined desired angular position is equated to the actual angular position, while the predefined angular

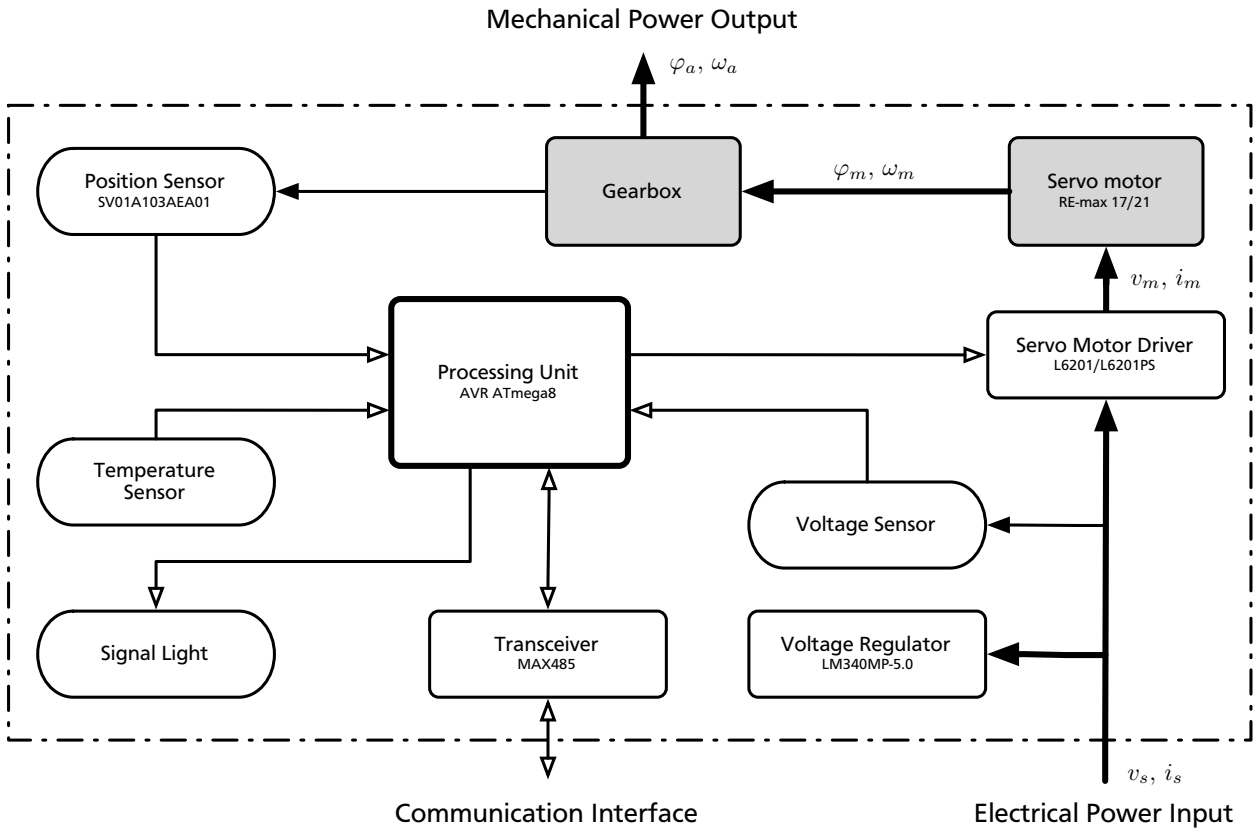

Figure 3.2.: Setup of the original RX-28 and RX-64 servo actuators.

speed is set to the maximum angular speed. Each value in the non-volatile and volatile memory can be accessed directly by a unique memory address. By writing to or reading from a specific memory address through the communication interface the appertaining value can be configured or requested. Changes of the volatile memory area are temporary and lost after the actuator is deactivated. Only the persistent configuration parameters in the non-volatile memory area can be changed permanently [43].

The protocol of the communication interface uses two different packet types. The instruction packet type is sent from a control unit to a servo actuator and contains a command identifier and command parameters. Depending on the configuration of the communication interface and the transmitted command identifier, the servo actuator returns a packet of the status packet type that contains status information and requested actuator values. The structure of each packet starts with two start bytes, one servo actuator identifier byte and one length byte followed by the packet data and one checksum byte. The servo actuator identifier gives a unique address to each actuator connected to the communication bus. A reserved broadcast address is used to contact all networked actuators with a single instruction packet. The write command and the read command allow to write or read data from the memory structure starting from a specific memory address. The registered write command corresponds to the write command, but the written data is kept inactive until a subsequent trigger command is sent. The synchronized write command can be used to write data to multiple actuators simultaneously. For testing the communication interface, the ping command requests a minimal status packet from the addressed actuator. The reset command restores all actuator values to the associated default values [43].

3.2 Mechanical Setup

The mechanical setup of the original RX-28 and RX-64 servo actuators comprises the servo motor, the gearbox and the actuator enclosure. The servo motor is driven by the power electronics and converts the electrical power input into mechanical power output with a high angular speed and a low torque. The gearbox is coupled to the servo motor and produces a mechanical advantage by transforming low-torque power input from the servo motor into high-torque power output of the actuator by reducing the angular speed. The gearbox output shaft is the mechanical interface of the servo actuator and provides a mount for fitted servo horns. Figure 3.2 presents a functional diagram of the setup of the original RX-28 and RX-64 servo actuators.

3.2.1 Servo Motor

Both servo actuator types use a brushed direct current motor of the RE-max series produced by Maxon Motor. The motors apply neodymium magnets in the stator and have a coreless armature without any magnetic cogging torque. The coreless design of the armature consists of a self-supporting winding structure without an iron core. This configuration reduces the inertia of the servo motor and increases the efficiency by avoiding magnetic core losses. The armature is connected with carbon brushes and supported by sintered bearing in the motor enclosure. Both servo actuator types apply a custom product variant of a standard motor series with a mounted pinion gear.

The motor used in the RX-28 type has the part number 275338 and is a product variant of a RE-max 17 series motor with an enclosure diameter of 17 millimeters and the part number 214897. The motor specifications rate the armature voltage at 12 volts and the power output at 4 watts. The armature temperature must not exceed 85 degrees Celsius. The thermal resistance between armature and ambient air is rated at 47 kelvin per watt [33]. The RX-64 type applies a motor with the part number 310002 that is a product variant of a RE-max 21 series motor with an enclosure diameter of 21 millimeters and the part number 250003. The armature voltage is rated at 15 volts and the power output is specified at 6 watts. The armature temperature needs to be kept below 125 degrees Celsius. The thermal resistance between armature and ambient air is rated at 36 kelvin per watt [34]. A summery of the technical specifications and parameters of the motors is listed in table 3.2.

3.2.2 Gearbox

The gearbox of both servo actuator types consist of two single and four double spur gears including the single pinion gear of the servo motor. In order to provide a high integration of the gearbox, the gears are installed in a stacked configuration. The double gears are made of steel or brass and run on plain bearings, while the single geared output shaft is made of aluminum and is supported by two ball bearings. For providing a mechanical interface for the actuator, the toothed extension of the torsionally stiff gearbox output shaft has a threaded center hole and is led through an opening in the actuator enclosure. The toothed shape and the threaded hole enable an interlocking and screw secured mounting of a fitted servo horn. The gearbox ratio defines the ratio of the input and output torque and corresponds to the mechanical advantage that is produced by the gearbox. The calculation of the gearbox ratio based on the gear dimensions and number of teeth results in a gearbox ratio of 192.6 for the gearbox of the RX-28 type and a gearbox ratio of 199.6 for the gearbox of the RX-64 type. The given specifications in table 3.1 approximate the calculated values of the gearbox ratio. A description of the calculation of the gearbox ratio parameters can be found in Appendix B.

Table 3.2.: Technical specifications of the motors RE-max 17 214897 and RE-max 21 250003 [33, 34].

	Unit	**RE-max 17 214897** (Maxon Motor)	**RE-max 21 250003** (Maxon Motor)
Rated armature voltage	V	12.0	15.0
Rated power output	W	4.0	6.0
Motor speed constant	$\frac{rad}{Vs}$	100.7	74.9
Motor torque constant	$\frac{mNm}{A}$	9.9	13.4
Armature inductance	mH	0.2	0.2
Armature resistance	Ω	8.3	6.3
Armature inertia	kgm^2	$86.4 \cdot 10^{-9}$	$217.0 \cdot 10^{-9}$
Enclosure diameter	mm	17.0	21.0

3.2.3 Enclosure

The servo actuator types are housed in different dimensioned enclosures that are composed of three parts. The top cover has an opening for the output shaft of the mechanical interface, while the bottom cover provides a transparent window for the signal light and slots for the connectors of the electrical interface. The covers are mounted on the center body that holds the mechanical and electronic components and maintains two openings for servo motor cooling. All parts are assembled by four screws and made of black, resistant plastic. A socket for a counter bearing on the opposite site of the mechanical interface and mounting bases around the actuator enclosure allow various actuator configurations and assembly structures. All mounting holes provide a nut retainer for ensuring simple installation.

3.2.4 Evaluation

The mechanical setup of the original RX-28 and RX-64 servo actuators employs high quality components and provides a flexible but simple construction and integration into robotic systems. All applied components are well suited and sufficiently dimensioned for the desired purpose. Damages of the gears or the servo motor result from exceeding specified electrical or mechanical limits and have to be prevented by the introduction of comprehensible safety limits. These properties allow the application of the unmodified mechanical setup in the enhanced DD-28 and DD-64 servo actuators.

3.3 Electronic Setup

The electrical setup of the original RX-28 and RX-64 servo actuators consists of a processing unit, sensor elements, a communication interface, power electronics and a signal light mostly in surface mounted technology (*SMT*). All components are assembled on double-sided printed circuit boards made of copper clad epoxy laminate with a thickness of 1 millimeter that are mounted inside of the actuator enclosure.

The processing unit manages configuration parameters as well as actual and desired values and implements the control concept and communication protocol. All operations of the actuator are controlled by the processing unit, making it the central component of the setup. The sensor elements measure actual actuator values that are used in the control algorithm or for monitoring safety limits. The communication interface comprising a transceiver and a serial interface of the processing unit provide a standardized bus configuration with a high electromagnetic compatibility for the control and configuration of multiple networked servo actuators. The power electronics include a driver for the servo motor and a voltage regulator. The servo motor driver powers the servo motor and allows the control of magnitude and polarity of the armature voltage within the range of the supply voltage. For ensuring a stable and low supply voltage for the electrical components with considering the variable and high supply voltage of the actuator, the voltage regulator provides a voltage reduction and stabilization. The operational status of the actuator is indicated with a configurable red signal light that is integrated into the actuator enclosure. Two reverse polarity protected connectors with four terminals for the supply voltage and the communication interface, that are led through slots in the actuator enclosure, are the electrical interface of the servo actuator. Figure 3.2 shows a functional diagram of the setup of the original RX-28 and RX-64 servo actuators. Detailed circuit diagrams of both servo actuator types are listed in Appendix F.

3.3.1 Processing Unit

The processing unit of both servo actuator types is the 8-bit microcontroller AVR ATmega8 produced by Atmel. The microcontroller is clocked by an external crystal oscillator with a clock rate of 16 megahertz an has a supply voltage range from 4.5 volts to 5.5 volts. The processor architecture is based on the reduced instruction set computer (*RISC*) design and supports 16 million instructions per second at the given clock rate. For interacting with other electronic components, the microcontroller provides twenty-three digital inputs and outputs and different analog and digital peripherals. The successive approximation analog-digital-converter (*ADC*) converts analog input voltages into proportional digital integers with a resolution of 10 bits on eight channels. The input channels are connected to a multiplexer and enable a sequent conversion with a conversion rate of up to 15.4 kilohertz per channel. The ADC is used for measuring actual analog values of the actuator. The two timers of the microcontroller provide a pulse width modulation (*PWM*) interface with three channels that allows to generate a digital voltage signal with a controllable duty cycle. Two channels have a resolution of 16 bits, while one channel is limited to an accuracy of 8 bits. The two high-resolution PWM channels are applied for actuating the servo motor driver. An additional watchdog timer allows to perform a reset of the microcontroller in case of a software-related malfunction. The universal synchronous and asynchronous receiver and transmitter (*USART*) is a configurable serial interface with a symbol rate of up to 2 megabits per second. In combination with an external transceiver the USART establishes the asynchronous communication interface of the actuator. The highly integrated circuit is housed in a thin quad flat package (*TQFP*) with thirty-two leads and a size of 7 by 7 millimeters. The allowed operating temperature ranges from -55 degrees Celsius to $+125$ degrees Celsius [7].

The memory configuration of the microcontroller is divided into volatile and non-volatile memory types. The non-volatile flash memory has a size of 8 kibibytes and stores the firmware of the servo actuator including the control algorithm and the handling of the communication protocol. The volatile static random access memory (*SRAM*) provides a size of 1 kibibyte and is applied as the working memory of the microcontroller for reading and writing working data continuously during the operation. The working memory includes the volatile memory area of the allocated memory structure for configuration parameters and actual and desired actuator values. The non-volatile electrically erasable programmable read-only memory (*EEPROM*) has a size of 0.5 kibibytes and stores the non-volatile memory area of the allocated memory structure with the persistent configuration parameters [7]. A list of the technical specifications of the microcontroller AVR ATmega8 is presented in table 3.3.

All values of the memory structure are stored and addressed as unsigned eight bit integer cells. Values with a range that exceeds the eight bit range are divided into a lower eight bit value and a higher eight bit value. The non-volatile address space contains twenty-four memory cells, while the volatile address space comprises twenty-six memory cells. Some memory addresses are not writable and store undocumented, actuator-specific calibration and configuration parameters [41, 42].

The microcontroller comes with an installed command-line bootloader that allows to change the firmware of the servo actuator. This bootloader communicates through the serial communication interface and can be activated by using the Dynamixel Wizard software provided by Robotis or by sending the hexadecimal code $0x23$ when powering up the servo actuator. A different method of programming the microcontroller is given by the usage of the in-system programming (*ISP*) interface that is connected to five pads on the circuit board and allows to access the non-volatile flash memory and additional configuration bits.

3.3.2 Sensor Elements

The sensor elements of both servo actuator types are applied for measuring the actual values of the angular position, servo motor temperature and supply voltage of the servo actuator. The actual angular

Table 3.3.: Technical specifications of the microcontroller AVR ATmega8 [7].

	Unit	**AVR ATmega8** (Atmel)
Supply voltage range	V	4.5 - 5.5
Clock speed limit	MHz	16.0
Flash memory size	KiB	8.0
SRAM size	KiB	1.0
EEPROM size	KiB	0.5
ADC channels		8
ADC resolution	bit	10
PWM channels		3
PWM resolution	bit	8 / 16
USART interfaces		1
USART symbol rate limit	$\frac{Mbit}{s}$	2.0
Digital inputs and outputs		23
Package dimensions	mm	7.0 x 7.0 x 1.2

position is used in the control algorithm, while the actual supply voltage and servo motor temperature are monitored to satisfy the specified safety limits. All measured values are converted into analog voltages and captured with the ADC of the microcontroller. The convertible voltage of the ADC is limited to a range from 0 volts to the operating voltage of the microcontroller of 5 volts.

3.3.2.1 Position Sensor

The actual angular position of the servo actuator is measured with a potentiometer that is mechanically linked to the output shaft of the gearbox. Both servo actuator types use the linear potentiometer SV01A103AEA01 produced by Murata Manufacturing with a rated total resistance of 10 kiloohms. This potentiometer has a specified measurement range of 5.8 radians, but is not mechanically restricted and allows a multiple turn operation. The linearity of the characteristic is rated at 2 percent with a durability of 10^6 cycles [38]. The potentiometer consists of a static, arcuate resistive element made of a carbon film and an actuated wiper. The wiper is slid over the linear resistive element and taps a fraction of the resistive value dependent on the angular position. This configuration works as an angular position-dependent voltage divider. The input voltage of 5 volts over the resistive element is provided by the voltage regulator and the output voltage is measured over the tapped resistance of the wiper. Figure 3.3a shows the reference output characteristic of a virgin potentiometer with the output voltage v against the angular position φ. Within the specified range and slightly beyond the output voltage is a linear function of the angular position. The rated linearity ensures a maximum deviation of 0.1 volts. All remaining angular positions result in an undefined output voltage. With the resolution of the ADC of 10 bits for the full input voltage range and the limited angular range of the servo actuator of ± 2.6 radians, the angular position is measured with a theoretical resolution r_m of

$$r_m = \frac{2 \cdot 2.6 rad}{2^{10}} = 5.1\ mrad. \tag{3.1}$$

Voltage signal noise affects the actual resolution and makes a low-pass filtering of the measured value necessary. Due to restricted installation space in the RX-28 type, the potentiometer is mounted on a dedicated circuit board that is connected to the main circuit board by a three-terminal connector. The installation space in the RX-64 type allows an integrated mounting next to the other components. In both servo actuator types, a lightweight plastic shaft is applied for the linkage of the potentiometer and the gearbox output shaft.

The actual angular speed and actuator load are not measured directly, but are derived from the value of the angular position. The angular speed is determined by differentiating the angular position with respect to time, while the actuator load results from the difference of the desired and the actual angular position. Both measurands are updated with a frequency of about 7.5 hertz [43, 44, 54].

During the operation of the servo actuator the continuous sliding of the wiper over the resistive element causes wear and stress in both components. Partial abrasion or damage of the carbon film of the resistive element changes the total resistance and disturbs the distribution of the resistive layer. These effects are increased by operating the potentiometer in a small angular range with a fast changing or oscillating motion. The change of the total resistance does not affect the performance of the potentiometer, but a non-uniform distribution of the resistive layer results in a nonlinear output characteristic and shifts the neutral angular position. An abrupt step in resistance causes a discontinuity of the output characteristic with a high change of the output voltage for a small change in angular position. Figure 3.3b represents an exemplary nonlinear output characteristic with a discontinuity of an used potentiometer taken from a damaged RX-28 servo actuator. A direction-dependent disturbance in the resistive layer results in a localized hysteresis loop within the output characteristic. In the affected area identical angular positions

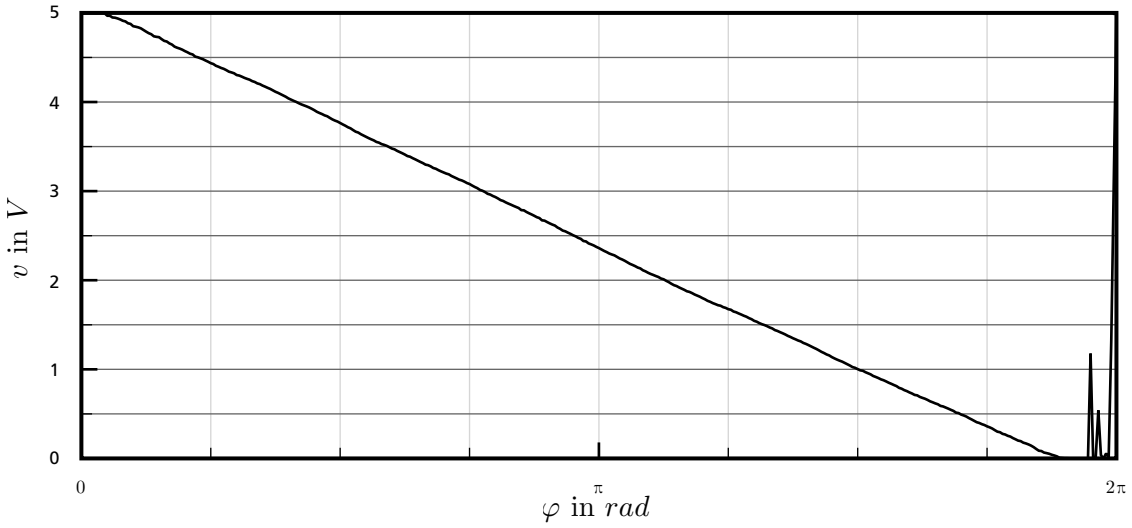

(a) Linear output characteristic.

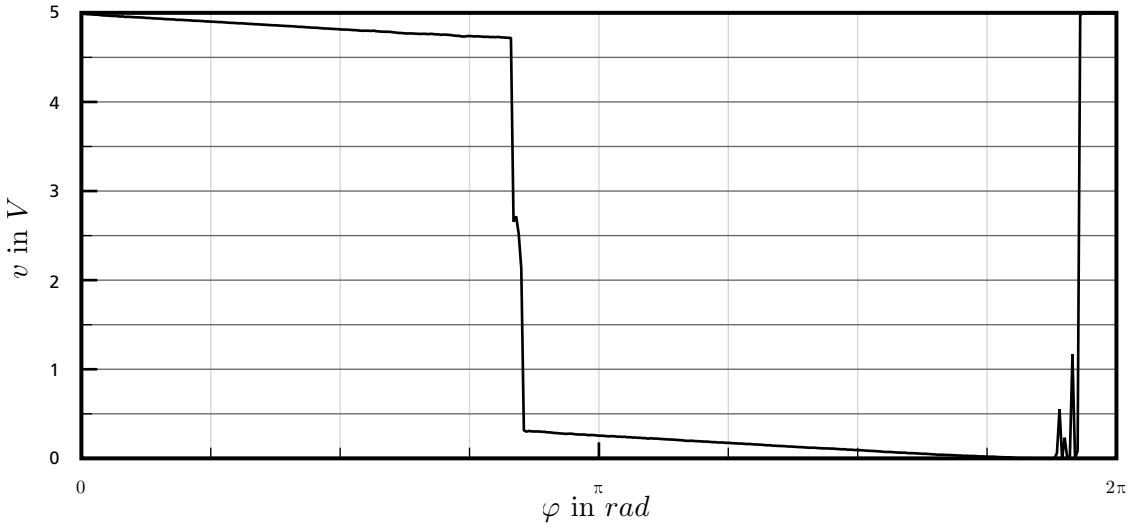

(b) Nonlinear output characteristic caused by a discontinuity.

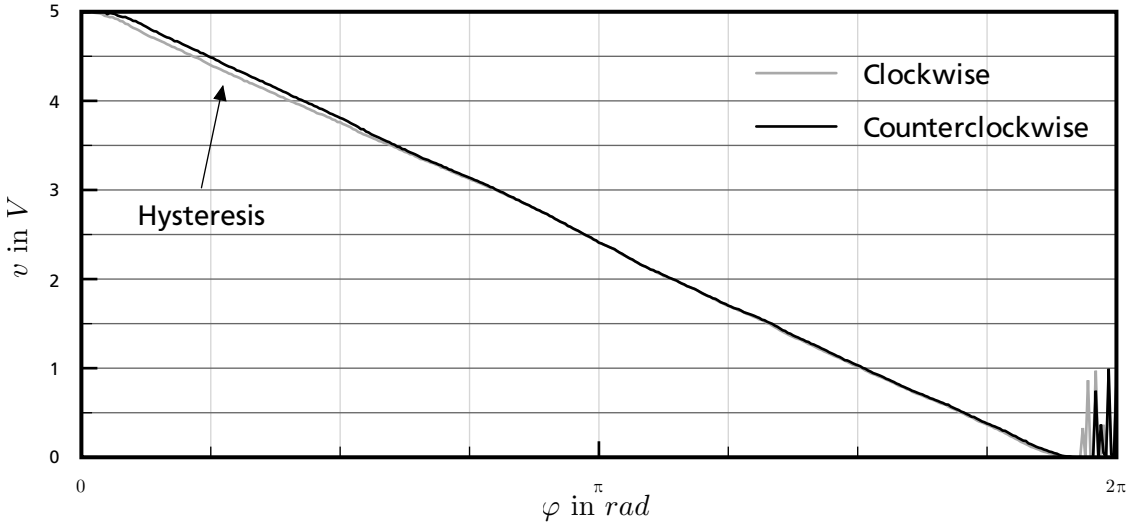

(c) Nonlinear output characteristic caused by a hysteresis.

Figure 3.3.: Linear and nonlinear characteristics of the SV01A103AEA01 potentiometer.

yield different output voltages dependent on the direction of motion. Figure 3.3c shows an exemplary nonlinear output characteristic with a hysteresis loop of an used potentiometer taken from a damaged RX-64 servo actuator. Both nonlinear effects have an influence on the measurement and feedback control of the angular position of the servo actuator. A small control error or control variable overshoot results in nonlinear angular position measurements and produces a disproportional control signal that causes an unstable and oscillating actuator motion. A precise angular positioning of the servo actuator becomes impossible.

3.3.2.2 Temperature Sensor

The actual servo motor temperature is indirectly measured by the interpretation of a thermistor that is placed near the servo motor. The thermistor has a negative temperature coefficient, that results in a nonlinear decrease of the resistance value with an increasing servo motor temperature. A series connection of the thermistor and a resistor with a rated resistance of 10 kiloohms forms a temperature-dependent voltage divider. The input voltage of 5 volts over the thermistor and resistor is provided by the voltage regulator, while the output voltage is measured over the thermistor and is proportional to the actual resistance value. The approximated actual servo motor temperature is obtained by applying the nonlinear inverse thermistor function to the determined actual resistance value. The theoretical measurement range and resolution depend on the unspecified temperature-dependent parameters of the thermistor. The tolerance of the resistance values and parameters as well as voltage signal noise affect the actual measurement range and resolution.

3.3.2.3 Voltage Sensor

For measuring the actual supply voltage of the servo actuator without exceeding the input voltage range of the ADC, the supply voltage is scaled with a voltage divider. This voltage divider is formed by two resistors connected in series with a rated resistance of 10 kiloohms and 3.3 kiloohms. The supply voltage is the input voltage over the resistors, while the proportionally reduced output voltage is measured over the low value resistor. With considering the maximum convertible voltage of 5 volts and neglecting the input current of the ADC, this configuration results in a theoretically measurable highest supply voltage $v_{s,h}$ of

$$v_{s,h} = 5\ V \cdot \frac{R_1 + R_2}{R_2} = 20.2\ V \tag{3.2}$$

where

$$R_1 = 10\ k\Omega, \tag{3.3}$$

$$R_2 = 3.3\ k\Omega. \tag{3.4}$$

With the resolution of the ADC of 10 bits for the full convertible voltage range, the supply voltage is measured with a theoretical resolution r_m of

$$r_m = \frac{v_{s,h}}{2^{10}} = 19.7\ mV. \tag{3.5}$$

The actual measurement range and resolution is affected by the tolerance of the resistance values and voltage signal noise affect.

3.3.3 Communication Interface

The communication interface is an asynchronous half-duplex serial interface based on the EIA-485 bus standard. This standard is widely used in industrial applications and provides a high electromagnetic compatibility paired with high symbol rates and large transmission distances. For rejecting common-mode interference, the digital signal is transmitted as an inverted and a noninverted voltage level on two differential bus lines. Terminal resistors on the end of the bus lines reduce signal noise and reflections. The standard provides a networked operation of multiple senders and receivers in a multi-drop or multi-point configuration with a supported cable length of 1200 meters.

Both servo actuator types use the integrated low-power transceiver MAX485 produced by Maxim Integrated Products as driver and receiver for the bus interface. This transceiver has a rated supply voltage of 5 volts and an operating current of 0.5 milliamperes. The supported symbol rate limit is specified at 2.5 megabits per second with up to thirty-two transceivers on the bus interface. The transceiver is housed in a small outline (*SO-8*) package with eight leads and a size of 4 by 5 millimeters that provide input, output and enable terminals for the driver and receiver. The allowed operating temperature ranges from +0 degrees Celsius to +70 degrees Celsius [31].

Due to the half-duplex operation, the inverting receiver input and driver output as well as the noninverting receiver input and driver output are bundled in two terminals and linked to the connectors of the servo actuator. The USART interface of the microcontroller is connected to the driver input and receiver output terminals. The driver enable and the inverted receiver enable terminals are bundled and controlled by a digital output of the microcontroller. This digital output sets the operational mode of the transceiver. In idle state the communication interface is in receiver mode and analyzes the incoming data for assigned instruction packets. For sending a status packet, the communication interface switches to transmitter mode until the packet is transmitted and subsequently switches back to receiver mode. Multiple servo actuators can be connected in an open daisy chain scheme terminated by terminal resistors with a typical resistance of 120 ohms. The applied transceiver supports a networked operation with up to thirty-two devices. In both servo actuator types, terminal resistors are not implemented and have to be attached externally. The configuration of the asynchronous serial interface defines eight data bits, no party bit and one stop bit [43].

3.3.4 Servo Motor Driver

The servo motor has an electrical power input and provides the mechanical power output of the servo actuator. The angular speed and rotating direction of the servo motor are controlled by the magnitude and polarity of the armature voltage. Both servo actuator types apply a full bridge motor driver with four double-diffused metal–oxide semiconductor field-effect transistors (*DMOSFET*) and integrated protective diodes for powering the servo motor. Caused by switching losses and the residual resistance of the transistors, electrical power is converted into thermal power and makes a sufficient heat sinking concept necessary.

The RX-28 type uses the integrated motor driver L6201 with a rated operating current of 1 ampere and a peak current of 2 amperes. The motor driver is housed in a small outline (*SO-20*) package with twenty leads and a size of 7.6 by 13 millimeters. Eight ground leads are designated for dissipating thermal power. The RX-64 type applies the integrated motor driver L6201PS with a specified operating current of 4 amperes and a peak current of 5 amperes. The motor driver is housed in a high power version of the small outline (*Power-SO-20*) package with twenty leads and a size of 11.1 by 16 millimeters. A pad on the bottom of the package is provided for dissipating thermal power. In both servo actuator types, the heat sink is an extensive ground plane on the circuit board. The motor drivers have a rated supply

voltage range from 12 volts to 48 volts and are produced by STMicroelectronics. The allowed junction temperature ranges from −40 degrees Celsius to +150 degrees Celsius. At a junction temperature of +150 degrees Celsius, the motor drivers initiate a thermal shutdown. The thermal resistance between junction and ambient air is specified at 85 kelvin per watt for the motor driver L6201 or 13 kelvin per watt for the motor driver L6201PS mounted on a heat sink [48].

The full bridge is powered by the supply voltage and has one digital enable terminal and one digital input terminal for each half bridge that are connected to the microcontroller. The enable terminal is controlled by a digital output, while the input terminals are driven by the high-resolution PWM interface. In idle state both input terminals are pulled to logical low and the servo motor is passively braked by shorting the armature winding. For actuating the servo motor, the full bridge is operated in one phase chopping. Depending on the desired rotating direction, one input terminal is pulled to logical high with driving the other input terminal by a PWM signal with a frequency of 15.6 kilohertz. In this configuration, the armature voltage of the servo motor is proportional to the inverse duty cycle of the PWM interface with a limit value equaling the supply voltage for both rotating directions. Electromagnetic interferences produced by the servo motor are suppressed by a filter capacitor in parallel connection to the servo motor. Further terminals of the motor driver are two bootstrap terminals, one reference voltage terminal and one current sense terminal on the low-side of the full bridge. The bootstrap terminals are connected to external bootstrap capacitors that are used by an internal charge pump circuit for driving the high-side transistors of the full bridge. By measuring the voltage drop of a sense resistor connected between the sense terminal and the negative supply voltage potential, the actual current that drives the servo motor can be determined. In both servo actuator types the reference voltage terminal is left unconnected and the sense terminal is bypassed with a zero-ohm resistor.

3.3.5 Power Supply

The components of the electrical setup excluding the servo motor driver are rated at a supply voltage of 5 volts. In order to provide a stable operating voltage from the variable supply voltage, both servo actuator types apply the linear voltage regulator LM340MP-5.0 produced by National Semiconductor. This active voltage regulator has a rated input voltage range from 7.5 to 20 volts and a fixed rated output voltage of 5 volts with a operating current of up to 1 ampere [39]. The voltage reduction and stabilization is achieved by continuously adjusting a voltage divider network and dissipating the intrinsic excess power as thermal power. The output voltage is further stabilized and smoothed by the connection of external filter capacitors to the input and output terminals of the voltage regulator. The principle of operation makes a sufficient heat sinking concept necessary and limits the operating current to the corresponding dissipatable power. With the rated quiescent current of 50 milliamperes and the maximum rated supply voltage of the servo actuators of 18.5 volts, the output power p_o of the voltage regulator is given by

$$p_o = 5\ V \cdot 50\ mA = 250\ mW. \tag{3.6}$$

Including the operating current of the voltage regulator of 8 milliamperes, the input power p_i and efficiency factor η_v are

$$p_i = 18.5\ V \cdot (50\ mA + 8\ mA) = 1073\ mW, \tag{3.7}$$

$$\eta_v = \frac{p_o}{p_i} = 23.3\ \%. \tag{3.8}$$

At the defined operating point, the dissipation power p_d of the voltage regulator results from the difference of the input power p_i and the output power p_o read as

$$p_d = p_i - p_o = 823\ mW. \tag{3.9}$$

The integrated voltage regulator is housed in a small outline transistor (*SOT-223*) package with a size of 3.6 by 6.5 millimeters and three leads as well as an additional ground lug that is designated to be connected to a heat sink. The allowed operating temperature ranges from +0 degrees Celsius to +125 degrees Celsius [39]. In both servo actuator types this heat sink is an extensive ground plane on the circuit board.

3.3.6 Signal Light

The operational status of the servo actuator is indicated by a signal light that is integrated into the actuator enclosure. The signal light is turned on when the actuator is activated and can be turned off or configured through the communication interface to blink in the event of a failure. In both servo actuator types the signal is produced by a red light-emitting diode (*LED*) mounted on the circuit board and is guided through a transparent plastic conductor to an opening in the actuator enclosure. The diode is connected to a series resistor of 470 ohms in order to limit the operating current. The signal light is controlled by a digital output of the microcontroller and has two switching states.

3.3.7 Evaluation

The electronic setup of the original RX-28 and RX-64 servo actuators have areas for improvement in durability, efficiency and performance. In intended operation, the applied position sensor is prone to partial damage resulting in a nonlinear output characteristic. This makes a precise angular positioning impossible and causes unstable and oscillating actuator motion. Replacing the damaged potentiometer is complex and requires the modification of undocumented calibration parameters. The applied linear voltage regulator has a low efficiency factor and increases the power consumption of the servo actuator. By dissipating the unused thermal power into the ambient air inside the actuator enclosure and into the circuit board, all components are loaded with high temperature and the heat sinking of the servo motor and the servo motor driver is impeded. The applied microcontroller has a basic processor architecture and is limited in computing power and memory space. These characteristics restrain the implementation of advanced control concepts and the introduction of a comprehensive set of operating data.

For enhancing the performance and durability of the servo actuators, a replacement of essential components and a redesign of the electronic setup is required. Particular attention is to be paid to the selection of the processing unit and the position sensor. The development of an enhanced electronic setup applied in the DD-28 and DD-64 servo actuators is described in Chapter 4.

3.4 Control Concept

The control concept of the original RX-28 and RX-64 servo actuators provides different control systems for each mode of operation. In joint mode the actuator is controlled by an angular position control, while in wheel mode an angular speed control is applied. Both control systems are implemented in the firmware of the microcontroller. A comparison of the binary sequence of the different firmware files reveals that the implementations on both servo actuator types are basically identical. In the firmware files with the version number 23 only the model number, the upper supply voltage limit and three actuator-specific calibration parameters for the measurement of the angular position have different values. This fact allows the analysis of the control concept of both servo actuator types by examining the characteristics of a single servo actuator.

In order to analyze the control law, the relation between the control error and the resulting control signal is determined. The control error corresponds to the difference of the desired and the actual

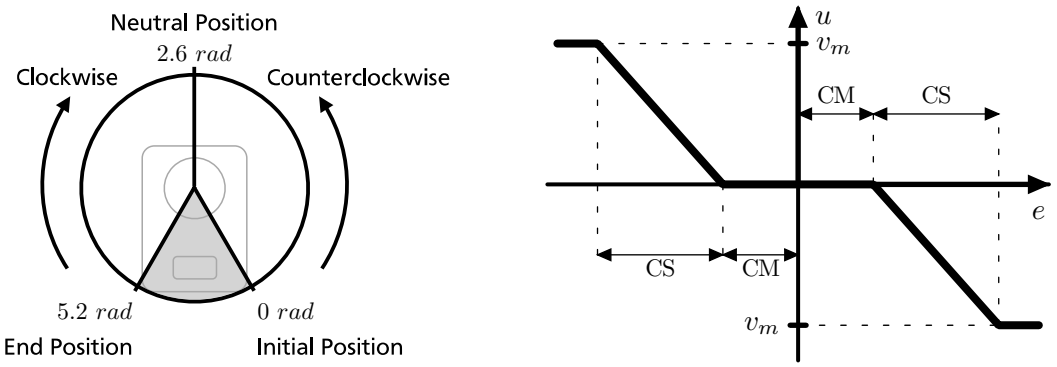

(a) Definition of the absolute angular position.

(b) Definition of the adjustment parameters.

Figure 3.4.: Parameters of the angular position control [43].

control variable. For applying a specific control error, the mechanical setup of an operative RX-28 servo actuator is modified. The mechanical linkage between the potentiometer that measures the actual control variable and the output shaft of the gearbox is removed and replaced by a stepping motor actuating the potentiometer with a step size of 15.7 milliradians. In combination with a static desired control variable, the stepping motor allows to specify the control error by applying a specific actual control variable. The control signal is the duty cycle of the PWM control voltage of the servo motor driver. The modulated control voltage for the clockwise rotating direction is demodulated by applying a passive second-order low-pass filter with a cutoff frequency of 1.5 kilohertz. The low-pass filter averages the modulated control voltage over time and yields the corresponding duty cycle as a continuous-time voltage within the range from 0 volts to 5 volts.

3.4.1 Angular Position Control

In joint mode the angular position control of both servo actuator types allows to drive the servo actuator to a desired angular position within the supported angular range. By setting a desired angular speed, the moving speed of the servo actuator can be specified. The angular position is defined as an absolute value between the index position at 0 radians and the end position at 5.2 radians. The neutral position at 2.6 radians is aligned to the actuator enclosure [43]. Figure 3.4a illustrates the definition of the absolute angular position.

The angular position control is a feedback control and compensates control errors and stabilizes the control variable. The characteristics of the control action can be customized by modifying two compliance-related adjustment parameters for each rotating direction. The compliance margin (*CM*) parameter specifies a dead zone around the desired angular position as an integer multiple of 5.1 milliradians. This dead zone equals to a maximum tolerated control error of the feedback control. The default compliance margin is set to the minimum value of 5.1 milliradians. The compliance slope (*CS*) parameter defines the width of an operating zone for the linear feedback control in seven steps with an undocumented unit. The width of the operating zone corresponds to the actuator stiffness in angular position. Outside of the compliance slope, the control signal saturates and the feedback control acts as a nonlinear two-step control. The default compliance slope has a value of 32. Figure 3.4b depicts the definition of the adjustment parameters with the control error e and the armature voltage of the servo motor v_m. An additional adjustment parameter for setting an increased gain for small control errors is documented, but not implemented in current firmware versions [43].

The linear feedback control law within the compliance slope is identified by applying the method of least-squares on a set of measured control signals resulting from a specified sequence of control errors. The control error e equals to the difference of the static desired angular position φ_d of 2.6 radians and an actual angular position φ_a that is applied by the stepping motor read as

$$e(t) = \varphi_d(t) - \varphi_a(t) = 2.6\ rad - \varphi_a(t). \tag{3.10}$$

The measured control signal u is the filtered control voltage of the servo motor driver $v_{d,f}$ that corresponds to the duty cycle of the modulated control voltage read as

$$u(t) = v_{d,f}(t). \tag{3.11}$$

By assuming the feedback control as an ideal proportional–integral–derivative control with the control gains K_P, K_I and K_D, the control law results in

$$u(t) = K_P\, e(t) + K_I \int_0^t e(\tau)\,\mathrm{d}\tau + K_D\, \dot{e}(t). \tag{3.12}$$

For making use of the method of least-squares, a sequence of n control error values is applied using the stepping motor and the appertaining set of n filtered control voltage values is measured. For the measurement, the compliance margin parameter is left at the default value, while the compliance slope parameter is set to the maximum value of 128 for not exceeding the linear operating zone. The applied control error values and the measured control signal values are combined into the input matrix $\boldsymbol{e}$ and the output vector $\boldsymbol{u}$ given by

$$\boldsymbol{e} = \begin{bmatrix} e(t_0) & \int_{t_0}^{t_0} e(\tau)\,\mathrm{d}\tau & \dot{e}(t_0) \\ e(t_1) & \int_{t_0}^{t_1} e(\tau)\,\mathrm{d}\tau & \dot{e}(t_1) \\ \vdots & \vdots & \vdots \\ e(t_{n-1}) & \int_{t_0}^{t_{n-1}} e(\tau)\,\mathrm{d}\tau & \dot{e}(t_{n-1}) \end{bmatrix}, \tag{3.13}$$

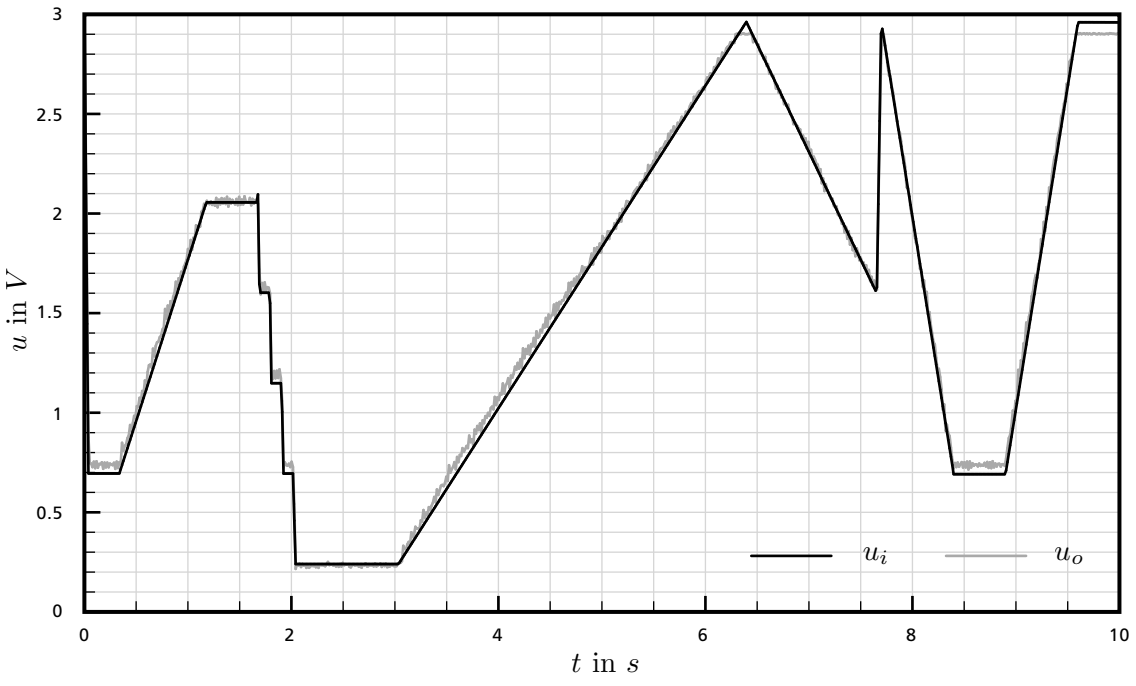

Figure 3.5.: Control action of the original and identified angular position control.

$$\boldsymbol{u}^T = \begin{bmatrix} u(t_0) & u(t_1) & \dots & u(t_{n-1}) \end{bmatrix}. \tag{3.14}$$

By inserting the input matrix and the output vector into the estimator function of the method of least-squares [20], the control gains of the feedback control K_P, K_I and K_D are estimated by

$$\begin{bmatrix} K_P & K_I & K_D \end{bmatrix}^T = \left(\boldsymbol{e}^T\,\boldsymbol{e}\right)^{-1}\,\boldsymbol{e}^T\,\boldsymbol{u}. \tag{3.15}$$

With a sequence of 31800 generic control error values, the normalized values of the control gains $K_{P,n}$, $K_{I,n}$ and $K_{D,n}$ result in

$$K_{P,n} = 1.0\ \tfrac{V}{rad}, \tag{3.16}$$

$$K_{I,n} = -0.3 \cdot 10^{-3}\ \tfrac{V}{radt}, \tag{3.17}$$

$$K_{D,n} = -2.1 \cdot 10^{-3}\ \tfrac{Vt}{rad}. \tag{3.18}$$

The scale of the normalized values shows that the integral control gain K_I and the derivative control gain K_D are negligible. Accordingly, the feedback control law within the linear operating zone is an adjustable proportional control with a control gain K_P that depends on the value of the compliance slope parameter. The executing frequency of the feedback control algorithm exceeds the rate of 1 kilohertz. Figure 3.5 presents the control action of the original angular position control u_o and the identified angular position control u_i resulting from an identical sequence of control errors.

Previous studies on the control accuracy of RX-28 servo actuators show that the local deviation of individual servo actuators can reach a maximum value of 70 milliradians. The system inherent accuracy of the angular position varies between the rated 5.1 milliradians and a maximum value of 10.2 milliradians. This variation is caused by a nonlinear interpolation of the actual angular position. Typically 16 percent of the 2^{10} measurable, equidistant angular position values are ignored in the measurement and are not considered in the feedback control [44].

3.4.2 Angular Speed Control

In wheel mode the angular speed control of both servo actuator types provides a continuous motion of the servo actuator with a desired angular speed. The angular range is not limited and the actuator is able to move in endless turn operation. The desired angular speed is defined as a percentage of the maximum value that depends on the applied supply voltage of the actuator. In continuous motion the angular position passes through the unspecified zone of the potentiometer causing unrelated values of the measured actual angular speed within this range [54].

For identifying the control law of the angular speed control, the relation between a specified control error and the resulting control signal is analyzed. The control error e equals to the difference of the static desired angular speed ω_d and an actual angular speed ω_a that is applied by the stepping motor. The desired angular speed is set to 5 radians per second corresponding to a value of 50 percent at a supply voltage of 19 volts read as

$$e(t) = \omega_d(t) - \omega_a(t) = 5.0\ \tfrac{rad}{s} - \omega_a(t). \tag{3.19}$$

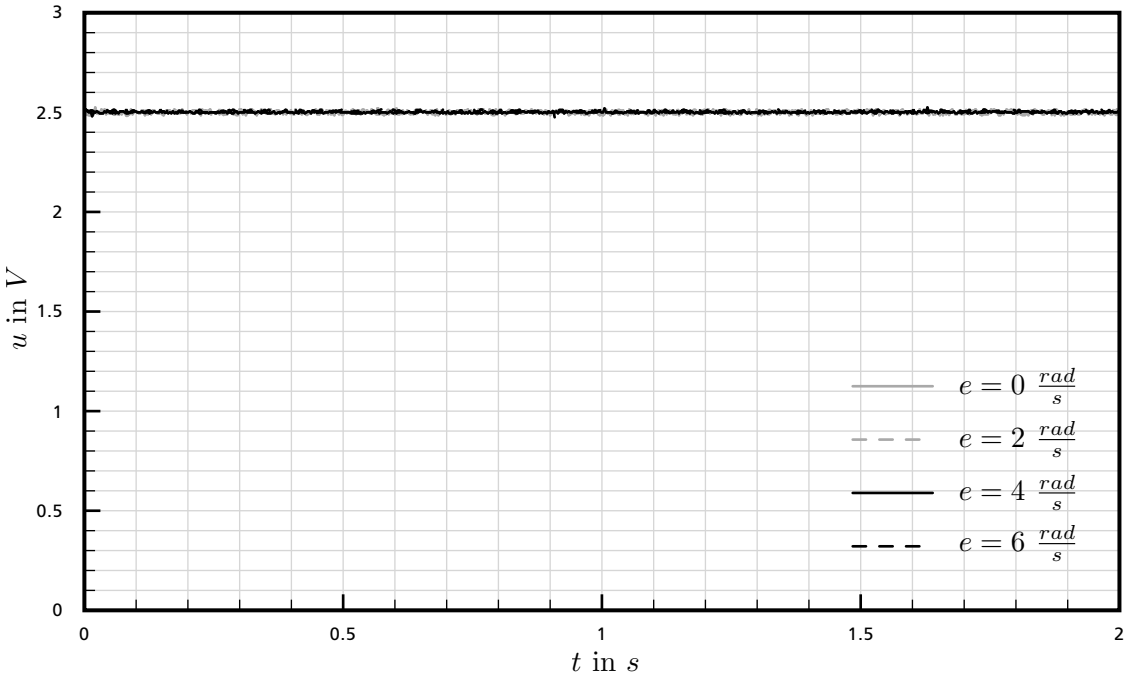

Figure 3.6.: Control action of the angular speed control.

The control signal u is the duty cycle of the modulated control voltage of the servo motor driver that is measured as the filtered control voltage $v_{d,f}$ read as

$$u(t) = v_{d,f}(t). \tag{3.20}$$

Figure 3.6 shows the control action of the control signal for different applied control errors. The control error does not influence the value of the control signal that remains constant over time. Accordingly, the angular speed control is a simple feedforward control that is not able to compensate control errors.

3.4.3 Evaluation

The control concept of the original RX-28 and RX-64 servo actuators implements a basic angular position and speed control without taking full use of the capacities of the actuators. The angular position control has a limited operating range with a nonlinear variation in control accuracy. Significant local deviations of individual servo actuators and the utilization of the compliance margin parameter further decrease the accuracy and repeatability of the angular positioning. For small control errors and a variable supply voltage, the simple proportional control law is not able to take advantage of the full input signal range and limits the control rate. The provided adjustment parameters do not have a fundamental influence on the control action and restrict the adjustment of the actuator trajectory to the desired angular speed. Due to the principle of operation, the angular speed control is not able to eliminate control errors resulting from load torque or parameter deviations. In endless turn operation, the measurement values of the angular position and the angular speed are partially unrelated and have a coarse temporal resolution.

Both control systems fail to meet the requirements for high performance applications. For enhancing the accuracy, repeatability and control rate of the servo actuators, an advanced and flexible control concept in combination with a precise measurement of related process variables is required. Special consideration needs to be given to the elimination of the steady-state control error for assuring high control accuracy and taking advantage of the full input signal range for maximizing the control rate.

The development of an enhanced control concept applied in the DD-28 and DD-64 servo actuators is described in Chapter 5.

4 Electronic Design

The upcoming chapter presents the design and development of the electronic setup applied in the enhanced servo actuators. The configuration and selection of components are related to the analysis of the original servo actuators and aligned to the defined requirements.

4.1 Design Considerations

The survey of the electronic setup implemented in the original RX-28 and RX-64 servo actuators in Section 3.3 identified a potential of improvement that can be attributed to the deficiencies of essential components. The configuration and performance of the processing unit provide a low computing power and restrict the options in control and firmware design. The impaired durability and restricted operating range of the position sensor affect the angular motion and positioning capabilities of the actuator. Caused by the low efficiency of the voltage regulator, the power consumption of the servo actuator is increased and the electronic components are loaded with high temperature.

The electronic setup of the enhanced DD-28 and DD-64 servo actuators is designated for improving the operating characteristics and eliminating the identified design-related deficiencies. The advanced electronic setup needs to comply with the specifications, dimensions and interfaces of the original servo actuators. The restricted installation space requires the limitation to a small number of highly integrated

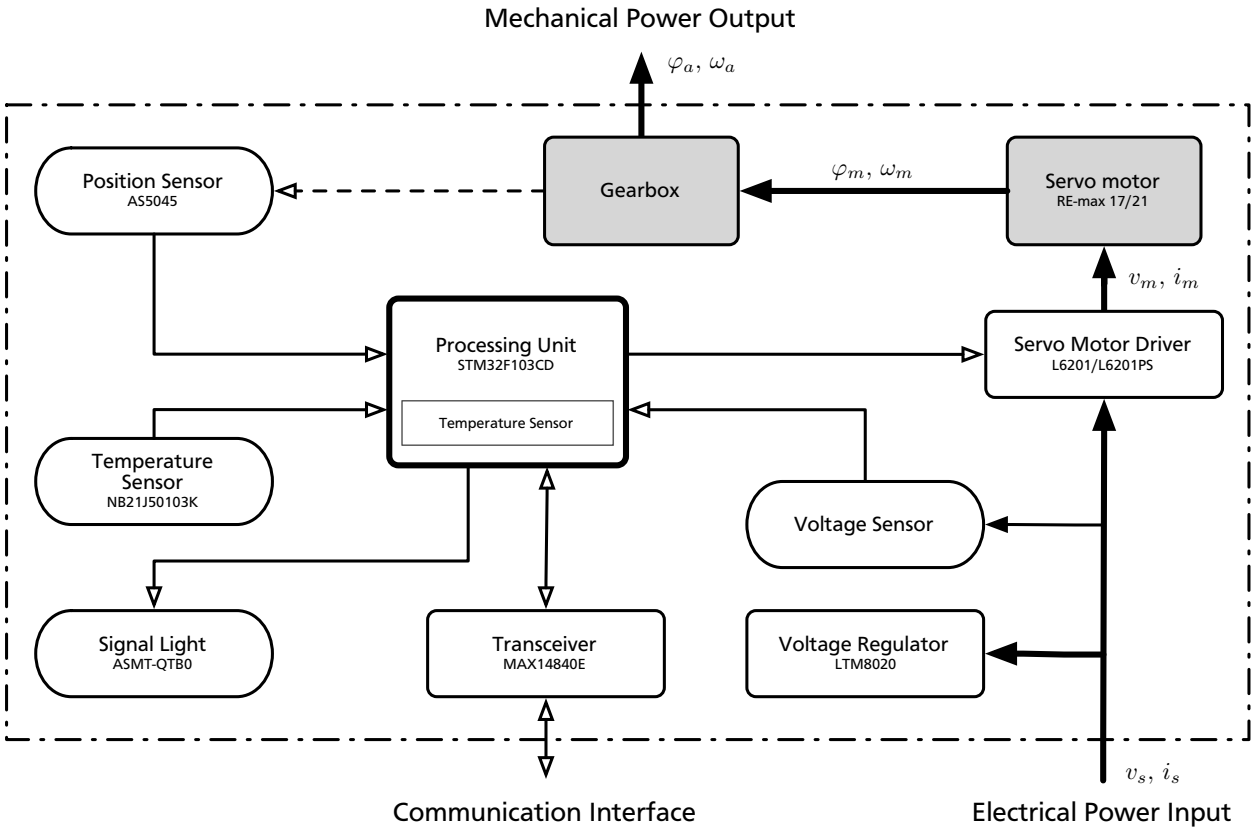

Figure 4.1.: Setup of the enhanced DD-28 and DD-64 servo actuators.

components and surface mounted technology (*SMT*). At any time the applied modifications have to be reversible. In order to improve the performance and durability of the actuator without violating these design requirements, the development of the enhanced electronic setup is based on replacing the deficient components with adopting the scheme of the original system. This design approach allows to increase the operating efficiency and functionality without affecting compatibility.

The requirements for the processing unit combine demands in performance, configuration and dimension. The implementation of an advanced control and firmware concept requires high computing power and sufficient memory space that gives an ample scope for further development. The introduction of a comprehensive set of operating data and reasonable measurements makes the processing of an extensive amount of data necessary. For interacting with other electronic components, the peripheral configuration of the processing unit needs to include all required analog and digital interfaces without exceeding the available installation space. The communication interface must cover an extended symbol rate range with assuring a reliable networked operation. In order to capture precise measurements of the angular motion over a wide measurement range, the position sensor has to provide a high angular resolution and support multiple turn operation. The sensor configuration needs to prevent wear-related failures and adapt to the given mechanical interface. The demands in the power supply comprise an improved efficiency and a broad range of supported supply voltages. The reduction of dissipation power avoids thermal load of adjacent components and decreases the overall power consumption. Caused by the mostly sealed enclosure and the limited heat sink capacities, the thermal power is a critical operating parameter and requires monitoring of the operating temperature and thermal distribution.

For ensuring compatibility and an uncomplicated installation, the layout of the printed circuit boards is to be aligned to the original double-sided circuit board and enclosure dimensions. The design and dimensioning of conducting paths and ground planes have to assure a reliable operation and consider electromagnetic compatibility in the context of the design requirements. Figure 4.1 shows a functional diagram of the setup of the enhanced DD-28 and DD-64 servo actuators. Detailed circuit diagrams and circuit board layouts of both servo actuator types are listed in Appendix F.

4.2 Processing Unit

Based on the requirements in performance and configuration, the 32-bit microcontroller STM32F103CD produced by STMicroelectronics is selected for the application in both servo actuator types. The microcontroller implements the Cortex-M3 architecture with the 16-bit Thumb2 instruction set introduced by ARM and derived from the reduced instruction set computer (*RISC*) design. The architecture supports hardware division and single cycle multiplication and bit-field manipulation [6]. An external crystal oscillator with a clock rate of 8 megahertz is connected to the configurable phase-locked loop (*PLL*) circuit of the microcontroller that multiplies the clock frequency and clocks the core, memory and main bus system with a clock rate of 72 megahertz. This clock configuration enables a processing speed of 90 million instructions per second. A number of peripherals and extra bus systems are clocked with a reduced clock rate. The microcontroller provides thirty-seven digital inputs and outputs and different analog and digital peripherals. The successive approximation analog-digital-converter (*ADC*) has 10 external and two internal channels and can convert analog measurement signals with a resolution of 12 bits. All channels are connected to a multiplexer that allows several single and continuous conversion modes with a conversion rate of up to 854.7 kilohertz. The internal channels can be used to measure the outputs of an internal temperature sensor or a reference voltage. The ADC is applied for capturing the actual values of the motor and microcontroller temperature as well as the supply voltage of the actuator. The advanced-control timer and the three general-purpose timers provide four independent pulse width modulation (*PWM*) interfaces with sixteen channels in total. Each channel is able to generate a digital voltage signal with a controllable duty cycle at a resolution of 16 bits. Two PWM channels drive the

input terminals of the servo motor driver. Two separate watchdog timers allow to generate a reset of the microcontroller in the event of a software-related malfunction. The configurable serial interface provided by one of the three universal synchronous and asynchronous receiver and transmitters (*USART*) has a symbol rate limit of 4.5 megabits per second. In combination with an external transceiver the USART establishes the asynchronous communication interface of the actuator. For interacting with external components, the microcontroller offers two serial peripheral interfaces (*SPI*) with a symbol rate of up to 18 megabits per second. One of the SPI connections is used to emulate the digital interface of the applied position sensor and read the actual angular position value. The integrated direct memory access (*DMA*) feature allows a direct data transfer between peripherals and memory as well as between memory and memory without any action of the processor core. This function increases the transfer rates and reduces the processor core load for repeated data transfers. The highly integrated circuit is housed in a low profile quad flat package (*LQFP*) with forty-eight leads and a size of 7 by 7 millimeters. The allowed operating temperature ranges from -40 degrees Celsius to $+105$ degrees Celsius [50, 51].

The memory configuration of the microcontroller consists of a volatile working memory and a non-volatile program memory. The volatile static random access memory (*SRAM*) has a size of 20 kibibytes and is used for storing and buffering working data during the operation including the transient configuration parameters and actual and desired actuator values. The non-volatile flash memory provides a size of 128 kibibytes and is applied for the storage of the persistent configuration parameters and the firmware of the servo actuator. In both memory types, data is encoded in little-endian byte order storing the least significant byte value at the lowest memory address [50,51]. A list of the technical specifications of the microcontroller STM32F103CD is presented in table 4.1.

The microcontroller provides a hardware extensions for advanced debugging that supports the joint test action group debug (*JTAG*) standard and the serial wire debug (*SWD*) standard. The debug interface can be used for programming firmware or data to the program memory of the microcontroller and allows to test the operating sequence as well as the memory usage during operation. The processor core and specified peripherals can be halted on a given instruction fetch appertaining to a breakpoint or data access corresponding to a watchpoint. The state of the halted system including register and memory values may be examined for finding and removing firmware or hardware errors. The execution can be resumed in single step or regular operation [50, 51]. Caused by the limited installation space, the debug interface is not led to pads on the circuit board, but can be accessed by connecting to the related terminals of the microcontroller. A different way of programming the program memory is provided by the embedded bootloader that can be interfaced through the communication interface. For activating the bootloader, one of the two boot terminals has to be pulled to logical high when powering up the microcontroller. An external resistor–capacitor circuit connected to a digital output allows to enter the bootloader mode without modifying the electronic setup. The capacitor is charged by the digital output and holds the voltage potential during the microcontroller performs a restart. In bootloader mode, the symbol rate of the communication interface is detected automatically and the programming or erasing of the program memory can be initiated by sending corresponding commands [53]. This configuration allows to change the firmware of the servo actuator without accessing the circuit board or applying an additional programming adapter. Due to the half-duplex operation of the communication interface, the reading of the program memory or the reception of data sent by the bootloader is not supported.

The firmware of the servo actuator is developed by applying the standard peripherals library provided by STMicroelectronics. This library comprises an extensive set of functions and header files written in the programming language C for accessing the microcontroller features and peripherals [52]. The free version of the integrated development environment TrueStudio developed by Atollic is used for programming and firmware generation [8].

Caused by the absence of an independent electrically erasable programmable read-only memory (*EEPROM*), the application of flash memory for the storage of the persistent configuration parame-

Table 4.1.: Technical specifications of the microcontroller STM32F103CB [50, 51].

	Unit	**STM32F103CB** (STMicroelectronics)
Supply voltage range	V	2.0 - 3.6
Clock speed limit	MHz	72.0
Flash memory size	KiB	128.0
SRAM size	KiB	20.0
ADC channels		12
ADC resolution	bit	12
PWM channels		16
PWM resolution	bit	16
USART interfaces		3
USART symbol rate limit	$\frac{Mbit}{s}$	4.5
SPI interfaces		2
SPI symbol rate limit	$\frac{Mbit}{s}$	18.0
Digital inputs and outputs		37
Package dimensions	mm	7.0 x 7.0 x 1.6

ters of the servo actuator is requisite. The flash memory provides a fast read and write access, but requires a time-consuming erase operation to free up memory space before new data can be rewritten to the same memory address. The memory space is divided into a set of memory pages with a size of 1 kibibyte. The erase operation clears memory in blocks and erases one memory page at once. These characteristics and the limited number of supported write and erase cycles necessitate the implementation of a flash memory management concept. For storing variable data to the flash memory, the concept allocates a virtual 16-bit memory address and a 16-bit data field for each data element. The virtual memory address allows to to read or modify data of a specific data element. When a data element is modified, the modified data associated with the virtual memory address is stored at a subsequent location of the flash memory. The actual value of an data element is read by returning the data field at the latest flash memory location. The functionality of the erase operation requires the utilization of at least two memory pages. One memory page is initially erased and can store actual data elements until all memory space is occupied. The other memory page is kept ready for taking over the data of the former, full memory page and allows an erase operation without any loss of data. The actual operating status of a memory page is saved in a header field with three possible states:

- *VALID PAGE*: The memory page contains valid data elements.

- *ERASED PAGE*: The memory page is erased and ready for taking over data elements.
- *RECEIVE DATA*: The memory page receives data elements from the former, full memory page.

By appending additional memory pages to the flash memory management, the non-volatile memory space can be extended [49]. This configuration results in a flexible and fast memory structure with a configurable memory space for the storage of persistent data. An implementation of the concept is provided by STMicroelectronics as a configurable extension of the standard peripherals library [52].

The applied microcontroller has a reduced supply voltage compared to the microcontroller used in the original system. The supply voltage range is rated from 2 volts to 3.6 volts. This characteristic makes a modification of the power supply configuration necessary. In regard to the limited installation space, the integration of an additional voltage regulator is not admissible. For this reason, the operating voltage of all components applied in the electronic setup excluding the servo motor driver is specified at 3.3 volts. This definition requires a replacement of incompatible components and influences the design and layout of the circuit boards.

4.3 Sensor Elements

The set of essential servo actuator values consists of the actual angular position and speed, load torque and armature current. The actual supply voltage and servo actuator temperatures are measured for complying with specified safety limits. The original system provides sensor elements for monitoring the actual angular position, operating voltage and servo motor temperature. The values of the actual angular speed and the load torque related load value are derived from the measured value of the actual angular position. For measuring the actual angular speed, load torque and armature current directly, additional sensor elements are required. The limited installation space impedes the implementation of these supplemental components. Depending on the operating principle of the sensor elements, the power consumption and power loss of the actuator is increased by converting the measurands. For these reasons, the electronic setup of both servo actuators types is not augmented by additional sensor elements. The unmeasured actuator values are estimated by a model-based state observer that uses the known control signal and captured measurands. The state observer matches the estimated actuator state to the actual actuator values based on the output error of the applied model. A detailed description of the functionality and design of the state observer can be found in Section 5.3.

The applied sensor elements measure the actual values of the angular position, supply voltage and servo actuator temperatures and support the decreased operating voltage of 3.3 volts. The angular position is read from the position sensor through the SPI of the microcontroller, while the supply voltage and servo actuator temperatures are converted into analog voltages and captured with the ADC of the microcontroller. The convertible voltage of the ADC is limited to a range from 0 volts to the reduced operating voltage of 3.3 volts.

4.3.1 Position Sensor

For measuring the actual angular position of the servo actuator, the contactless absolute position sensor AS5045 produced by austriamicrosystems is selected for the application in both servo actuator types. The position sensor uses an array of Hall effect sensors for detecting the magnetic field across the sensor surface. In combination with a diametral magnet mechanically linked to the output shaft of the gearbox, the sensor is able to infer the absolute angular position of the servo actuator from the distribution of the magnetic field. An integrated digital signal processing (*DSP*) unit evaluates the measurement values and provides a digital representation of the angular position. The implemented spinning-current technology

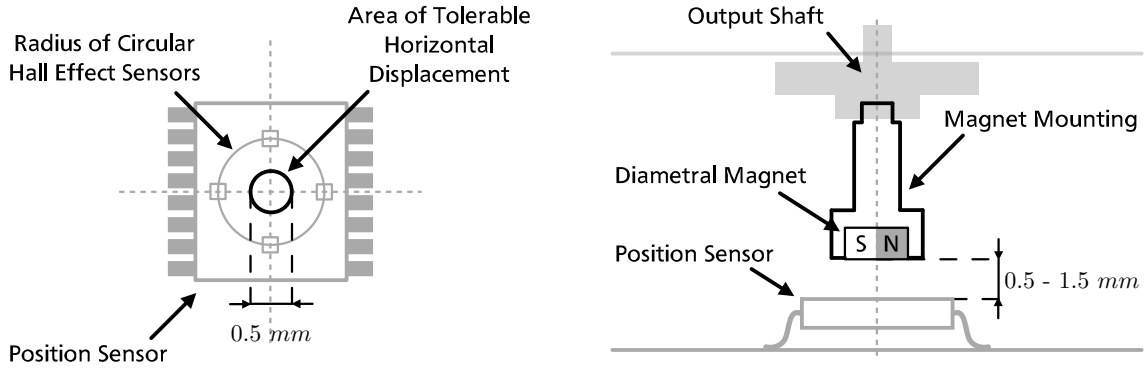

(a) Configuration of the position sensor.

(b) Mounting of the diametral magnet.

Figure 4.2.: Setup of the position sensor with the diametral magnet [9].

reduces the offset value of the measurement signal. Due to the applied differential measurement method and a Hall effect sensor conditioning circuit, the sensor is tolerant to magnetic stray fields and a finite misalignment of the diametral magnet [9]. Figure 4.2a shows the configuration of the position sensor with the arrangement of the Hall effect sensor array.

An integrated voltage regulator allows the operation of the position sensor with a supply voltage of 3.3 volts or 5 volts. The typical operating current is rated at 16 milliamperes. Resulting from the contactless configuration, the sensor provides a wearless operation and supports multiple turn operation. The measurement range covers a full turn of 2π radians with a resolution of 12 bits and a sampling rate of 10.4 kilohertz. The integrated circuit of the sensor is housed in a shrink small outline package (*SSOP-16*) with sixteen leads and a size of 5.3 by 6.2 millimeters. The allowed operating temperature ranges from -40 degrees Celsius to $+125$ degrees Celsius [9].

Disturbances in the conversion of the measurement signal cause an additive noise signal that interferes the measurement. The noise signal is assumed to be zero-mean and normally distributed with a variance of 1.1 square milliradians. The activation of an internal noise filter reduces the variance of the noise signal to 0.3 square milliradians, but is accompanied by a decrease of the sampling rate to 2.6 kilohertz [9]. With the resolution of 12 bits over the angular range of 2π radians, the angular position is measured with a theoretical resolution r_m of

$$r_m = \frac{2\pi\ rad}{2^{12}} = 1.5\ mrad. \tag{4.1}$$

Besides the additive noise signal, the actual resolution is affected by magnet displacement and fluctuation in operating temperature. The tolerable horizontal displacement of the magnet relative to the center of the Hall effect sensor array is rated at 0.25 millimeters [9]. The applied diametral magnet is made of an alloy of neodymium, iron and boron and measures 6 millimeters in diameter and 2.5 millimeters in height. The remanence is rated at 1.2 telsa with a maximum operation temperature of 120 degrees Celsius [37]. The correct measurement of the angular position is ensured by placing the magnet within the tolerable horizontal displacement and a vertical distance range from 0.5 millimeters to 1.5 millimeters to the sensor surface [9]. To satisfy these specifications and provide a mechanical link to the output shaft of the gearbox, a lightweight magnet mounting is constructed. The mounting is made of selective-laser-sintered polyamide with a medium flexibility and a high strength. A tenon and edgewise tongues allow to insert the mounting into the existing notch of the output shaft and result in a positive locking. A bore on the opposite side holds the diametral magnet. By taking advantage of the flexibility, the magnet mounting is installed by clamping and does not necessitate any permanent conversions. Figure 4.2b

illustrates the mounting of the diametral magnet in relation to the position sensor. Detailed technical drawings of the magnet mounting of both servo actuator types can be found in Appendix G.

In order to retrieve the measured angular position, the position sensor provides a synchronous serial interface (*SSI*) with a supported symbol rate limit of 1 megabit per second. The interface is connected to SPI of the microcontroller. By pulling the chip select terminal to logical low, the position sensor initiates the transmission of a data word with a length of 19 bits that contains the digital representation of the angular position and additional status data. The transmitted data is read by the serial data in terminal and clocked by the serial clock terminal of the microcontroller. The interface is configured to retrieve the actual value of the angular position with a rate of 2.5 kilohertz.

For decreasing the power consumption and reducing the installation space, the applied sensor can be replaced with the novel position sensor AS5055 produced by austriamicrosystems. The supply voltage is rated at 3.3 volts, while the average operating current has a maximum value of 8 milliamperes dependent on the applied retrieving rate. The integrated circuit of the position sensor is housed in a quad flat no leads package with sixteen terminals (*QFN-16*) and a size of 4 by 4 millimeters [10].

4.3.2 Temperature Sensors

In addition to the temperature sensor applied for the measurement of the servo motor temperature, the internal temperature sensor of the microcontroller allows to approximate the temperature of the electronic components and the circuit board. The thermal load of the servo motor and the electronic components differ in magnitude and rate of change. By monitoring the actual temperature at different points inside of the actuator enclosure, the observation of the thermal distribution and the specification of differentiated safety limits is possible.

4.3.2.1 Microcontroller Temperature Sensor

The internal temperature sensor of the microcontroller is connected to a dedicated channel of the ADC. The actual microcontroller temperature θ_c in degrees Celsius is computed from the converted voltage v_c by applying the reference voltage v_t, the temperature parameter A_t and the temperature offset θ_o read as

$$\theta_c(t) = \frac{v_t - v_c(t)}{A_t} + 25\ ^\circ C + \theta_o. \tag{4.2}$$

The reference voltage is rated at 1430 millivolts and has a tolerance of 6 percent. The temperature parameter is specified at 4.3 millivolts per degree Celsius with a tolerance of 7 percent. Due to production variation, the temperature offset cannot be defined generally, but is guaranteed to be smaller than 45 degrees Celsius [50, 51]. The actual temperature offset is identified by using the measurement value of the temperature sensor applied for measuring the servo motor temperature. When the servo actuator is activated for the first time, all servo actuator components are assumed to have the same temperature and the temperature offset θ_o results from the measured servo motor temperature θ_m and the offset-free measured microcontroller temperature $\tilde{\theta}_c$ read as

$$\theta_o = \theta_m(t_0) - \tilde{\theta}_c(t_0). \tag{4.3}$$

The determined value of the temperature offset is stored as a persistent configuration parameter in the non-volatile memory area. In order to assure a correct measurement, the servo actuator needs to have an equal temperature distribution when activated for the first time.

The measurement range of the sensor is given by the range of the converted voltage v_c. Dependent on the temperature offset θ_o and with the lowest value $v_{c,l}$ and highest value $v_{c,h}$ of the converted voltage, the theoretically measurable lowest temperature $\theta_{c,l}$ and highest temperature $\theta_{c,h}$ of the microcontroller result in

$$\theta_{c,l} = \frac{v_t - v_{c,h}}{A_t} + 25\ ^\circ C + \theta_o = -409.9\ ^\circ C + \theta_o, \tag{4.4}$$

$$\theta_{c,h} = \frac{v_t - v_{c,l}}{A_t} + 25\ ^\circ C + \theta_o = 357.6\ ^\circ C + \theta_o \tag{4.5}$$

where

$$v_{c,l} = 0\ V, \tag{4.6}$$

$$v_{c,h} = 3.3\ V, \tag{4.7}$$

$$v_t = 1430\ mV, \tag{4.8}$$

$$A_t = 4.3\ \tfrac{mV}{^\circ C}. \tag{4.9}$$

The actual measurement range is limited by the allowed operating temperature of the microcontroller that ranges from -40 degrees Celsius to $+105$ degrees Celsius [50]. With the resolution of the ADC of 12 bits for the full convertible voltage range, the microcontroller temperature is measured with a theoretical resolution r_m of

$$r_m = \frac{\theta_{c,h} - \theta_{c,l}}{2^{12}} = 187.4\ m^\circ C. \tag{4.10}$$

The tolerance of the parameters and voltage signal noise affect the actual measurement range and resolution. For reducing the influence of the signal noise, a moving average low-pass filter over four measurement values is implemented. By neglecting the temperature offset and applying the specified tolerances of the reference voltage of 6 percent and the temperature parameter of 7 percent, the maximum relative measurement error ϵ_m at a temperature of 25 degrees Celsius is given by

$$\epsilon_m = \left| \frac{\tilde{\theta}_c - \theta_c}{\theta_c} \right| = \left| \frac{\left(\frac{\tilde{v}_t - 1430\ mV}{\tilde{A}_t} + 25\ ^\circ C \right) - \left(\frac{v_t - 1430\ mV}{A_t} + 25\ ^\circ C \right)}{\frac{v_t - 1430\ mV}{A_t} + 25\ ^\circ C} \right| = 85.8\ \% \tag{4.11}$$

where

$$\tilde{v}_t = 0.94 \cdot v_t = 1344.2\ mV, \tag{4.12}$$

$$\tilde{A}_t = 1.07 \cdot A_t = 4.6\ \tfrac{mV}{^\circ C}. \tag{4.13}$$

This result shows that the internal temperature sensor of the microcontroller gives a rough approximation of the actual temperature value by applying the rated parameters. For improving the measurement accuracy, the specific parameters of each temperature sensor have to be determined by performing a reference measurement.

4.3.2.2 Servo Motor Temperature Sensor

The configuration for measuring the actual servo motor temperature of the servo actuator is based on the measurement method of the original system. A thermistor with a negative temperature coefficient placed near the servo motor and a resistor are connected in series and form a voltage divider. The voltage divider provides a temperature-dependent voltage that is captured with the ADC of the microcontroller. In order to adapt to the reduced operating voltage and cover a wide temperature range, the scaling factor of the voltage divider needs to be adjusted By applying high value resistors, the power consumption of the configuration and the measurement error resulting from intrinsic dissipation power is minimized. The thermistor NB21J50103K produced by AVX is used in both servo actuator types. The resistance at a temperature of 25 degrees Celsius is rated at 10 kiloohms and has a tolerance of 10 percent. The temperature parameter is specified at 3480 kelvin with a tolerance of 3 percent [12]. The resistor is a metal film resistor with a low temperature dependency. The resistance is rated at 68 kiloohm and has a tolerance of 1 percent. The input voltage over the thermistor and resistor is the reduced operating voltage of 3.3 volt, while the output voltage is measured over the thermistor and is proportional to the actual resistance value. By neglecting the input current of the ADC and the temperature dependency of the resistor, the actual resistance of the thermistor R_t is computed with the resistor R_1 and the converted voltage v_c read as

$$R_t(t) = \frac{R_1 \; v_c(t)}{3.3 \; V - v_c(t)}. \tag{4.14}$$

The nonlinear decrease of the resistance R_t with an increasing servo motor temperature can be approximated by an exponential function [4]. Dependent on the rated resistance R_2 at the temperature θ_t and the temperature parameter B_t of the thermistor, the measured servo motor temperature θ_m in kelvin is given by

$$\theta_m(t) = \frac{B_t \; \theta_t}{B_t + \ln\left(\frac{R_t(t)}{R_2}\right) \; \theta_t}. \tag{4.15}$$

To decrease the computational effort during operation, the nonlinear relation between the servo motor temperature and the measured voltage is precalculated and stored as a persistent lookup table in the non-volatile memory area. Caused by the indirect measurement method, the measured value approximates the temperature of the servo motor, but does not represent the actual value. Changes in actual temperature are measured with an offset and delay that has to be considered in the specification of safety limits.

For estimating the measurement range and resolution of the sensor, the highest and lowest values of the converted voltage v_c are shifted by one resolution step of the ADC. The lowest value $v_{c,l}$ and highest value $v_{c,h}$ of the converted voltage are determined from the maximum convertible voltage of 3.3 volts and the resolution of the ADC of 12 bits read as

$$v_{c,l} = 0 \; V + \frac{3.3 \; V}{2^{12}} = 0.8 \; mV, \tag{4.16}$$

$$v_{c,h} = 3.3 \; V - \frac{3.3 \; V}{2^{12}} = 3299.2 \; mV. \tag{4.17}$$

The theoretically measurable lowest resistance $R_{t,l}$ and highest resistance $R_{t,h}$ of the thermistor as well as the lowest temperature $\theta_{m,l}$ and highest temperature $\theta_{m,h}$ of the servo motor are given by

$$\theta_{m,l} = \frac{B_t\ \theta_t}{B_t + \ln\left(\frac{R_{t,h}}{R_2}\right)\ \theta_t} = 158.9\ K \mathrel{\widehat{=}} -144.3\ ^\circ C, \tag{4.18}$$

$$\theta_{m,h} = \frac{B_t\ \theta_t}{B_t + \ln\left(\frac{R_{t,l}}{R_2}\right)\ \theta_t} = 660.7\ K \mathrel{\widehat{=}} 387.5\ ^\circ C \tag{4.19}$$

where

$$R_1 = 68\ k\Omega, \tag{4.20}$$

$$R_{t,l} = \frac{R_1\ v_{c,l}}{3.3\ V - v_{c,l}} = 16.5\ \Omega, \tag{4.21}$$

$$R_{t,h} = \frac{R_1\ v_{c,h}}{3.3\ V - v_{c,h}} = 280.4\ M\Omega, \tag{4.22}$$

$$B_t = 3480\ K, \tag{4.23}$$

$$R_2 = 10\ k\Omega, \tag{4.24}$$

$$\theta_t = 298.2\ K \mathrel{\widehat{=}} 25\ ^\circ C. \tag{4.25}$$

The actual measurement range is limited by the allowed operating temperature of the thermistor that ranges from −55 degrees Celsius to +150 degrees Celsius [12]. With the resolution of the ADC of 12 bits for the full convertible voltage range, the servo motor temperature is measured with a theoretical resolution r_m of

$$r_m = \frac{\theta_{m,h} - \theta_{m,l}}{2^{12}} = 1.3\ mK. \tag{4.26}$$

The actual measurement range and resolution is affected by the tolerance of the resistance values and parameters as well as voltage signal noise. For reducing the influence of the signal noise, a moving average low-pass filter over four measurement values is implemented. By applying the rated tolerances of the thermistor of 10 percent and the temperature parameter of 3 percent, the maximum relative measurement error ϵ_m at a temperature of 25 degrees Celsius is given by

$$\epsilon_m = \left|\frac{\tilde{\theta}_m - \theta_m}{\theta_m}\right| = \left|\frac{\frac{\tilde{B}_t\ \theta_t}{\tilde{B}_t + \ln\left(\frac{10\ k\Omega}{\tilde{R}_2}\right)\ \theta_t} - \frac{B_t\ \theta_t}{B_t + \ln\left(\frac{10\ k\Omega}{R_2}\right)\ \theta_t}}{\frac{B_t\ \theta_t}{B_t + \ln\left(\frac{10\ k\Omega}{R_2}\right)\ \theta_t}}\right| = 0.9\ \% \tag{4.27}$$

where

$$\tilde{R}_2 = 0.90 \cdot R_2 = 9000\ \Omega, \tag{4.28}$$

$$\tilde{B}_t = 0.99 \cdot B_t = 3375.6\ K. \tag{4.29}$$

4.3.3 Voltage Sensor

For measuring the actual supply voltage of both servo actuator types, the configuration of the original system is adopted. A voltage divider scales the supply voltage and allows to capture the proportionally reduced voltage with the ADC of the microcontroller. The scaling factor of the voltage divider needs to be modified in order to cover the extended supply voltage range and adapt to the reduced operating voltage. By applying high value resistors, the power consumption of the configuration is minimized. The voltage divider is formed by two resistors connected in series with a rated resistance of 68 kiloohms and 10 kiloohms. Both resistors are metal film resistors with a low temperature dependency and a rated tolerance of 1 percent. The supply voltage is the input voltage over both resistors, while the scaled output voltage is measured over the low value resistor. With considering the maximum convertible voltage of 3.3 volts and neglecting the input current of the ADC and the temperature dependency of the resistors, this configuration results in a theoretically measurable highest supply voltage $v_{s,h}$ of

$$v_{s,h} = 3.3\ V \cdot \frac{R_1 + R_2}{R_2} = 25.7\ V \tag{4.30}$$

where

$$R_1 = 68\ k\Omega, \tag{4.31}$$

$$R_2 = 10\ k\Omega. \tag{4.32}$$

With the resolution of the ADC of 12 bits for the full convertible voltage range, the supply voltage is measured with a theoretical resolution r_m of

$$r_m = \frac{v_{s,h}}{2^{12}} = 6.3\ mV. \tag{4.33}$$

The tolerance of the resistance values and voltage signal noise affect the actual measurement range and resolution. For reducing the influence of the signal noise, a moving average low-pass filter over four measurement values is implemented. By applying the specified tolerance of the resistors of 1 percent, the maximum relative measurement error ϵ_m is given by

$$\epsilon_m = \left| \frac{\tilde{v}_s - v_s}{v_s} \right| = \left| \frac{\frac{\tilde{R}_2}{\tilde{R}_1 + \tilde{R}_2} - \frac{R_2}{R_1 + R_2}}{\frac{R_2}{R_1 + R_2}} \right| = 1.8\ \% \tag{4.34}$$

where

$$\tilde{R}_1 = 0.99 \cdot R_1 = 67320\ \Omega, \tag{4.35}$$

$$\tilde{R}_2 = 1.01 \cdot R_2 = 10100\ \Omega. \tag{4.36}$$

4.4 Communication Interface

Resulting from the demand in compatibility with the original system, the communication interface provides an asynchronous half-duplex serial interface based on the EIA-485 bus standard. The USART interface of the microcontroller is connected to a transceiver that is used as driver and receiver for the bus interface. The used transceiver ensures a reliable networked operation and supports the reduced operating voltage of 3.3 volts.

In both servo actuator types, the integrated high-speed transceiver MAX14840E produced by Maxim Integrated Products is applied. This transceiver has a rated supply voltage of 3.3 volts and a typical operating current of 1.5 milliamperes. The symbol rate limit is specified at 40 megabits per second with up to thirty-two transceivers on the bus interface. The transceiver is housed in a thin quad flat no leads package with eight terminals (*TQFN-8*) and a size of 3 by 3 millimeters. The allowed operating temperature ranges from -40 degrees Celsius to $+125$ degrees Celsius [32].

The configuration of the communication interface covers the desired symbol rate range from 9600 kilobits per second to 4 megabits per second and permits the operation of the specified thirty devices in networked operation. The actual symbol rate is restricted by the USART interface of the microcontroller that has a symbol rate limit of 4.5 megabits per second. The functionality and terminal configuration of the transceiver are compatible to the original transceiver and allow an integration without necessitating changes of the electronic setup.

For further increasing the number of supported networked devices, the applied transceiver can be replaced with the transceiver MAX13431E produced by Maxim Integrated Products. This transceiver allows to operate up to two hundred and fifty-six transceivers on the bus interface with a symbol rate limit of 16 megabits per second [32].

4.5 Servo Motor Driver

The servo motor drivers applied in the original system are matched to the servo motors and provide high performance with a compact design. The integrated full bridges of efficient field-effect transistors support a wide supply voltage range and ensure low switching losses. The digital input terminals that are controlled by a digital output and two PWM channels of the microcontroller have a low threshold voltage of 2 volts and can be driven with the reduced operating voltage of 3.3 volts [48]. Based on these specifications, the original motor drivers L6201 and L6201PS produced by STMicroelectronics are maintained in the electronic setup of the servo actuators.

Two PWM channels of the microcontroller actuate the two half bridges of the motor driver and control the magnitude and polarity of the armature voltage. The absolute value of the armature voltage is bounded by the supply voltage. The timer of the PWM interface provides a resolution of 12 bits per rotating direction at an operating frequency of 17.6 kilohertz. Electromagnetic interferences produced by the servo motor are suppressed by a filter capacitor of 100 nanofarads in parallel connection to the servo motor as well as a connection between the servo motor case and ground.

The extended supply voltage range of the servo actuators from 12 volts to 25 volts results in an increased armature current of the servo motor at high armature voltages and load torques. This increased armature current and the arising temperature load have to be considered in the definition of safety limits in order to comply with the rated specifications of the servo motor and the motor driver.

4.6 Power Supply

The power supply provides the stable, reduced operating voltage of 3.3 volts for the components of the electrical setup excluding the servo motor driver. For supporting a wide supply voltage range and decreasing the power consumption of the servo actuator, a switched-mode voltage regulator with high efficiency factor is applied. The voltage regulator reduces and stabilizes the output voltage by switching an inductor into different configurations. The inductor stores electrical energy when connected to the input voltage and supplies the electrical load when discharged. The duty cycle of the switching operation defines the value of the output voltage. Both servo actuator types use the integrated voltage regulator LTM8020 produced by Linear Technology. This voltage regulator has a rated input voltage range from 4 volts to 36 volts and provides an adjustable output voltage from 1.25 volts to 5 volts with an efficiency factor of up to 80 percent. The output voltage is set to 3.3 volts by connecting a resistor of 301 kiloohms to the adjustment terminal. Two external filter capacitors of 2.2 microfarads connected to the input terminal and 10 microfarads connected to the output terminal further stabilize and smooth the output voltage. The maximum operating current is specified at 200 milliamperes. The voltage regulator is housed in a land grid array (*LGA*) package with a size of 6.3 by 6.3 millimeters and twenty-one leads. The allowed operating temperature ranges from -40 degrees Celsius to $+85$ degrees Celsius [26].

The principle of operation results in a high efficiency with low dissipation power. With an approximated operating current of 120 milliamperes and the maximum supply voltage of the servo actuators of 25 volts, the output power p_o of the voltage regulator results in

$$p_o = 3.3\ V \cdot 120\ mA = 396\ mW. \tag{4.37}$$

At the defined operating point, the efficiency factor η_v of the voltage regulator is rated at 70 percent [26]. The input power p_i is given by

$$p_i = \frac{1}{\eta_v}\, p_o = 565.7\ mW \tag{4.38}$$

where

$$\eta_v = 70\ \%. \tag{4.39}$$

The dissipation power p_d of the voltage regulator results from the difference of the input power p_i and the output power p_o read as

$$p_d = p_i - p_o = 169.7\ mW. \tag{4.40}$$

The configuration of the power supply covers the desired supply voltage range from 12 volts to 25 volts and reduces the thermal load and power consumption of the servo actuator.

4.7 Signal Light

In order to enhance the optical feedback and indication of different operating states of the servo actuator, the monochrome signal light of the original system is replaced by a multicolor signal light. This component combines three separate signal lights with the primary colors red, green and blue in one package. The primary signal lights can be operated individually through three control terminals that

are connected the microcontroller. This configuration allows to modulate the luminous intensity of each color and reproduce a broad array of additive mixed colors.

In both servo actuator types, the common anode light-emitting diode (*LED*) ASMT-QTB0 produced by Avago Technologies is applied. The red diode has a typical forward voltage of 2.1 volts and produces a luminous intensity of 620 millicandelas with an operating current of 20 milliamperes. The green and blue diodes have a typical forward voltage of 3.2 volts where the luminous intensity with an operating current of 20 milliamperes reaches 1200 millicandelas for the green diode and 280 millicandelas for the blue diode. The signal light is housed in a plastic leaded chip carrier (*PLCC-4*) package with four leads and a size of 2.8 by 3.2 millimeters. The allowed operating temperature ranges from −40 degrees Celsius to +110 degrees Celsius [11].

The signal of the diode mounted on the circuit board is guided through a transparent plastic conductor to an opening in the actuator enclosure. The three cathode terminals for the individual colors are connected to three PWM channels of the microcontroller, while the common anode terminal is powered by the operating voltage of 3.3 volts. A series resistor for each channel limits the operating current to a maximum value of 20 milliamperes. The resistance value of the series resistor is 56 ohms for the red diode and 4.7 ohms for the green and blue diodes. In this configuration, the luminous intensity is a function of the inverse duty cycle of the PWM interface.

Due to the nonlinear characteristic of the human eyes, a correction of the duty cycle progression is required in order to assure a linear gradient of the signal light. The relation between the magnitude of luminance l_s and the appertaining dimensionless perceived intensity ψ_e is described by Steven's power law defined by

$$\psi_e(t) = l_s^{c_p}(t) \; \frac{m^2}{cd} \tag{4.41}$$

where c_p is the correction factor that depends on the source of light [47]. This relation can be applied for mapping the duty cycle of the PWM interface that is related to the luminance of the signal light to a corrected duty cycle sequence. The correction factor of the applied diode combined with the transparent plastic conductor can be approximated by 0.5. The timer of the PWM interface provides a resolution of 16 bits at a frequency of 1.1 kilohertz. The linear gradient of the signal light is specified to have a reduced resolution of 8 bits. With the floor function $\lfloor \cdot \rfloor$ that returns the largest integer not greater than the argument, the corrected duty cycle progression N_p is given by

$$N_p(n) = \left\lfloor (2^{16} - 1) \cdot \left(\frac{n}{2^8 - 1} \right)^{\frac{1}{0.5}} \right\rfloor \quad \forall \, n \in \{0, \ldots, (2^8 - 1)\}. \tag{4.42}$$

To decrease the computational effort during operation, the sequence of corrected duty cycles is precalculated and stored as a persistent lookup table in the non-volatile memory area. The reduced resolution of 8 bits per primary color results in a theoretical color depth of 24 bits.

5 Control Design

The upcoming chapter presents the control design of the enhanced servo actuators for angular position and speed control. With regard to the defined requirements, a novel model predictive control approach is proposed and compared to a competitive loop-shaping control approach.

5.1 Design Considerations

The identification and analysis of the control concept applied in the original RX-28 and RX-64 servo actuators in Section 3.4 pointed out the limitations of the implemented angular position and speed control. The performance of the angular position feedback control is affected by a limited operating range and a nonlinear variation in control accuracy. At a variable supply voltage, the control rate is restricted by a limited utilization of the input signal range. The adjustability of the actuator trajectory is reduced to the definition of the desired angular speed and does not support further control of the angular motion. Due to the principle of operation, the angular speed feedforward control depends on the supply voltage and is not able to compensate control errors caused by an external load torque or parameter deviations.

The control concept of the enhanced DD-28 and DD-64 servo actuators needs to provide a universal feedback control of angular position and speed. The requirements for the control action comprise high steady-state accuracy and repeatability in combination with high actuator performance. The control rate is to be maximized without overshooting the desired value of the control variable or exceeding mechanical or electronic limits. For adapting the angular motion to the demands of the application, the trajectory of the actuator needs to be adjustable in angular speed and acceleration with avoiding impulsive discontinuities. The capture of unmeasured operating data and the variable input signal saturation resulting from the bounded power supply with changing supply voltages have to be considered in the control design process. The implementation of the control system on the digital processing unit of the electronic setup necessitate the application of digital control. To ensure a continuous operation of the servo actuators, the performance requirements and implementation costs of the control concept are to be aligned to the performance abilities of the system.

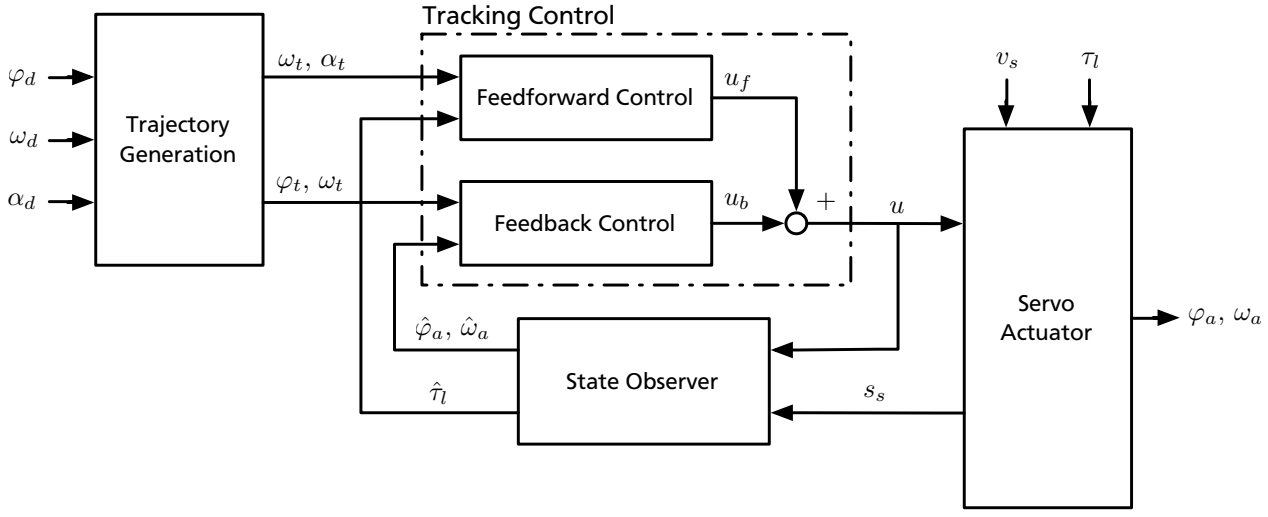

Figure 5.1.: Structure of the combined feedforward and feedback tracking control.

For meeting these design requirements, the control system of both servo actuator types consists of an angular position control for positioning in segmental or multiple turn operation and an angular speed control for driving in endless turn operation. Both control systems provide a combined digital feedforward and feedback tracking control with a highly adjustable desired trajectory. The preceding feedforward control presets the control signal depending on the desired trajectory and estimated disturbances, while the succeeding feedback control eliminates uncompensated errors of the control variable. Adjusting the desired trajectory allows to customize the actuator motion and reduce the mechanical load by controlling the acceleration and deceleration characteristics of the servo actuator. This configuration ensures a high performance of the controlled system with guaranteed offset-free tracking. Based on the measured actuator values, a model-based state observer estimates unmeasured actuator values and provides the actual actuator state. This actuator state contains essential operating data including the actual control variable. Figure 5.1 shows a functional diagram of the control concept of the enhanced DD-28 and DD-64 servo actuators.

The separation of the control concept into an invariable tracking control and an adjustable desired trajectory results in meaningful adjustment parameters and a flexible control system. The generation of the desired trajectory is independent from the tracking control and can be modified at any time without affecting the control action. This characteristic allows to specify arbitrary actuator paths within the mechanical or electronic limits by defining the complying desired trajectories.

The servo actuators are considered as linear time-invariant systems with a time-variant input constraint caused by the variable input signal saturation. In order to investigate different angular position and speed control strategies for this type of controlled system, two separate control approaches are applied and validated in the design process of the feedback control. The first approach introduces a novel model predictive control for arbitrary trajectory tracking that optimizes a quadratic performance index over the desired trajectory with respecting input and state constraints. The second approach implements a competitive loop-shaping control with an attuned transfer characteristic and a conditional anti-windup scheme for considering input signal saturation. Both control systems are simulated using an extensive nonlinear model of the controlled system and evaluated by the characteristics of the control action in respect to the defined requirements. A concluding evaluation summarizes the simulation results with identifying the assets and deficiencies of the different control approaches. A detailed description and derivation of the process models used in the control design process can be found in Appendix C.

5.2 Trajectory Generation

The application of a tracking control in the servo actuator allows to follow any desired control variable progression over time within the mechanical or electronic limits. The trajectory generation computes a sequence of desired values that reproduces the desired progression. To enable a universal actuator motion, the applied trajectory generation is based on point to point motion. This type of motion is characterized by moving the actuator from an arbitrary initial state to a desired final state. The desired trajectory is representable by a polynomial function corresponding to the control variable progression over time between the initial value and the desired final value. By defining constraints for the polynomial function and its time derivatives, the desired trajectory can be adjusted to customize the actuator motion. More complex actuator motions can be generated by applying a time-shifted sequence of desired trajectories resulting in an actuator path through specified transition points [46].

The control system of both servo actuator types provides an angular position control and an angular speed control that are used in two different operating modes. The trajectory generation needs to support the computation of desired trajectories for each mode of operation. In positioning mode, the actuator has to move with a desired angular speed to a desired angular position. The driving mode requires the actuator to hold a desired angular speed. For permitting further customization of the actuator motion,

the acceleration and deceleration characteristics in both operating modes need to be adjustable by complying with a desired angular acceleration limit. The actuator motion has to be continuous and without any angular jerk impulses to avoid vibrational modes in the actuator and ensure tracking control accuracy. The angular speed ω_t, acceleration α_t and jerk ι_t correspond to the time derivatives of the angular position φ_t of the desired trajectory

$$\omega_t(t) = \dot{\varphi}_t(t), \tag{5.1}$$

$$\alpha_t(t) = \ddot{\varphi}_t(t) = \dot{\omega}_t(t), \tag{5.2}$$

$$\iota_t(t) = \dddot{\varphi}_t(t) = \ddot{\omega}_t(t) = \dot{\alpha}_t(t). \tag{5.3}$$

All equations of the trajectory generation are given in continuous-time formulation. For the application in the discrete-time control system, the progression of the desired trajectory needs to be computed at the sampling instants of the applied feedback control.

5.2.1 Position Trajectory

The desired trajectory in angular position control has to move the actuator with a desired angular speed to a desired angular position. The constraints for the desired trajectory comprise the initial and final value of the angular position as well as additional demands in the angular speed, acceleration and jerk. In order to combine a continuous actuator motion with a constant angular speed, the polynomial function of the desired trajectory is divided into three segments. In the first segment, the actuator is accelerated from the initial state to the desired angular speed; the angular speed is held within the second segment; in the third segment, the actuator is decelerated from the desired angular speed to the idle state. The adjacent segments are merged at the blend times $t_{b,1}$ and $t_{b,2}$. Figure 5.2 illustrates the segmentation of the desired trajectory.

The constraints for the segmented trajectory at the initial time t_0, final time t_f and blend times $t_{b,1}$ and $t_{b,2}$ are specified by the desired values of the angular position φ_d, the angular speed ω_d and the angular acceleration limit α_d as well as the initial values of the angular position φ_0 and the angular speed ω_0. For the first segment, the constraints ensure conformance of the initial values and set the angular acceleration and angular jerk at the initial time and blend time to zero. The maximum angular acceleration at the half term of the segment is equated to the desired angular acceleration limit. With these specifications, the constraints for the first segment are given by

$$\varphi_{t,p,1}(t_0) = \varphi_0, \qquad \omega_{t,p,1}(t_0) = \omega_0, \qquad \omega_{t,p,1}(t_{b,1}) = \omega_d,$$

$$\alpha_{t,p,1}(t_0) = 0, \qquad \alpha_{t,p,1}\left(\tfrac{t_{b,1}}{2}\right) = \alpha_d, \qquad \alpha_{t,p,1}(t_{b,1}) = 0,$$

$$\iota_{t,p,1}(t_0) = 0, \qquad \iota_{t,p,1}(t_{b,1}) = 0.$$

The second segment provides a constant angular speed equaling the desired value and needs to comply with the blend conditions of the angular position. The constraints for the second segment are covered by

$$\varphi_{t,p,1}(t_{b,1}) = \varphi_{t,p,2}(t_{b,1}), \qquad \varphi_{t,p,2}(t_f - t_{b,2}) = \varphi_{t,p,3}(t_f - t_{b,2}), \qquad \omega_{t,p,2}(t) = \omega_d.$$

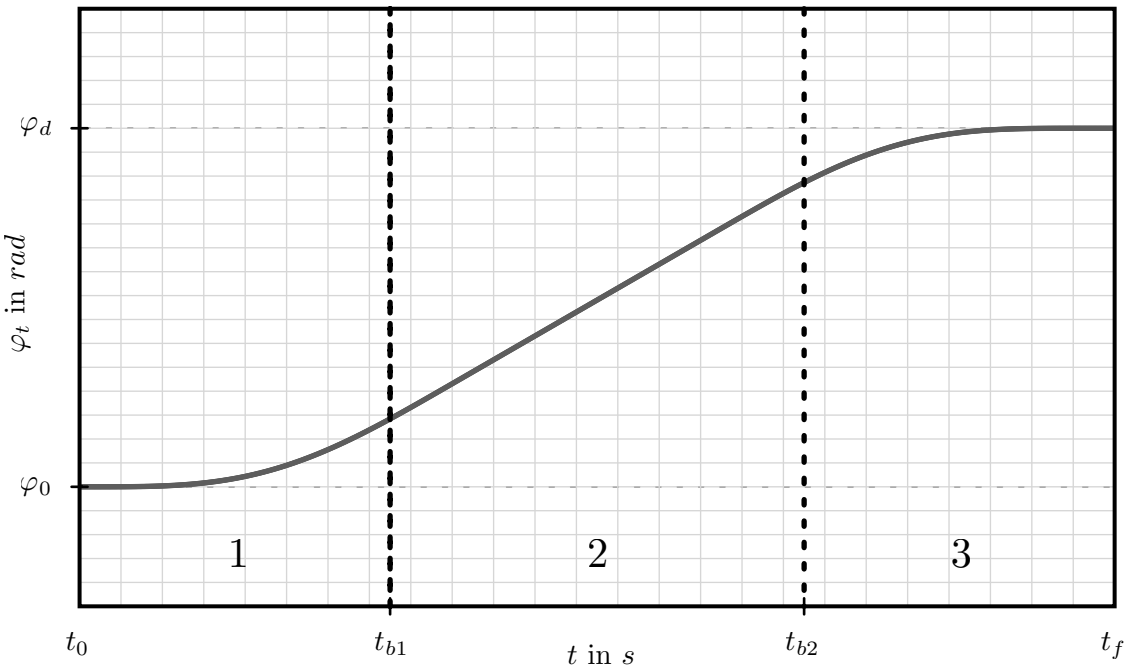

Figure 5.2.: Segmentation of the desired trajectory.

The requirements for the third segment correspond to the specified conditions of the first segment with substituting the final for the initial values. The constraints for the third segment result in

$$\varphi_{t,p,3}(t_f) = \varphi_d, \qquad \omega_{t,p,3}(t_f - t_{b,2}) = \omega_d, \qquad \omega_{t,p,3}(t_f) = 0,$$

$$\alpha_{t,p,3}(t_f - t_{b,2}) = 0, \qquad \alpha_{t,p,3}\left(t_f - \tfrac{t_{b,2}}{2}\right) = \alpha_d, \qquad \alpha_{t,p,3}(t_f) = 0,$$

$$\iota_{t,p,3}(t_f - t_{b,2}) = 0, \qquad \iota_{t,p,3}(t_f) = 0.$$

Respecting the desired actuator motion and the number of conditions, the polynomial functions of the first and third segment have a degree of six, while the polynomial function of the second segment is linear with a degree of one. The remaining constraints are used to set the final time and blending times. The desired trajectory φ_t is piecewise composed of the polynomial functions and the initial and desired final angular position

$$\varphi_{t,p}(t) = \begin{cases} \varphi_0 & \text{for } t < t_0, \\ \varphi_{t,p,1}(t) & \text{for } t_0 \leq t < t_{b,1}, \\ \varphi_{t,p,2}(t) & \text{for } t_{b,1} \leq t \leq t_{b,2}, \\ \varphi_{t,p,3}(t) & \text{for } t_{b,2} < t \leq t_f, \\ \varphi_d & \text{for } t > t_f. \end{cases} \tag{5.4}$$

The parameters of the polynomial functions of each segment can be determined by applying the defined constraints to the polynomial function and the time derivatives. With setting the initial time t_0 to zero, the polynomial functions are given by

$$\varphi_{t,p,1}(t) = \frac{\omega_d - \omega_0}{t_{b,1}^5}\, t^6 - 3\,\frac{\omega_d - \omega_0}{t_{b,1}^4}\, t^5 + \frac{5}{2}\,\frac{\omega_d - \omega_0}{t_{b,1}^3}\, t^4 + \omega_0\, t + \varphi_0, \tag{5.5}$$

$$\varphi_{t,p,2}(t) = \omega_d \; t - \frac{t_{b,1}}{2} \left(\omega_d - \omega_0\right) + \varphi_0, \tag{5.6}$$

$$\varphi_{t,p,3}(t) = \frac{\omega_d}{t_{b,2}^5} \left(t_f - t\right)^6 + 3 \, \frac{\omega_d}{t_{b,2}^4} \left(t_f - t\right)^5 + \frac{5}{2} \, \frac{\omega_d}{t_{b,2}^3} \left(t_f - t\right)^4 + \varphi_d. \tag{5.7}$$

The blend times $t_{b,1}$ and $t_{b,2}$ depend on the desired angular speed ω_d and angular acceleration limit a_d and result in

$$t_{b,1} = \frac{15}{8} \, \frac{|\omega_d - \omega_0|}{a_d}, \tag{5.8}$$

$$t_{b,2} = \frac{15}{8} \, \frac{|\omega_d|}{a_d}. \tag{5.9}$$

The desired trajectory reaches the desired angular position φ_d at the final time t_f that is computed from the blend times $t_{b,1}$ and $t_{b,2}$ and the moving duration in the second segment

$$t_f = \frac{t_{b,1} + t_{b,2}}{2} + \frac{\varphi_d - \varphi_0 - \frac{t_{b,1} \, \omega_0}{2}}{\omega_d}. \tag{5.10}$$

The progression of the defined trajectory ensures a continuous actuator motion for a constant desired angular position. If the desired value is changed during the acceleration or deceleration process and the desired trajectory is recomputed, the progression of the angular acceleration has a discontinuity generating a jerk impulse. This characteristic needs to be considered when driving the servo actuator.

An exceptional case occurs, if the desired angular speed can not be reached with the desired angular acceleration limit before the desired trajectory arrives at the desired angular position. This situational condition results from a small desired angular acceleration limit paired with a small difference between the initial and the desired angular position. Consequently, the computed final time t_f is smaller than the sum of the blend times $t_{b,1}$ and $t_{b,2}$

$$t_f < t_{b,1} + t_{b,2}. \tag{5.11}$$

and the desired trajectory becomes discontinuous. To avoid this interference of the actuator motion, a different desired trajectory that neglects the desired angular acceleration limit is applied in occurrence of the exceptional case. Because of the small position difference, the actuator is not able to hold the desired angular speed and has to move with a variable angular acceleration. The exceptional trajectory $\varphi_{t,e}$ is represented by a single polynomial function with a degree of five and has to comply with the constraints specified by

$$\varphi_{t,e}(t_0) = \varphi_0, \qquad \varphi_{t,e}(t_f) = \varphi_d, \qquad \omega_{t,e}(t_0) = \omega_0,$$

$$\omega_{t,e}(t_f) = 0, \qquad \alpha_{t,e}(t_0) = 0, \qquad \alpha_{t,e}(t_f) = 0.$$

By inserting the defined constraints into the polynomial function and the time derivatives and setting the initial time t_0 to zero, the exceptional trajectory results in

$$\begin{aligned} \varphi_{t,e}(t) = {} & \frac{6 \left(\varphi_d - \varphi_0\right) - 3 \; t_f \; \omega_0}{t_f^5} \; t^5 - \frac{15 \left(\varphi_d - \varphi_0\right) - 8 \; t_f \; \omega_0}{t_f^4} \; t^4 \\ & + \frac{10 \left(\varphi_d - \varphi_0\right) - 6 \; t_f \; \omega_0}{t_f^3} \; t^3 + \omega_0 \; t + \varphi_0. \end{aligned} \tag{5.12}$$

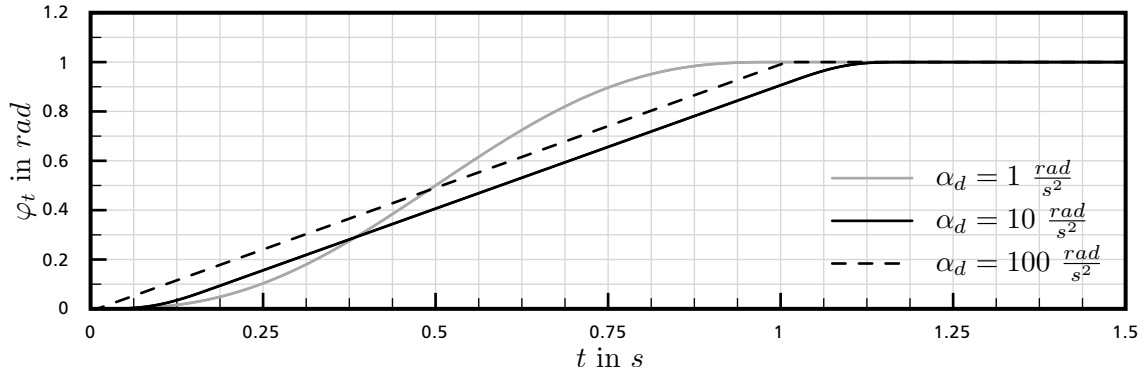

(a) Progression of the angular position with $\varphi_0 = 0\ rad$, $\varphi_d = 1\ rad$, $\omega_0 = 0\ \frac{rad}{s}$ and $\omega_d = 1\ \frac{rad}{s}$.

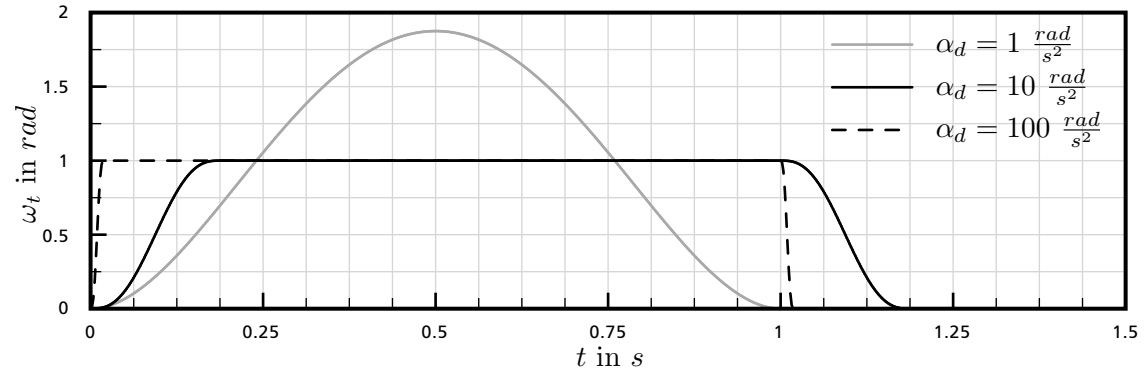

(b) Progression of the angular speed with $\varphi_0 = 0\ rad$, $\varphi_d = 1\ rad$, $\omega_0 = 0\ \frac{rad}{s}$ and $\omega_d = 1\ \frac{rad}{s}$.

Figure 5.3.: Angular position trajectories with different desired angular acceleration limits.

The desired angular position φ_d is reached at the final time t_f that is specified by the position difference and the desired angular speed ω_d

$$t_f = \frac{|\varphi_d - \varphi_0|}{\omega_d}. \tag{5.13}$$

The final time equals to the moving duration of the actuator. Caused by the additional time needed for acceleration and deceleration, the actual angular speed of the desired trajectory exceeds the desired value. The exceptional trajectory can be avoided by setting the desired angular acceleration limit to a reasonable value regarding the desired angular speed and the position difference.

The introduced trajectory generation of the angular position control ensures a continuous actuator motion with avoiding impulsive discontinuities. Besides the desired angular position, the absolute values of the desired angular speed and angular acceleration limit can be adjusted within the mechanical or electronic limits of the servo actuator. Figure 5.3 shows three exemplary trajectories with different desired angular acceleration limits. The exceptional case occurs for the desired angular acceleration limit of 1 radian per square seconds.

5.2.2 Speed Trajectory

The desired trajectory in angular speed control has to accelerate the actuator to the desired angular speed that is held until the desired value changes. The constraints for the desired trajectory are specified by the desired values of the angular speed ω_d and the angular acceleration limit α_d as well as the

initial value of the angular speed ω_0. At the initial time t_0 and the final time t_f, the constraints ensure conformance with the initial and desired values and set the angular acceleration and angular jerk to zero. The maximum angular acceleration at the half term of the desired trajectory is equated to the desired angular acceleration limit. With these definitions, the constraints for the desired trajectory $\omega_{t,s}$ are given by

$$\omega_{t,s}(t_0) = \omega_0, \qquad \omega_{t,s}(t_f) = \omega_d, \qquad \alpha_{t,s}(t_0) = 0,$$

$$\alpha_{t,s}\left(\frac{t_f}{2}\right) = \alpha_d, \qquad \alpha_{t,s}(t_f) = 0, \qquad \iota_{t,s}(t_0) = 0,$$

$$\iota_{t,s}(t_f) = 0.$$

In order to respect the desired actuator motion and the number of conditions, the polynomial function has a degree of five where the parameters can be determined by applying the defined constraints. The remaining constraint is used to set the final time. With setting the initial time t_0 to zero, the desired trajectory results in

$$\omega_{t,s}(t) = 6\,\frac{\omega_d - \omega_0}{t_f^5}\,t^5 - 15\,\frac{\omega_d - \omega_0}{t_f^4}\,t^4 + 10\,\frac{\omega_d - \omega_0}{t_f^3}\,t^3 + \omega_0 \tag{5.14}$$

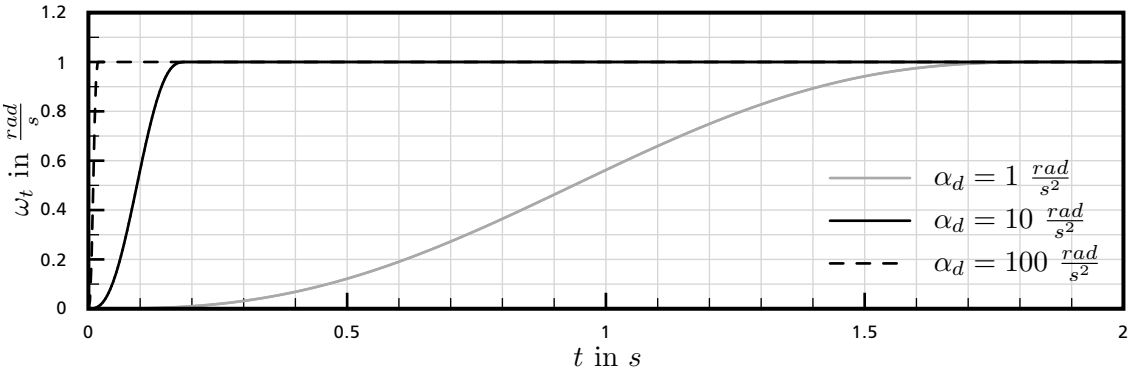

(a) Angular speed progressions with $\omega_0 = 0\ \frac{rad}{s}$ and $\omega_d = 1\ \frac{rad}{s}$.

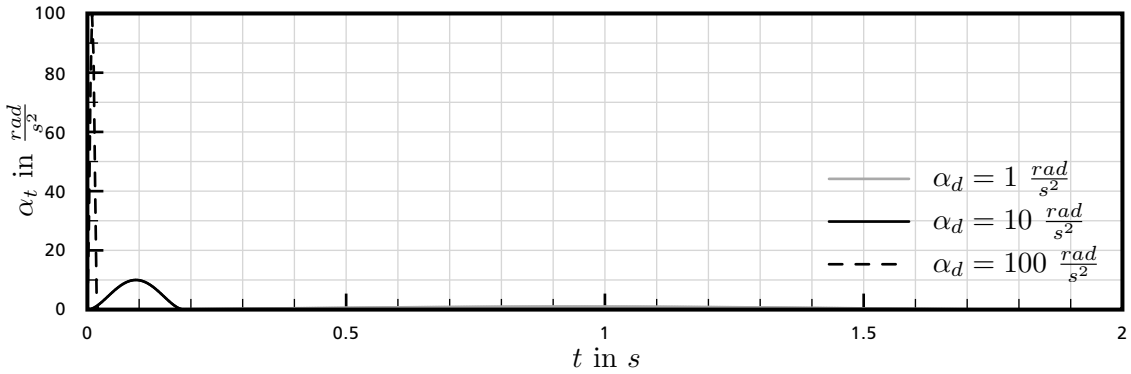

(b) Angular acceleration progressions with $\omega_0 = 0\ \frac{rad}{s}$ and $\omega_d = 1\ \frac{rad}{s}$.

Figure 5.4.: Angular speed trajectories with different desired angular acceleration limits.

The desired trajectory reaches the desired angular speed ω_d at the final time t_f that is specified by the speed difference and the desired angular acceleration limit α_d

$$t_f = \frac{15}{8} \frac{|\omega_d - \omega_0|}{a_d} \tag{5.15}$$

The introduced trajectory generation of the angular speed control assures a continuous angular acceleration characteristic for a desired angular speed within the mechanical or electronic limits of the servo actuator. Changing the desired value during the acceleration process results in a discontinuity of the angular acceleration and generates a jerk impulse. This characteristic has to be regarded when driving the servo actuator. Figure 5.4 presents three exemplary trajectories with different desired angular acceleration limits.

5.3 State Observer Design

The sensor elements measure actual values of the angular position, supply voltage and servo actuator temperatures. Additionally, the actual angular speed, load torque and armature current are required for the application of the control concept or the verification of safety limits. These unmeasured actuator values have to be estimated from the measurands and known system parameters. The estimation is affected by undefined disturbances and interferences of the sensor elements and system parameters that cause stochastic noise signals.

The control concept uses a model-based state observer for ensuring an accurate determination of the actuator state. Due to the significant noise signals, the state observer of both servo actuator types is implemented as a digital Kalman filter that provides a precise estimation of the actuator values with reducing the influence of process and measurement noise. The Kalman filter applies an output injection to make the residual error between the actual and estimated actuator state converge to zero. The discrete-time estimation procedure is divided into a prediction phase and an update phase. The actuator values are initially predicted by deploying a model of the observed system and the actual value of the control variable. The difference between the predicted output values and the actual measurements is subsequently used to update the predicted values resulting in an advanced estimate of the actuator state. In this phase, the computed difference is weighted with the Kalman gain that depends on the covariances of the process and measurement noise. A dynamic Kalman filter updates the Kalman gain in each iteration of the estimation procedure and is able to adapt to changing noise characteristics. Under conditions where the noise covariances are in fact stationary, the Kalman gain will quickly stabilize and remain constant. This simplification is utilized in a stationary Kalman filter that applies a precomputed constant Kalman gain and possesses a reduced computational complexity. In order to decrease the performance requirements and implementation costs, the state observer is realized as a stationary Kalman filter [18, 57]. Figure 5.5 presents a functional diagram of the state observer.

The design of the state observer is based on a linear, time-invariant, discrete-time and observable state space model of the servo actuators. The state vector $\boldsymbol{x}_o$ includes the angular position φ_a, angular speed ω_a and load torque τ_l of the servo actuator. To regard stochastic noise signals, the model is extended by a generalized process noise $\boldsymbol{a}_n$ and measurement noise b_n. Compared to speed changes in the mechanical subsystem of the servo motor, transitions of the armature current i_m resulting from a changing armature voltage v_m are presumed to be instantaneous. Based on this assumption, the influence of the armature inductance L_m is supposed to be insignificant and the armature current i_m of the servo motor is not contained in the specified model. In order to ensure a correct estimation of the state vector, the nonlinear saturation of the input signal is considered in the input variable. A detailed derivation of the process

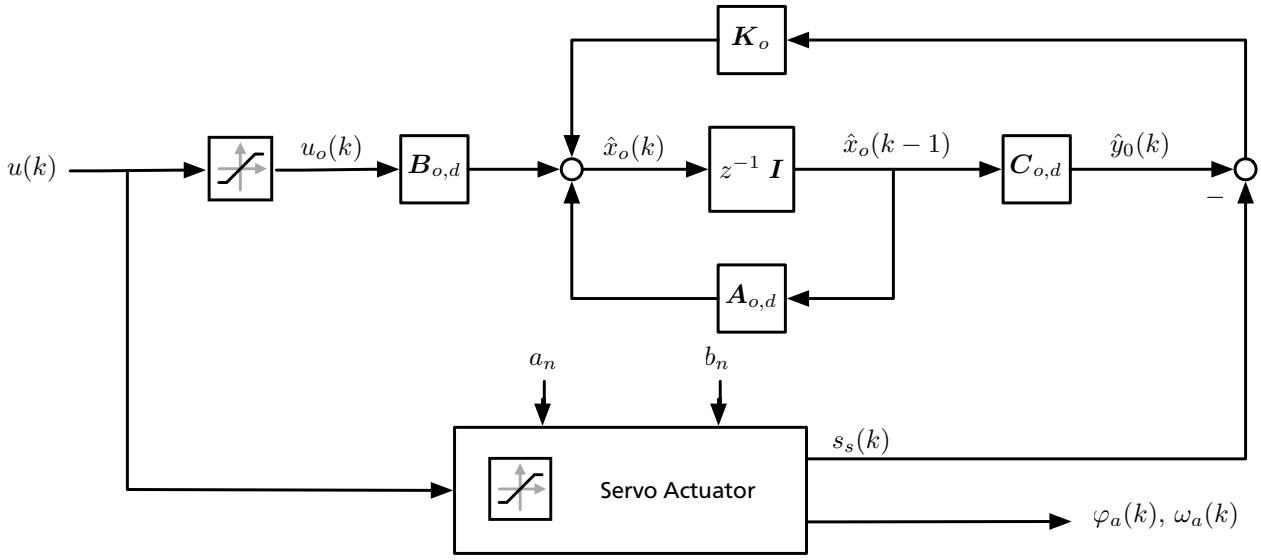

Figure 5.5.: Structure of the state observer.

model and the proof of observability can be found in Appendix C. With the input variable u_o, the state vector $\boldsymbol{x}_o$ and the output variable y_o specified by

$$u_o(k) = \text{sat}[v_m(k)], \tag{5.16a}$$

$$\boldsymbol{x}_o(k) = \begin{bmatrix} \varphi_a(k) & \omega_a(k) & \tau_l \end{bmatrix}^T, \tag{5.16b}$$

$$y_o(k) = \frac{1}{r_s}\,\varphi_a(k), \tag{5.16c}$$

the state space model is given by

$$\boldsymbol{x}_o(k) = \boldsymbol{A}_{o,d}\,\boldsymbol{x}_o(k-1) + \boldsymbol{B}_{o,d}\,u_o(k) + \boldsymbol{a}_n(k-1), \tag{5.17a}$$

$$y_o(k) = \boldsymbol{C}_{o,d}\,\boldsymbol{x}_o(k-1) + b_n(k). \tag{5.17b}$$

The process noise $\boldsymbol{a}_n$ includes system parameter uncertainties and disturbances, while the measurement noise b_n contains uncertainties, disturbances and quantization noise of the position sensor. Both noise signals are assumed to be independent, zero-mean, white and normal distributed with the constant, symmetric covariances $\boldsymbol{Q}_n$ and R_n where

$$P\{\boldsymbol{a}_n(t)\} \sim \mathcal{N}(0, \boldsymbol{Q}_n), \tag{5.18}$$

$$P\{b_n(t)\} \sim \mathcal{N}(0, R_n). \tag{5.19}$$

The estimation equations of the Kalman filter perform the described prediction-update procedure to estimate the actual values of the angular position, angular speed and load torque. In the initial prediction phase, the model of the observed system and the saturated actual control signal $u_o(k)$ project the predicted state vector ${}^+\hat{\boldsymbol{x}}_o$. In the subsequent update phase, the estimated state vector $\hat{\boldsymbol{x}}_o$ is computed from

a linear combination of the predicted state vector ${}^{+}\hat{\boldsymbol{x}}_o$ and the weighted difference between the actual measurement value of the position sensor s_s and the estimated output value $\hat{y}_o$ read as

$${}^{+}\hat{\boldsymbol{x}}_o(k) = \boldsymbol{A}_{o,d}\,\hat{\boldsymbol{x}}_o(k-1) + \boldsymbol{B}_{o,d}\,u_o(k), \qquad \textit{prediction phase} \tag{5.20}$$

$$\hat{\boldsymbol{x}}_o(k) = {}^{+}\hat{\boldsymbol{x}}_o(k) + \boldsymbol{K}_o\left(s_s(k) - \hat{y}_o(k)\right) \qquad \textit{update phase} \tag{5.21}$$

where

$$\hat{\boldsymbol{x}}_o(k) = \begin{bmatrix} \hat{\varphi}_a(k) & \hat{\omega}_a(k) & \hat{\tau}_l \end{bmatrix}^T, \tag{5.22}$$

$$\hat{y}_o(k) = \frac{1}{r_s}\,\hat{\varphi}_a(k). \tag{5.23}$$

The Kalman gain $\boldsymbol{K}_o$ is chosen to minimize the influence of the process noise $\boldsymbol{a}_n$ and measurement noise b_n on the estimated state vector $\hat{\boldsymbol{x}}_o$. The corresponding minimization problem is defined by the trace of the estimate error covariance $\boldsymbol{P}_e$ resulting from the expectation value of the estimation error [28, 57]. The quadratic cost objective J is given by

$$J = \operatorname{tr}\left\{\boldsymbol{P}_e\right\} = \operatorname{tr}\left\{E\{(\boldsymbol{x}_o - \hat{\boldsymbol{x}}_o)\,(\boldsymbol{x}_o - \hat{\boldsymbol{x}}_o)^T\}\right\} \tag{5.24}$$

For solving this minimization problem dependent on the Kalman gain $\boldsymbol{K}_o$, the discrete-time Riccati equation with the noise covariances $\boldsymbol{Q}_n$ and R_n is applied to calculate the symmetric, positive definite estimate error covariance $\boldsymbol{P}_e$

$$\boldsymbol{A}_{o,d}\,\boldsymbol{P}_e\,\boldsymbol{A}_{o,d}^T - \boldsymbol{P}_e - \boldsymbol{A}_{o,d}\,\boldsymbol{P}_e\,\boldsymbol{C}_{o,d}^T\,(\boldsymbol{C}_{o,d}\,\boldsymbol{P}_e\,\boldsymbol{C}_{o,d}^T + R_n)^{-1}\,\boldsymbol{C}_{o,d}\,\boldsymbol{P}_e\,\boldsymbol{A}_{o,d}^T = -\boldsymbol{Q}_n. \tag{5.25}$$

With the measurement noise covariance R_n and the obtained estimate error covariance $\boldsymbol{P}_e$, the Kalman gain $\boldsymbol{K}_o$ can be determined from

$$\boldsymbol{K}_o = (\boldsymbol{C}_{o,d}\,\boldsymbol{P}_e\,\boldsymbol{C}_{o,d}^T + R_n)^{-1}\,\boldsymbol{C}_{o,d}\,\boldsymbol{P}_e\,\boldsymbol{A}_{o,d}^T. \tag{5.26}$$

The presented Kalman filter is able to estimate the actual angular position, angular speed and load torque of the servo actuator. The armature current i_m of the servo motor can be approximated with the known armature voltage v_m and the estimated angular speed of the servo actuator $\hat{\omega}_a$ by using

$$i_m(k) = \frac{v_m(k) - \frac{r_g}{k_\omega}\,\hat{\omega}_a(k)}{R_m}. \tag{5.27}$$

The introduced state observer based on a stationary Kalman filter provides an accurate estimate of the essential actuator values. The choice of the Kalman gain and the presented structure of the Kalman filter ensure a decreasing estimate error and a minimized influence of stochastic noise signals. The estimated actuator values and the measurement values of the sensor elements yield all relevant operating data of the servo actuator. This set of actual actuator values enables the introduction and monitoring of comprehensive safety limits to prevent the exceeding of electrical or mechanical limits and increase the durability of the servo actuator. The computational effort of the estimation equations is low and allows to iterate the estimation procedure with a small sampling time giving an ample scope for the control design and further development. The state observers of both servo actuator types operate with a sampling time

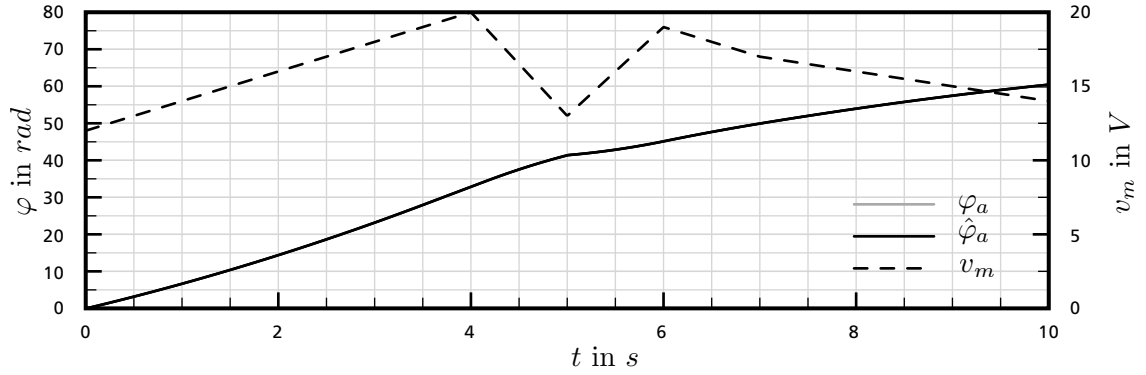

(a) Progressions of the actual and estimated angular position.

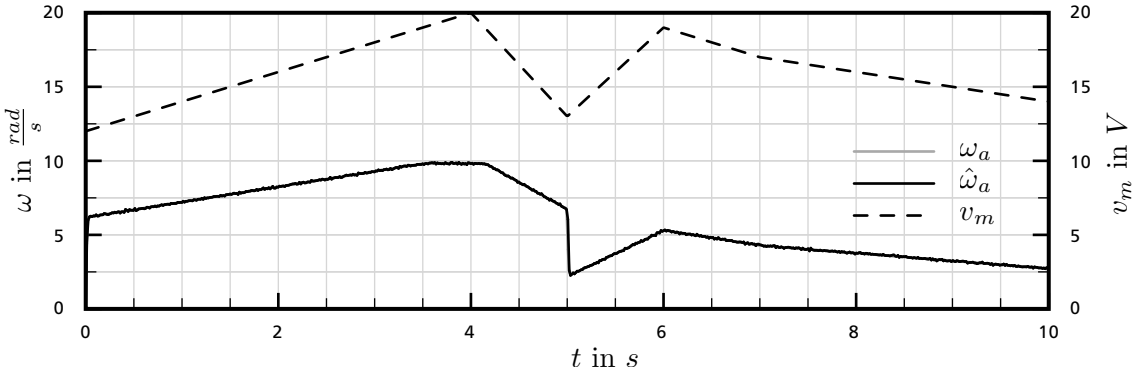

(b) Progressions of the actual and estimated angular speed.

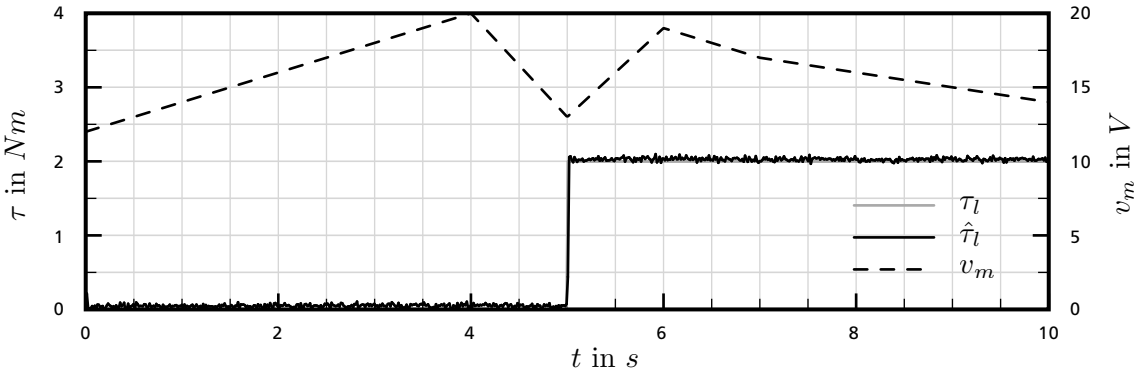

(c) Progressions of the actual and estimated load torque.

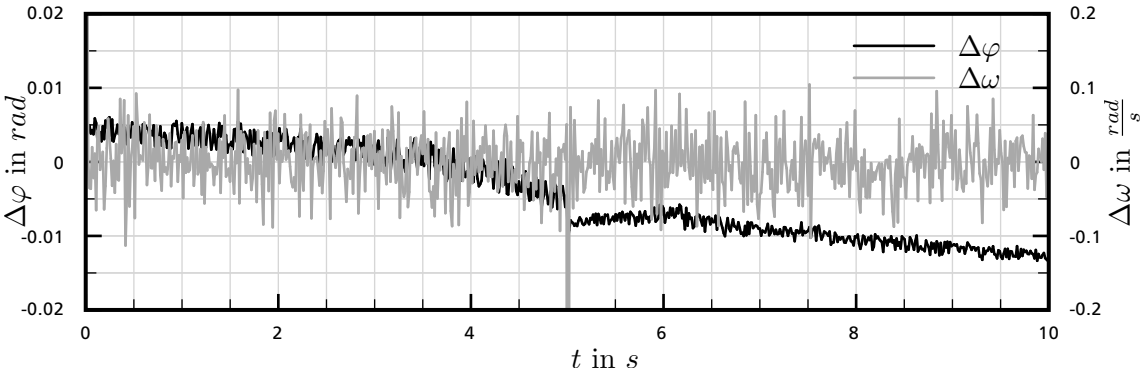

(d) Absolute estimation error of the angular position and angular speed.

Figure 5.6.: Performance of the state observer of the DD-28 servo actuator.

of 0.5 milliseconds and are designed with emphasis on high estimation accuracy. All applied design parameters and the resulting Kalman gains are listed in Appendix E.

In order to evaluate the performance and estimation accuracy, the state observer of the DD-28 servo actuator is simulated with an extensive nonlinear model. Figure 5.6 presents the progressions of the estimated actuator values and the absolute estimation errors of the angular position and angular speed. The armature voltage has a variable progression with a minimum value of 12 volts and a maximum value of 20 volts. After 5 seconds a load torque of 2 newton meters is applied on the simulated servo actuator. The simulation demonstrates the high performance of the state observer. All estimated actuator values reproduce the actual values at low and and high rates of change. Steps in the armature voltage result in a short overshoot of the estimated angular speed and load torque that are compensated quickly. The relative estimation error of the estimated angular position is negligible, while the estimated angular speed is interfered by a minor residual noise signal. The overall performance of the state observer ensures a sufficient accuracy of the estimated actual actuator values and forms a solid basis for the development of the angular position and speed control.

5.4 Feedforward Control Design

The control concepts of angular position and speed control consist of a combined digital feedforward and feedback tracking control. This configuration provides a compound control signal that consists of the partial control signals of each control type. The partial control signal of the preceding feedforward control is computed by applying desired motion values derived from the desired trajectory and known disturbances on an inverse model of the controlled system. This procedure results in a pilot control for the desired motion values and a disturbance compensation for the known disturbances. The succeeding feedback control generates a superimposed control signal to eliminate uncompensated control errors. By utilizing the advantages of both control types, the feedforward controller provides an increased control rate and relieves the feedback controller that assures offset-free tracking [27].

The feedforward controller of both servo actuator types implements a pilot control for the desired values of the angular speed ω_d and angular acceleration α_d as well as a compensation of the actual load torque τ_l. The desired angular speed and acceleration results from the time derivatives of the desired trajectory φ_t provided by the trajectory generation

$$\omega_d(t) = \dot{\varphi}_t(t), \tag{5.28}$$

$$\alpha_d(t) = \ddot{\varphi}_t(t) = \dot{\omega}_t(t). \tag{5.29}$$

The actual value of the load torque is determined by the state observer and given as the estimate load torque $\hat{\tau}_l$. The control signal corresponds to the armature voltage of the servo motor v_m. For establishing a linear inverse model of the controlled system, the linear differential equations of the mechanical and electronic subsystem of the servo actuator are applied

$$\dot{\omega}_a(t) = \frac{r_g\, k_\tau\, i_m(t) - \tau_f(t) - \tau_l(t)}{\Theta_a}, \tag{5.30}$$

$$\dot{i}_m(t) = \frac{v_m(t) - R_m\, i_m(t) - \frac{r_g}{k_\omega}\, \omega_a(t)}{L_m}. \tag{5.31}$$

A detailed derivation of both differential equations can be found in Appendix C. By canceling unwanted actuator values and solving the reduced equations for the armature voltage v_m, the inverse transfer functions $K_{f,\omega}$, $K_{f,\alpha}$ and $K_{f,\tau}$ are specified by

$$K_{f,\omega} = \frac{v_m(t)}{\omega_a(t)} = \frac{r_g}{k_\omega}, \tag{5.32a}$$

$$K_{f,\alpha} = \frac{v_m(t)}{\alpha_a(t)} = \frac{R_m\,\Theta_a}{k_\tau\,r_g}, \tag{5.32b}$$

$$K_{f,\tau} = \frac{v_m(t)}{\tau_l(t)} = \frac{R_m}{k_\tau\,r_g} \tag{5.32c}$$

where

$$\alpha_a(t) = \dot{\omega}_a(t). \tag{5.33}$$

The control law of the feedforward controller results from summing up the inverse transfer functions applied with the desired angular speed ω_d and angular acceleration α_d as well as the estimated load torque $\hat{\tau}_l$. The inverse transfer functions equate to the control gains of the control law. With this definition, the partial feedforward control signal u_f is given by

$$u_f(t) = K_{f,\omega}\,\omega_d(t) + K_{f,\alpha}\,\alpha_d(t) + K_{f,\tau}\,\hat{\tau}_l(t). \tag{5.34}$$

The introduced feedforward control is independent of the control variable type and can be used for the control of the angular position or angular speed. The control law does not regard the variable saturation of the input signal and conforms to the applied desired and estimated values at any time. The determined feedforward control gains of both servo actuator types are listed in Appendix E.

All equations of the feedforward control are given in continuous-time formulation. For the application in the discrete-time control system, the partial feedforward control signal has to be computed at the sampling instants of the applied feedback control.

5.5 Feedback Control Design

For the design of an appropriate feedback control, both servo actuator types are considered as linear time-invariant systems. The application of a combined digital feedforward and feedback tracking control as provided in the control concept distributes the tracking control problem among the different control types. While the preceding feedforward control provides a compensation of known disturbances and a pilot control for the desired motion sequence, the succeeding feedback control eliminates uncompensated control errors of the control variable to ensure offset-free tracking. The uncompensated control errors arise from unknown or incompletely compensated disturbances, initial deviations in the trajectory generation or saturation of the input signal. The rejection of disturbances and initial deviations in linear systems is a primary objective of feedback control and can be achieved by means of a linear control law. The input signal saturation results from the bounded supply voltage that can vary within the supported supply voltage range. Caused by this variable limitation of the control signal, the servo actuators have to be regarded as systems with a time-variant input constraint. Generally, this type of controlled system requires the application of a nonlinear control law in order to obtain a stable control action and

adequate performance. Two specific control approaches for designing a nonlinear controller for linear systems with input constraints are anti-windup control and model predictive control. In anti-windup control, a linear feedback controller that is designed for the unsaturated linear system is extended by an anti-windup scheme. This anti-windup scheme prevents internal controller states from exceeding acceptable limits and ensures stable operation in the case of input signal saturation. In model predictive control, the future progression of the control signal is optimized in respect to the desired trajectory of the control variable as well as input and state constraints by applying a process model. The optimization is achieved by continuously solving an open-loop optimal control problem over a finite prediction horizon. The optimized control signal is then used to actuate the controlled system [2, 13].

The difference in structure and methodological approach of anti-windup control and model predictive control results in particular stability characteristics and computational requirements. For investigating the performance and implementability of both control methods in the servo actuators, a novel model predictive control approach for arbitrary trajectory tracking is proposed and compared to a competitive loop-shaping control with an conditional anti-windup scheme. The control approaches are applied and evaluated in the design process of the angular position and speed control. In combination with the introduced state observer and feedforward control, the designed control systems are simulated using an extensive nonlinear model of the controlled system and validated by the characteristics of the control action in respect to the defined requirements.

5.5.1 Model Predictive Control

Model predictive control is an established and widely used digital control method in industrial applications. Especially in the chemical and process industries, this type of control is used for complex multivariable control problems. The control method provides a nonlinear control law and can be applied on linear and nonlinear controlled systems with considering existing input and state constraints [2, 13]. These capabilities result in powerful and universal control systems with a wide scope of application.

The fundamental principle of model predictive control is based on a finite open-loop optimal control problem. For the computation of the control signal, a continuous-time or discrete-time process model is used to predict the future progression of the control variable. Starting from the known actual state,

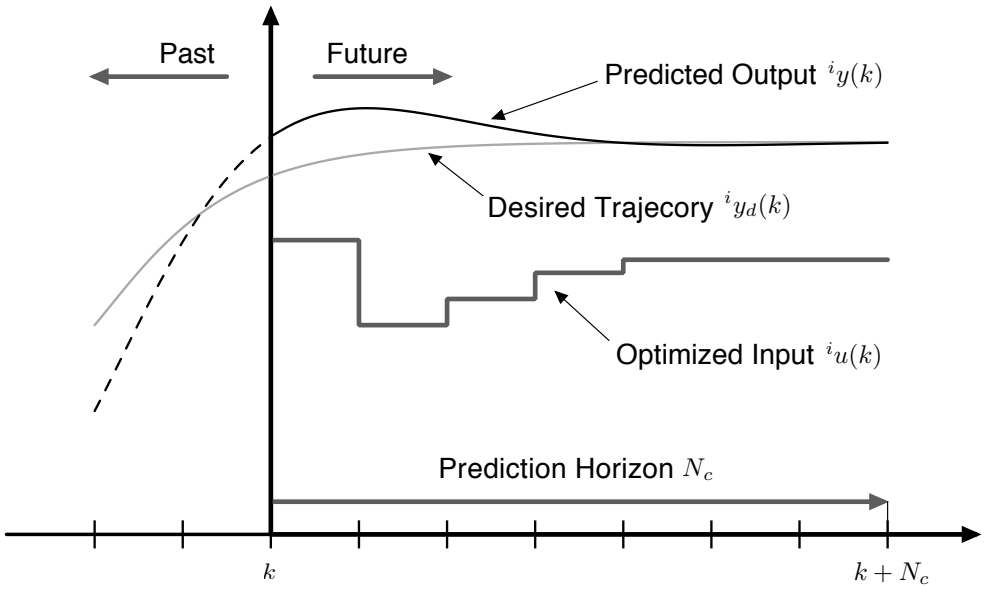

Figure 5.7.: Scheme of model predictive control [2].

the future control signal progression is optimized over a finite prediction horizon to match the predicted control variable progression to the desired trajectory. The optimization of the control signal sequence minimizes a linear or quadratic cost objective in regard to the desired values of the control variable as well as input and state constraints. At each sampling instant, the first element of the optimized control signal sequence is applied on the controlled system and the optimization is repeated for the new state over a shifted prediction horizon. This procedure leads to a moving horizon approach that respects all input and state constraints as well as interfering disturbances with optimizing a linear or quadratic performance index. The stability and performance of the control system depends on the size of the prediction horizon and the applied weighting factors of the cost objective. Figure 5.7 illustrates the described scheme of model predictive control [2, 13, 36].

The finite optimization problem implicitly defines the model predictive control law and corresponds to a linear or quadratic program. In controlled operation, the optimization problem has to be solved on-line at each sampling instant to determine the optimal control signal. The resulting significant on-line computational effort restricts the applicability of model predictive control in implicit form to slow processes or small control problems. In order to reduce the on-line computational requirements and provide a universal adaptability, the linear or quadratic program of the optimization problem can be transformed into a complying multi-parametric quadratic program. This transformation allows to compute the optimal solution off-line with preserving performance and stability characteristics of the control system. The precomputed solution explicitly defines the model predictive control law as a piecewise affine function of the state by partitioning the constrained state space into a set of polyhedral regions. The application of model predictive control in explicit form does not require any on-line optimization and limits the computational complexity to the evaluation of a piecewise affine function [13].

For considering standard model predictive control in a stabilization problem of a linear, time-invariant, discrete-time and controllable system, the state space model with the input vector $\boldsymbol{u}$ of the dimension m, the state vector $\boldsymbol{x}$ of the dimension n and the output vector $\boldsymbol{y}$ is given by

$$\boldsymbol{x}(k+1) = \boldsymbol{A}\,\boldsymbol{x}(k) + \boldsymbol{B}\,\boldsymbol{u}(k), \tag{5.35a}$$

$$\boldsymbol{y}(k) = \boldsymbol{C}\,\boldsymbol{x}(k) + \boldsymbol{D}\,\boldsymbol{u}(k). \tag{5.35b}$$

The actual state at time k is denoted by $\boldsymbol{x}(k)$, while ${}^{i}\boldsymbol{x}(k)$ indicates the predicted state, ${}^{i}\boldsymbol{y}(k)$ indicates the predicted output and ${}^{i}\boldsymbol{u}(k)$ indicates the optimized input at time $k+i$ given the state at time k. The state vector $\boldsymbol{x}$ and the input vector $\boldsymbol{u}$ are constrained by

$$\boldsymbol{x} \in \mathbb{X} \subset \mathbb{R}^n, \qquad\qquad \boldsymbol{u} \in \mathbb{U} \subset \mathbb{R}^m$$

where $\mathbb{X}$ and $\mathbb{U}$ are compact polyhedral sets containing the origin. With the value function V_N and the quadratic cost objective J over the prediction horizon N_c, the finite optimization problem results in

$$V_N = \min_{{}^{0}u(k),\ldots,{}^{N_c-1}u(k)} \left\{ J = {}^{N_c}\boldsymbol{x}^T(k)\,\boldsymbol{Q_c}\,{}^{N_c}\boldsymbol{x}(k) + \sum_{i=0}^{N_c-1} \left[{}^{i}\boldsymbol{x}^T(k)\,\boldsymbol{P_c}\,{}^{i}\boldsymbol{x}(k) + {}^{i}\boldsymbol{u}^T(k)\,\boldsymbol{R_c}\,{}^{i}\boldsymbol{u}(k) \right] \right\} \tag{5.36a}$$

subject to

$${}^{0}\boldsymbol{x}(k) = \boldsymbol{x}(k), \tag{5.36b}$$

$${}^{i+1}\boldsymbol{x}(k) = \boldsymbol{A}\,{}^{i}\boldsymbol{x}(k) + \boldsymbol{B}\,{}^{i}\boldsymbol{u}(k) \quad \forall\, i \in \{0,\ldots,N_c-1\}, \tag{5.36c}$$

$$^{i}\boldsymbol{u} \in \mathbb{U} \quad \forall\, i \in \{0, ..., N_c - 1\}, \tag{5.36d}$$

$$^{i}\boldsymbol{x} \in \mathbb{X} \quad \forall\, i \in \{1, ..., N_c - 1\}, \tag{5.36e}$$

$$^{N_c}\boldsymbol{x} \in \mathbb{T}. \tag{5.36f}$$

The model predictive control law is implicitly defined by the quadratic program of the specified finite optimization problem. In combination with the size of the prediction horizon N_c, the weighting factors $\boldsymbol{Q_c}$, $\boldsymbol{P_c}$ and $\boldsymbol{R_c}$ of the quadratic cost objective J determine the performance and stability of the control system. The positive definite matrix $\boldsymbol{R_c}$ weights the optimized control signal sequence and keeps the control signal within reasonable limits. The positive semidefinite matrices $\boldsymbol{P_c}$ and $\boldsymbol{Q_c}$ weight the predicted state sequence for assuring stabilization of the controlled system. The terminal cost F_T in the quadratic cost objective J given by

$$F_T = {}^{N_c}\boldsymbol{x}^T(k)\, \boldsymbol{Q_c}\, {}^{N_c}\boldsymbol{x}(k) \tag{5.37}$$

is an additional constraint that forces the predicted state sequence to reach the compact polyhedral terminal set $\mathbb{T}$ at the end of the prediction horizon N_c. Together with the terminal set $\mathbb{T}$, the terminal cost F_T specifies the stability characteristics of the control system. For linear systems with input and state constraints, the terminal cost F_T can be chosen to equal to the value function of the unconstrained infinite optimal control problem $\bar{V}_\infty$ defined by

$$\bar{V}_\infty = \min_{^0u(k),^1u(k),...} \left\{ J = \sum_{i=0}^{\infty} \left[{}^{i}\boldsymbol{x}^T(k)\, \boldsymbol{P_c}\, {}^{i}\boldsymbol{x}(k) + {}^{i}\boldsymbol{u}^T(k)\, \boldsymbol{R_c}\, {}^{i}\boldsymbol{u}(k) \right] \right\}. \tag{5.38}$$

The corresponding weighting factor of the terminal cost $\boldsymbol{Q_c}$ is computed by applying the discrete-time Riccati equation with the weighting factors $\boldsymbol{P_c}$ and $\boldsymbol{R_c}$

$$\boldsymbol{A}\, \boldsymbol{P}_c\, \boldsymbol{A}^T - \boldsymbol{P}_c - \boldsymbol{A}\, \boldsymbol{P}_c\, \boldsymbol{C}^T\, (\boldsymbol{C}\, \boldsymbol{P}_c\, \boldsymbol{C}^T + \boldsymbol{R}_c)^{-1}\, \boldsymbol{C}\, \boldsymbol{P}_c\, \boldsymbol{A}^T = -\boldsymbol{Q}_c. \tag{5.39}$$

With this choice of the weighting factor $\boldsymbol{Q_c}$, the terminal cost F_T becomes a Lyapunov function and ensures exponential stability within the terminal set $\mathbb{T}$. This terminal set $\mathbb{T}$ permits the replacement of the constrained infinite optimal control problem by the unconstrained infinite value function $\bar{V}_\infty$. The domain of attraction is specified by the set of states that can be controlled with the applied prediction horizon N_c. These stability characteristics assure a stable control action in case of an adequate size of the prediction horizon N_c [13, 36].

The specified finite optimization problem provides an implicit definition of the model predictive control law and requires an on-line optimization to compute the optimized control signal sequence. In order to derive the explicit form of the control system, the finite optimization problem has to be transformed from a quadratic program into a complying multi-parametric quadratic program. With the value function $\tilde{V}_N$, the cost objective $\tilde{J}$ and the substitution

$${}^{i+1}\boldsymbol{x}(k) = \boldsymbol{A}^i\, \boldsymbol{x}(k) + \sum_{j=0}^{i-1} \boldsymbol{A}^j\, \boldsymbol{B}\, \left({}^{i-1-j}\boldsymbol{u}(k) \right), \tag{5.40}$$

the optimization problem (5.36) can be reformulated as

$$\tilde{V}_N = \boldsymbol{x}^T(k)\, \boldsymbol{Y}\, \boldsymbol{x}(k) + \min_{\boldsymbol{U}_N} \left\{ \tilde{J} = \boldsymbol{U}_N^T\, \boldsymbol{H}\, \boldsymbol{U}_N + \boldsymbol{x}^T(k)\, \boldsymbol{F}\, \boldsymbol{U}_N \right\} \tag{5.41a}$$

subject to

$$\boldsymbol{G}\,\boldsymbol{U}_N \leq \boldsymbol{W} + \boldsymbol{E}\,\boldsymbol{x}(k). \tag{5.41b}$$

The column vector $\boldsymbol{U}_N$ of the dimension $m \cdot N_c$ contains the optimized control signal sequence, while the matrices $\boldsymbol{Y}$, $\boldsymbol{H}$, $\boldsymbol{F}$, $\boldsymbol{G}$, $\boldsymbol{W}$ and $\boldsymbol{E}$ can be obtained from the optimization problem (5.36) as well as the model (5.35). Resulting from the transformation, the optimized control signal sequence is provided as a function of the state vector $\boldsymbol{x}$ implicitly defined by the transformed optimization problem. By considering the state as a vector of individual parameters, the quadratic problem is translated into a multi-parametric quadratic problem that can be solved over the constrained state space $\mathbb{X}$. The solution can be computed off-line and equals to a piecewise affine function of the state vector $\boldsymbol{x}$ specified over a polyhedral partition of the constrained state space $\mathbb{X}$. This piecewise affine function corresponds to the explicitly defined model predictive control with a control law read as

$$\boldsymbol{U}_N(\boldsymbol{x}(k)) = \boldsymbol{L}\,\boldsymbol{x}(k) + \boldsymbol{M} \quad \forall \boldsymbol{x} \in R_p \tag{5.42}$$

for each region R_p of the constrained state space $\mathbb{X}$ under the assumptions of stability and feasibility of the closed-loop system. The number of regions R_p depends on the dimension of the state vector n and the number of degrees of freedom $m \cdot N_c$ [2, 13].

The explicit definition of the model predictive control law reduces the computational complexity to the evaluation of a piecewise affine function with preserving the performance and stability characteristics. The computational requirements are shifted from a high demand in computing power for solving the implicit optimization problem to an increased consumption of memory space for storing the explicit model predictive control law. These properties enhance the applicability of model predictive control and allows an efficient implementation in a wide range of application.

5.5.1.1 Tracking Control Structure

The design of a model predictive control for trajectory tracking requires a modification of the standard model predictive control to ensure an offset-free tracking of the desired trajectory. The presence of an unmeasured sustained disturbance can cause an enduring offset from the desired progression that is not rejected by standard model predictive control. Existing methods for offset-free tracking are based on the introduction of an integral constraint with considering the last control signal or the application of an trajectory and disturbance observer to regard uncertainties and disturbances. The integral constraint corresponds to an integral term in the control system that assures steady-state accuracy for asymptotically constant progressions of the desired values. The trajectory and disturbance observer allows for more general types of trajectories, but requires a model of the disturbance and trajectory dynamics. In the case of a modified trajectory generation, the control system needs to be adjusted to the changed trajectory dynamics. Both tracking control approaches do not support the desired flexible control system that permits an independent generation of the desired trajectory without affecting the control action [13, 30].

For providing a universal model predictive control for arbitrary trajectory tracking, a novel tracking control strategy is proposed and designed for the angular position and speed control of both servo actuator types. The finite optimization problem of the standard model predictive control is divided into a feedforward and feedback control with two partial control signals. The control signal of the feedforward control provides a compensation of known disturbances and a pilot control for desired motion values. The control signal of the feedback control eliminates uncompensated control errors of the control variable and ensures offset-free tracking. By applying the trajectory generation to project the future progression of desired motion values, the compound control signal sequence is optimized for

the desired trajectory within the limits of input and state constraints. This optimization is not restricted to specific types of trajectories and generalizes offset-free tracking to arbitrary motion. For covering variable input signal saturation, the input constraint is assumed to be time-variant.

The design of the tracking control is based on a linear, time-invariant, discrete-time and controllable model of the controlled system extended by an additive disturbance. With the input variable u, the state vector $\boldsymbol{x}$, the output variable y and the disturbance variable d, the state space model is given by

$$\boldsymbol{x}(k+1) = \boldsymbol{A}\,\boldsymbol{x}(k) + \boldsymbol{B}\,u(k) + \boldsymbol{V}\,d(k), \tag{5.43a}$$

$$y(k) = \boldsymbol{C}\,\boldsymbol{x}(k). \tag{5.43b}$$

The integrated operation of a feedforward and feedback control results in a compound control signal u that comprises the partial control signals of each control type

$$u(k) = u_b(k) + u_f(k) \tag{5.44}$$

where u_b is generated by the feedback control and u_f is generated by the feedforward control. While the control signal of the feedback control u_f is obtained by solving the finite optimization problem, the control signal of the feedforward control is given by the feedforward control law as a function of the disturbance d and the desired motion values summarized in the trajectory vector $\boldsymbol{r}$

$$u_f(k) = f_f(d(k), \boldsymbol{r}(k)). \tag{5.45}$$

In order to consider the future progression of desired motion values, the known disturbance and the variable input constraint in the computation of the control signal sequence, the finite optimization problem has to be extended by additional time-variant parameters. This is achieved by augmenting the state vector $\boldsymbol{x}$ and the model of the controlled system. The disturbance and the variable input constraint are assumed to change slowly in relation to the sampling time. For this reason, both values are expected to be constant over the finite prediction horizon N_c and are updated at the regular sampling instant only. The desired motion values are precomputed for each prediction step by applying the trajectory generation. The number of required motion values depends on the size of the trajectory vector $\boldsymbol{r}$ and the finite prediction horizon N_c. With the disturbance variable d, the constraint variable q and the trajectory vector $\boldsymbol{r}$, the augmented state vector $\tilde{\boldsymbol{x}}$ is defined by

$$\tilde{\boldsymbol{x}}(k) = \begin{bmatrix} \boldsymbol{x}^T(k) & \boldsymbol{r}^T(k) & \cdots & \boldsymbol{r}^T(k+N_c) & d(k) & q(k) \end{bmatrix}^T. \tag{5.46}$$

According to the augmented state vector $\tilde{\boldsymbol{x}}$, the augmented model for the computation of the predicted state sequence is given by

$$\tilde{\boldsymbol{x}}(k+1) = \tilde{\boldsymbol{A}}\,\tilde{\boldsymbol{x}}(k) + \tilde{\boldsymbol{B}}\,u(k), \tag{5.47a}$$

$$y(k) = \tilde{\boldsymbol{C}}\,\tilde{\boldsymbol{x}}(k) \tag{5.47b}$$

where

$$\tilde{\boldsymbol{A}} = \begin{bmatrix} \boldsymbol{A} & \boldsymbol{0} & \cdots & \boldsymbol{0} & \boldsymbol{V} & \boldsymbol{0} \\ \boldsymbol{0} & 1 & \cdots & 0 & 0 & 0 \\ \vdots & \vdots & \ddots & \vdots & \vdots & \vdots \\ \boldsymbol{0} & 0 & \cdots & 1 & 0 & 0 \\ \boldsymbol{0} & 0 & \cdots & 0 & 1 & 0 \\ \boldsymbol{0} & 0 & \cdots & 0 & 0 & 1 \end{bmatrix}, \qquad \tilde{\boldsymbol{B}} = \begin{bmatrix} \boldsymbol{B} \\ 0 \\ \vdots \\ 0 \\ 0 \\ 0 \end{bmatrix}, \qquad \tilde{\boldsymbol{C}} = \begin{bmatrix} \boldsymbol{C} \\ 0 \\ \vdots \\ 0 \\ 0 \\ 0 \end{bmatrix}^T.$$

The additive disturbance matrix $\boldsymbol{V}$ is included in the augmented system matrix $\tilde{\boldsymbol{A}}$. This is necessary for applying the disturbance on the predicted state sequence to ensure an aligned control action of the feedforward and feedback control. Without the consideration of the disturbance in the prediction process, the feedback control compensates the control signal of the feedforward control and counteracts the desired disturbance compensation. Generally, the augmented model is not completely controllable and violates a requirement of model predictive control. This restriction does not affect the tracking control of the desired variables in the state vector $\boldsymbol{x}$ as long as the state vector $\boldsymbol{x}$ is controllable. The controllability of the state vector $\boldsymbol{x}$ contained in the augmented state vector $\tilde{\boldsymbol{x}}$ can be verified by performing a Kalman decomposition of the augmented model.

Based on the specified extensions, the modified finite optimization problem of the tracking control with the value function V_N and the quadratic cost objective J over the prediction horizon N_c results in

$$\begin{aligned} V_N = \min_{{}^0u(k),\ldots,{}^{N_c-1}u(k)} \Big\{ J = & \left({}^{N_c}\boldsymbol{x}(k) - \boldsymbol{w}(k+N_c)\right)^T \boldsymbol{Q_c} \left({}^{N_c}\boldsymbol{x}(k) - \boldsymbol{w}(k+N_c)\right) \\ & + \sum_{i=0}^{N_c-1} \Big[\left({}^{i}\boldsymbol{x}(k) - \boldsymbol{w}(k+i)\right)^T \boldsymbol{P_c} \left({}^{i}\boldsymbol{x}(k) - \boldsymbol{w}(k+i)\right) \\ & + \left({}^{i}u_f(k) - f(d(k), \boldsymbol{r}(k+i))\right)^T R_c \left({}^{i}u_f(k) - f(d(k), \boldsymbol{r}(k+i))\right) \Big] \Big\} \end{aligned} \tag{5.48a}$$

subject to

$${}^0\tilde{\boldsymbol{x}}(k) = \tilde{\boldsymbol{x}}(k), \tag{5.48b}$$

$${}^{i+1}\tilde{\boldsymbol{x}}(k) = \tilde{\boldsymbol{A}}\,{}^{i}\tilde{\boldsymbol{x}}(k) + \tilde{\boldsymbol{B}}\,{}^{i}u(k) \quad \forall\, i \in \{0,\ldots,N_c-1\}, \tag{5.48c}$$

$${}^{i}u(k) = {}^{i}u_b(k) + {}^{i}u_f(k) \quad \forall\, i \in \{0,\ldots,N_c-1\}, \tag{5.48d}$$

$$-q(k) \leq {}^{i}u \leq q(k) \quad \forall\, i \in \{0,\ldots,N_c-1\}, \tag{5.48e}$$

$$-\boldsymbol{m} \leq {}^{i}\boldsymbol{x} \leq \boldsymbol{m} \quad \forall\, i \in \{1,\ldots,N_c-1\}, \tag{5.48f}$$

$$-\boldsymbol{m} \leq {}^{N_c}\boldsymbol{x} \leq \boldsymbol{m}. \tag{5.48g}$$

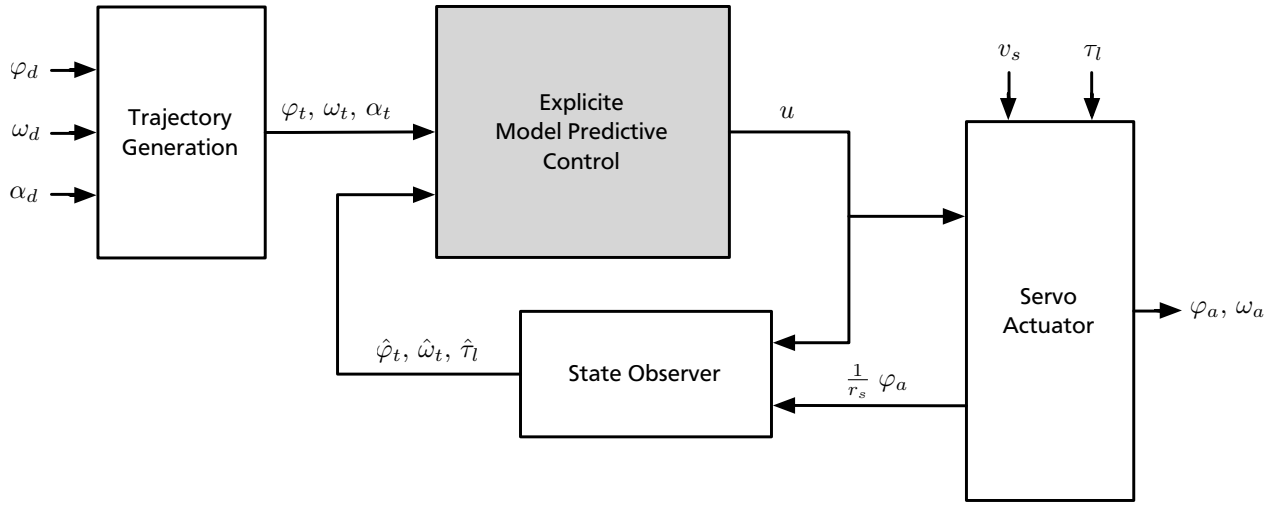

Figure 5.8.: Structure of the model predictive control for trajectory tracking.

The modified quadratic cost function J minimizes the deviation between the state vector $\boldsymbol{x}$ and the reference vector $\boldsymbol{w}$ as well as the deviation between the control signal of the feedforward control u_f and the result of the feedforward control law $f(d(k), \boldsymbol{r}(k))$. The weighting factors are the scalar R_c and the positive semidefinite matrices $\boldsymbol{P_c}$ and $\boldsymbol{Q_c}$. The reference vector $\boldsymbol{w}$ comprises the desired values of the states contained in the trajectory vector $\boldsymbol{r}$. Contrary to the control signal of the feedforward control u_f, the control signal of the feedback control u_b is not explicitly included in the cost objective J. The feedback control law is implicitly defined by the predicted state sequence and the constraint of the compound control signal u corresponding to standard model predictive control. The compound control signal u is restricted by the constraint variable q, while the augmented state vector $\tilde{\boldsymbol{x}}$ computed by the augmented model is bounded by the margin vector $\boldsymbol{m}$. The optimal terminal set equals to the desired trajectory in state space that cannot be predefined in the modified optimization problem. Because of the variable progression of the desired trajectory each state in the constrained state space can become part of the terminal set. For this reason, the terminal set is maximized and equated with the constrained state space bounded by the margin vector $\boldsymbol{m}$.

The introduced model predictive control for trajectory tracking is applied in the design of the angular position and speed control of both servo actuator types. The desired trajectory is provided by the trajectory generation and the disturbance is estimated by the state observer. In order to ensure an efficient implementation of the tracking control, the implicitly defined model predictive control law is transformed to the explicit form defined over the constrained state space. Figure 5.8 shows a functional diagram of the model predictive control structure for trajectory tracking.

For the design and simulation of the model predictive control as well as the computation of the explicitly defined control law, the generally available toolboxes MPT and YALMIP for the numerical computing environment MATLAB/SIMULINK developed by MathWorks are applied [24, 29].

5.5.1.2 Angular Position Control

The design of the model predictive control for angular position tracking is based on a linear, time-invariant, discrete-time and controllable state space model of the servo actuators with an additive disturbance. The state vector $\boldsymbol{x}_p$ includes the angular position φ_a and angular speed ω_a of the servo actuator. The additive disturbance is the load torque τ_l that is estimated by the state observer and given

as the estimated load torque $\hat{\tau}_l$. With the input variable u_p, the state vector $\boldsymbol{x}_p$, the output variable y_p and the disturbance variable d_p defined by

$$u_p(k) = v_m(k), \tag{5.49a}$$

$$\boldsymbol{x}_p(k) = \begin{bmatrix} \varphi_a(k) & \omega_a(k) \end{bmatrix}^T, \tag{5.49b}$$

$$y_p(k) = \varphi_a(k), \tag{5.49c}$$

$$d_p(k) = \hat{\tau}_l(k), \tag{5.49d}$$

the state space model is given by

$$\boldsymbol{x}_p(k+1) = \boldsymbol{A}_{p,d}\, \boldsymbol{x}_p(k) + \boldsymbol{B}_{p,d}\, u_p(k) + \boldsymbol{V}_{p,d}\, d_p(k), \tag{5.50a}$$

$$y_p(k) = \boldsymbol{C}_{p,d}\, \boldsymbol{x}_p(k) \tag{5.50b}$$

A detailed derivation of the process model and the proof of controllability can be found in Appendix C. The desired motion values summarized in the trajectory vector $\boldsymbol{r}_p$ comprise the angular position φ_t, angular speed ω_t and angular acceleration α_t provided by the trajectory generation. The constraint variable q_p is the measured supply voltage of the servo actuator v_s. The finite prediction horizon $N_{c,p}$ has to be kept down in order to ensure a compact explicitly defined model predictive control law. For the angular position tracking of both servo actuator types, the prediction horizon $N_{c,p}$ is specified by

$$N_{c,p} = 2 \tag{5.51}$$

The augmented state vector $\tilde{\boldsymbol{x}}_p$ and the augmented model for the computation of the predicted state sequence result in

$$\tilde{\boldsymbol{x}}_p(k+1) = \tilde{\boldsymbol{A}}_{p,d}\, \tilde{\boldsymbol{x}}_p(k) + \tilde{\boldsymbol{B}}_{p,d}\, u_p(k), \tag{5.52a}$$

$$y_p(k) = \tilde{\boldsymbol{C}}_{p,d}\, \tilde{\boldsymbol{x}}_p(k) \tag{5.52b}$$

where

$$\tilde{\boldsymbol{x}}_p(k) = \begin{bmatrix} \boldsymbol{x}_p^T(k) & \boldsymbol{r}_p^T(k) & \boldsymbol{r}_p^T(k+1) & \boldsymbol{r}_p^T(k+2) & d_p(k) & q_p(k) \end{bmatrix}^T, \tag{5.53}$$

$$\boldsymbol{r}_p(k) = \begin{bmatrix} \varphi_t(k) & \omega_t(k) & \alpha_t(k) \end{bmatrix}^T, \tag{5.54}$$

$$q_p(k) = v_s(k), \tag{5.55}$$

$$\tilde{\boldsymbol{A}}_{p,d} = \begin{bmatrix} \boldsymbol{A}_{p,d} & \boldsymbol{0} & \boldsymbol{0} & \boldsymbol{0} & \boldsymbol{V}_{p,d} & \boldsymbol{0} \\ \boldsymbol{0} & 1 & 0 & 0 & 0 & 0 \\ \boldsymbol{0} & 0 & 1 & 0 & 0 & 0 \\ \boldsymbol{0} & 0 & 0 & 1 & 0 & 0 \\ \boldsymbol{0} & 0 & 0 & 0 & 1 & 0 \\ \boldsymbol{0} & 0 & 0 & 0 & 0 & 1 \end{bmatrix}, \qquad \tilde{\boldsymbol{B}}_{p,d} = \begin{bmatrix} \boldsymbol{B}_{p,d} \\ 0 \\ 0 \\ 0 \\ 0 \\ 0 \end{bmatrix}, \qquad \tilde{\boldsymbol{C}}_{p,d} = \begin{bmatrix} \boldsymbol{C}_{p,d} \\ 0 \\ 0 \\ 0 \\ 0 \\ 0 \end{bmatrix}^T.$$

A Kalman decomposition on the augmented model shows that the control variables φ_a and ω_a are controllable and observable, the estimated load torque $\hat{\tau}_l$ is observable only and all other states are nether controllable nor observable. The reference vector $\boldsymbol{w}_p$ comprises the desired values of the angular position φ_t and the angular speed ω_t provided by the trajectory generation and is contained in the trajectory vector $\boldsymbol{r}_p$. The constrained state space and the terminal set that are bounded by the margin vector $\boldsymbol{m}_p$ are symmetrically restricted to an angular position of ±4000 radians and an angular speed of ±40 radians per second. All other states are limited to related reasonable values. These constraints specify the operating range of the controlled servo actuators and are based on the expected scope of application.

The modified finite optimization problem of the model predictive control for angular position tracking with the value function $V_{N,p}$ and the quadratic cost objective J_p over the prediction horizon $N_{c,p}$ results in

$$\begin{aligned} V_{N,p} = \min_{{}^0u_p(k),\ldots,{}^{N_{c,p}-1}u_p(k)} \Big\{ J_p &= \left({}^{N_{c,p}}\boldsymbol{x}_p(k) - \boldsymbol{w}_p(k+N_{c,p})\right)^T \boldsymbol{Q_{c,p}} \left({}^{N_{c,p}}\boldsymbol{x}_p(k) - \boldsymbol{w}_p(k+N_{c,p})\right) \\ &+ \sum_{i=0}^{N_{c,p}-1} \Big[\left({}^{i}\boldsymbol{x}_p(k) - \boldsymbol{w}_p(k+i)\right)^T \boldsymbol{P_{c,p}} \left({}^{i}\boldsymbol{x}_p(k) - \boldsymbol{w}_p(k+i)\right) \\ &+ \left({}^{i}u_{f,p}(k) - f_f(d_p(k), \boldsymbol{r}_p(k+i))\right)^T R_{c,p} \left({}^{i}u_{f,p}(k) - f_f(d_p(k), \boldsymbol{r}_p(k+i))\right) \Big] \Big\} \end{aligned} \tag{5.56a}$$

subject to

$$f_f(d_p(k), \boldsymbol{r}_p(k)) = K_{f,\omega}\, \omega_t(k) + K_{f,\alpha}\, \alpha_t(k) + K_{f,\tau}\, \hat{\tau}_l(k), \tag{5.56b}$$

$${}^0\tilde{\boldsymbol{x}}_p(k) = \tilde{\boldsymbol{x}}_p(k), \tag{5.56c}$$

$${}^{i+1}\tilde{\boldsymbol{x}}_p(k) = \tilde{\boldsymbol{A}}_{p,d}\, {}^{i}\tilde{\boldsymbol{x}}_p(k) + \tilde{\boldsymbol{B}}_{p,d}\, {}^{i}u_p(k) \quad \forall\, i \in \{0,\ldots,N_{c,p}-1\}, \tag{5.56d}$$

$${}^{i}u_p(k) = {}^{i}u_{b,p}(k) + {}^{i}u_{f,p}(k) \quad \forall\, i \in \{0,\ldots,N_{c,p}-1\}, \tag{5.56e}$$

$$-q_p(k) \leq {}^{i}u_p \leq q_p(k) \quad \forall\, i \in \{0,\ldots,N_{c,p}-1\}, \tag{5.56f}$$

$$-\boldsymbol{m}_p \leq {}^{i}\tilde{\boldsymbol{x}}_p \leq \boldsymbol{m}_p \quad \forall\, i \in \{1,\ldots,N_{c,p}-1\}, \tag{5.56g}$$

$$-\boldsymbol{m}_p \leq {}^{N_{c,p}}\tilde{\boldsymbol{x}}_p \leq \boldsymbol{m}_p. \tag{5.56h}$$

The model predictive control for angular position tracking of both servo actuator types is designed with emphasis on a maximized control rate and avoiding control variable overshoot. The explicit definition of the model predictive control law reduces the computational complexity and allows to use a small sampling time to improve the dynamic response of the tracking control. The model predictive control of both servo actuator types operates with a sampling time of 1 millisecond.

In order to evaluate the control action, the model predictive control of the DD-28 servo actuator is simulated with an extensive nonlinear model. Figure 5.9 presents the progressions of the angular position

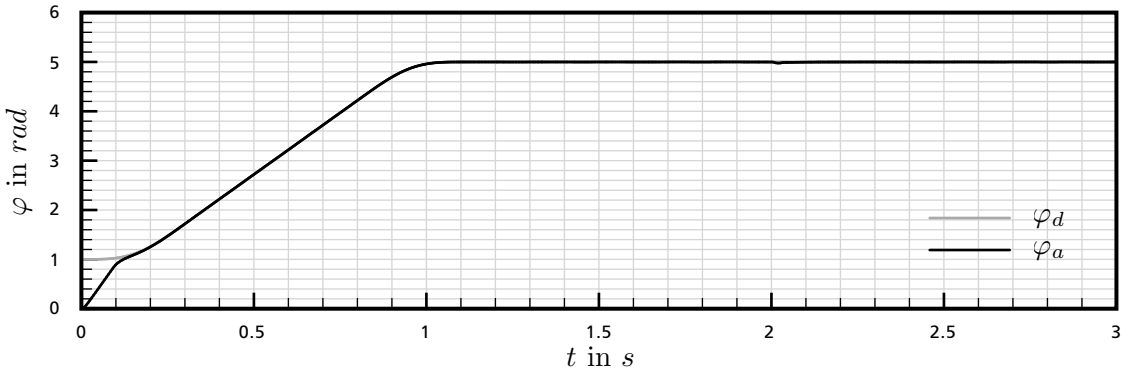

(a) Progression of the angular position with $\varphi_d = 5\ rad$, $\omega_d = 5\ \frac{rad}{s}$ and $\alpha_d = 30\ \frac{rad}{s^2}$.

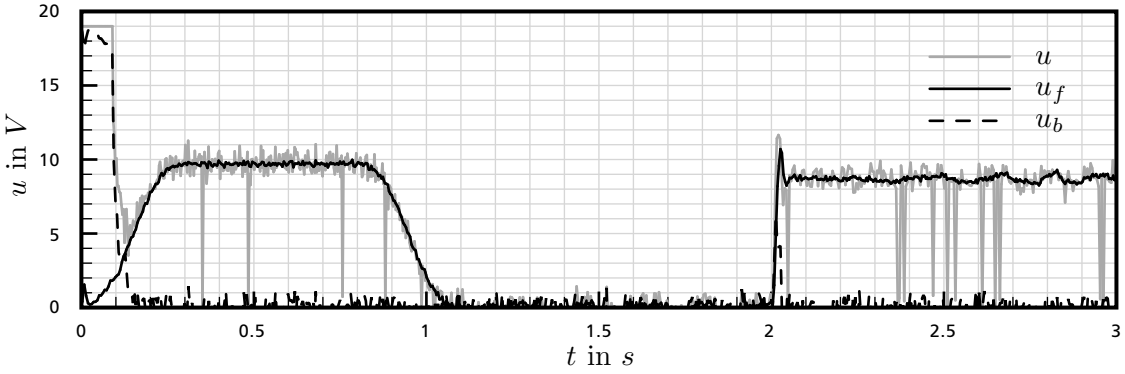

(b) Progressions of the control signals with $\varphi_d = 5\ rad$, $\omega_d = 5\ \frac{rad}{s}$ and $\alpha_d = 30\ \frac{rad}{s^2}$.

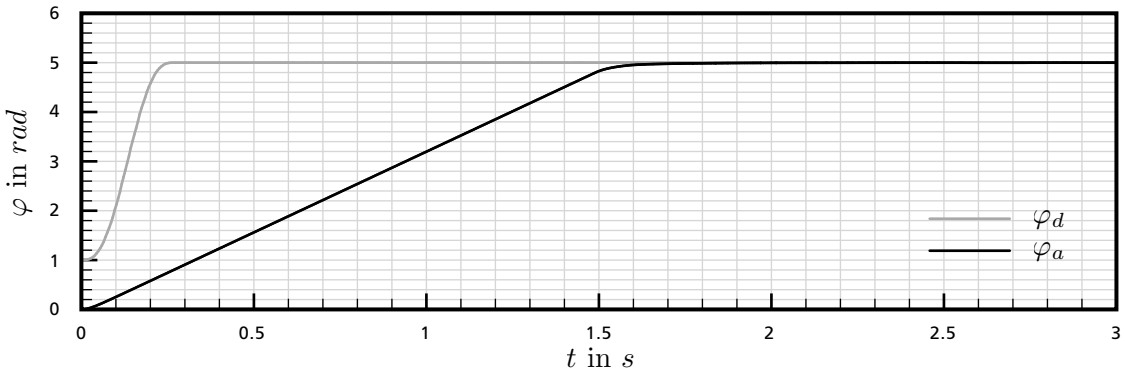

(c) Progression of the angular position with $\varphi_d = 5\ rad$, $\omega_d = 15\ \frac{rad}{s}$ and $\alpha_d = 100\ \frac{rad}{s^2}$.

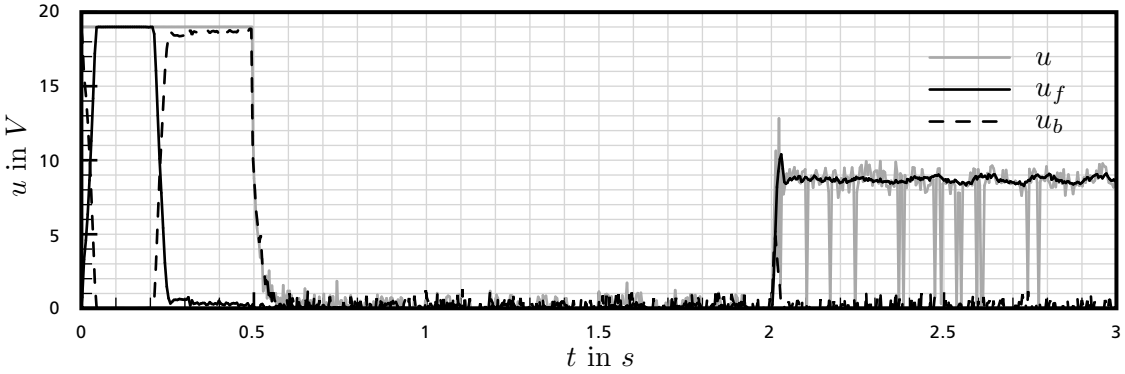

(d) Progressions of the control signals with $\varphi_d = 5\ rad$, $\omega_d = 15\ \frac{rad}{s}$ and $\alpha_d = 100\ \frac{rad}{s^2}$.

Figure 5.9.: Performance of the model predictive position control of the DD-28 servo actuator.

and the saturated control signals for two different desired angular speeds and accelerations. The simulations engender unsaturated and saturated operation of the servo actuator. For demonstration, the initial deviation of the angular position is set to a relatively high value of 1 radian. The armature voltage has a constant value of 19 volts. After 2 seconds, a load torque of 2 newton meters is applied on the simulated servo actuator. In unsaturated operation, the initial deviation is compensated quickly and the desired trajectory is tracked without any offset. In saturated operation, the full input signal range is utilized and the desired angular position is reached without any overshoot of the control variable. The applied load torque is rejected immediately by the feedforward control and the resulting deviation of the angular position is corrected by the feedback control. The overall performance of the control action is characterized by an excellent trajectory tracking and a fast disturbance compensation with high steady-stated accuracy.

The designed model predictive control law in explicit form requires six hundred and twenty-nine regions for the DD-28 servo actuator and three hundred and seventy-seven regions for the DD-64 servo actuator. All applied design parameters are listed in Appendix E.

5.5.1.3 Angular Speed Control

The design of the model predictive control for angular speed tracking is based on a linear, time-invariant, discrete-time and controllable state space model of the servo actuators with an additive disturbance. The state variable x_s corresponds to the angular speed ω_a of the servo actuator. The additive disturbance is the load torque τ_l that is estimated by the state observer and given as the estimated load torque $\hat{\tau}_l$. A detailed derivation of the process model and the proof of controllability can be found in Appendix C. With the input variable u_s, the state variable x_s, the output variable y_s and the disturbance variable d_s defined by

$$u_s(k) = v_m(k), \tag{5.57a}$$

$$x_s(k) = \omega_a(k), \tag{5.57b}$$

$$y_s(k) = \omega_a(k), \tag{5.57c}$$

$$d_s(k) = \tau_l(k), \tag{5.57d}$$

the state space model is given by

$$x_s(k+1) = A_{s,d}\, x_s(k) + B_{s,d}\, u_s(k) + V_{s,d}\, d_s(k), \tag{5.58a}$$

$$y_s(k) = C_{s,d}\, x_s(k) + D_{s,d}\, u_s(k) \tag{5.58b}$$

The desired motion values summarized in the trajectory vector $\boldsymbol{r}_s$ comprise the angular speed ω_t and angular acceleration α_t provided by the trajectory generation. The constraint variable q_s is the measured supply voltage of the servo actuator v_s. The finite prediction horizon $N_{c,p}$ has to be kept down in order to ensure a compact explicitly defined model predictive control law. For the angular speed tracking of both servo actuator types, the prediction horizon $N_{c,s}$ is specified by

$$N_{c,s} = 2 \tag{5.59}$$

The augmented state vector $\tilde{\boldsymbol{x}}_s$ and the augmented model for the computation of the predicted state sequence result in

$$\tilde{\boldsymbol{x}}_s(k+1) = \tilde{\boldsymbol{A}}_{s,d}\, \tilde{\boldsymbol{x}}_s(k) + \tilde{\boldsymbol{B}}_{s,d}\, u_s(k), \tag{5.60a}$$

$$y_s(k) = \tilde{\boldsymbol{C}}_{s,d}\, \tilde{\boldsymbol{x}}_s(k) \tag{5.60b}$$

where

$$\tilde{\boldsymbol{x}}_s(k) = \begin{bmatrix} x_s(k) & \boldsymbol{r}_s^T(k) & \boldsymbol{r}_s^T(k+1) & \boldsymbol{r}_s^T(k+2) & d_s(k) & q_s(k) \end{bmatrix}^T, \tag{5.61}$$

$$\boldsymbol{r}_s(k) = \begin{bmatrix} \omega_t(k) & \alpha_t(k) \end{bmatrix}^T, \tag{5.62}$$

$$q_s(k) = v_s(k), \tag{5.63}$$

$$\tilde{\boldsymbol{A}}_{s,d} = \begin{bmatrix} A_{s,d} & 0 & 0 & 0 & V_{s,d} & 0 \\ 0 & 1 & 0 & 0 & 0 & 0 \\ 0 & 0 & 1 & 0 & 0 & 0 \\ 0 & 0 & 0 & 1 & 0 & 0 \\ 0 & 0 & 0 & 0 & 1 & 0 \\ 0 & 0 & 0 & 0 & 0 & 1 \end{bmatrix}, \qquad \tilde{\boldsymbol{B}}_{s,d} = \begin{bmatrix} B_{s,d} \\ 0 \\ 0 \\ 0 \\ 0 \\ 0 \end{bmatrix}, \qquad \tilde{\boldsymbol{C}}_{s,d} = \begin{bmatrix} C_{s,d} \\ 0 \\ 0 \\ 0 \\ 0 \\ 0 \end{bmatrix}^T.$$

A Kalman decomposition on the augmented model shows that the control variable ω_a is controllable and observable, the estimated load torque $\hat{\tau}_l$ is observable only and all other states are nether controllable nor observable. The reference variable w_s equals to the desired value of the angular speed ω_t provided by the trajectory generation and is contained in the trajectory vector $\boldsymbol{r}_s$. The constrained state space and the terminal set that are bounded by the margin vector $\boldsymbol{m}_s$ are symmetrically restricted to an angular speed of ±40 radians per second. All other states are limited to related reasonable values. These constraints specify the operating range of the controlled servo actuators and are based on the expected scope of application.

The modified finite optimization problem of the model predictive control for angular position tracking with the value function $V_{N,s}$ and the quadratic cost objective J_s over the prediction horizon $N_{c,s}$ results in

$$\begin{aligned} V_{N,s} = \min_{{}^0u_s(k),\ldots,{}^{N_{c,s}-1}u_s(k)} \Big\{ J_s &= \left({}^{N_{c,s}}x_s(k) - w_s(k+N_{c,s})\right)^T\, Q_{c,s}\, \left({}^{N_{c,s}}x_s(k) - w_s(k+N_{c,s})\right) \\ &+ \sum_{i=0}^{N_{c,s}-1} \Big[\left({}^{i}x_s(k) - w_s(k+i)\right)^T\, P_{c,s}\, \left({}^{i}x_s(k) - w_s(k+i)\right) \\ &+ \left({}^{i}u_{f,s}(k) - f_f(d_s(k), \boldsymbol{r}_s(k+i))\right)^T\, R_{c,s}\, \left({}^{i}u_{f,s}(k) - f_f(d_s(k), \boldsymbol{r}_s(k+i))\right) \Big] \Big\} \end{aligned} \tag{5.64a}$$

subject to

$$f_f(d_s(k), \boldsymbol{r}_s(k)) = K_{f,\omega}\ \omega_t(k) + K_{f,\alpha}\ \alpha_t(k) + K_{f,\tau}\ \hat{\tau}_l(k), \tag{5.64b}$$

$${}^{0}\tilde{\boldsymbol{x}}_s(k) = \tilde{\boldsymbol{x}}_s(k), \tag{5.64c}$$

$${}^{i+1}\tilde{\boldsymbol{x}}_s(k) = \tilde{\boldsymbol{A}}_{s,d}\ {}^{i}\tilde{\boldsymbol{x}}_s(k) + \tilde{\boldsymbol{B}}_{s,d}\ {}^{i}u_s(k) \quad \forall\ i \in \{0, ..., N_{c,s} - 1\}, \tag{5.64d}$$

$${}^{i}u_s(k) = {}^{i}u_{b,s}(k) + {}^{i}u_{f,s}(k) \quad \forall\ i \in \{0, ..., N_{c,s} - 1\}, \tag{5.64e}$$

$$-q_s(k) \leq {}^{i}u_s \leq q_s(k) \quad \forall\ i \in \{0, ..., N_{c,s} - 1\}, \tag{5.64f}$$

$$-\boldsymbol{m}_s \leq {}^{i}\tilde{\boldsymbol{x}}_s \leq \boldsymbol{m}_s \quad \forall\ i \in \{1, ..., N_{c,s} - 1\}, \tag{5.64g}$$

$$-\boldsymbol{m}_s \leq {}^{N_{c,s}}\tilde{\boldsymbol{x}}_s \leq \boldsymbol{m}_s. \tag{5.64h}$$

The model predictive control for angular speed tracking of both servo actuator types is designed with emphasis on a maximized control rate and avoiding control variable overshoot. The explicit definition of the model predictive control law reduces the computational complexity and allows to use a small sampling time to improve the dynamic response of the tracking control. The model predictive control of both servo actuator types operates with a sampling time of 1 millisecond.

In order to evaluate the control action, the model predictive control of the DD-28 servo actuator is simulated with an extensive nonlinear model. Figure 5.10 presents the progressions of the angular speed and the saturated control signals for two different desired angular speeds and accelerations. The simulations engender unsaturated and saturated operation of the servo actuator. For demonstration, the initial deviation of the angular speed is set to a relatively high value of 1 radian per second. The armature voltage has a constant value of 19 volts. After 2 seconds, a load torque of 2 newton meters is applied on the simulated servo actuator. In unsaturated operation, the initial deviation is compensated quickly by the feedforward control with a slight overshoot, while the desired trajectory is tracked without any offset. A deflection caused by a noise impulse interferes the progression of the angular speed at about 0.25 seconds. The applied load torque is rejected immediately by the feedforward and feedback control. In saturated operation, the full input signal range is utilized and the actual angular speed is maximized at the specified armature voltage. The applied load torque causes an reduction of the actual angular speed that cannot be compensated due to input signal saturation. Because of the residual noise signal of the estimated angular speed, the control action is superimposed by a minor interference. The overall performance of the control action is characterized by an excellent trajectory tracking and a fast disturbance compensation with slight overshoot.

The designed model predictive control law in explicit form requires one hundred and twenty-five regions for the DD-28 servo actuator and eighty-three regions for the DD-64 servo actuator. All applied design parameters are listed in Appendix E.

5.5.2 Loop-Shaping Control

Loop-shaping control is a popular and universally used control method for many types of application. The control action is exceedingly adjustable and can be implemented with low computational requirements.

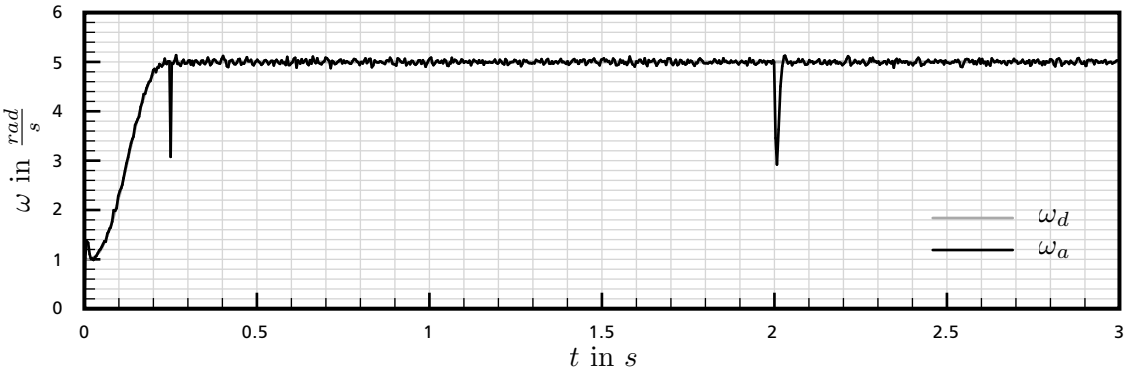

(a) Progression of the angular speed with $\omega_d = 5\ \frac{rad}{s}$ and $\alpha_d = 30\ \frac{rad}{s^2}$.

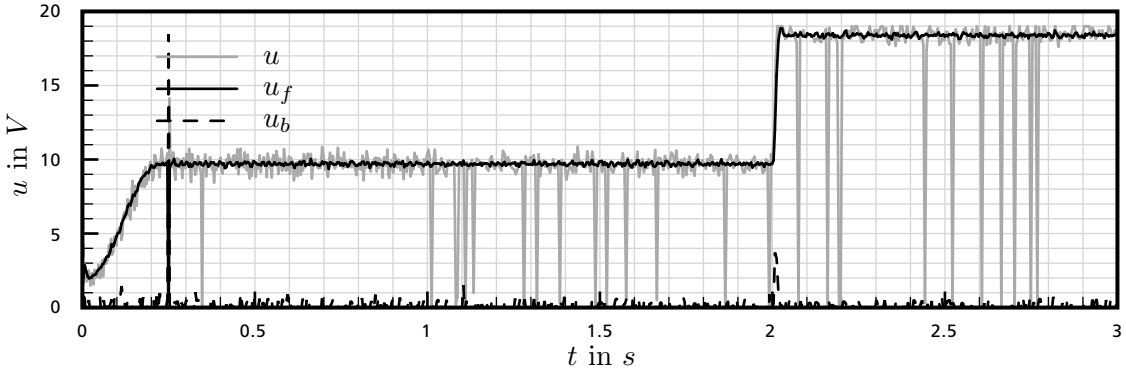

(b) Progressions of the control signals with $\omega_d = 5\ \frac{rad}{s}$ and $\alpha_d = 30\ \frac{rad}{s^2}$.

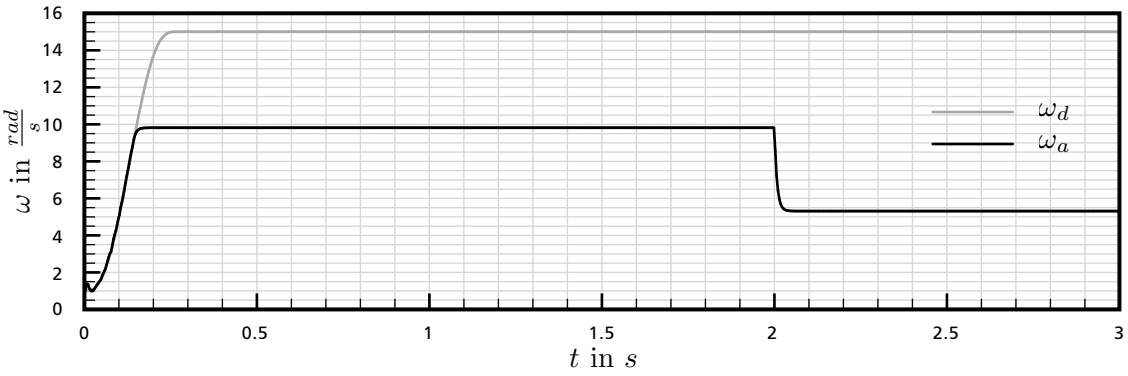

(c) Progression of the angular speed with $\omega_d = 15\ \frac{rad}{s}$ and $\alpha_d = 100\ \frac{rad}{s^2}$.

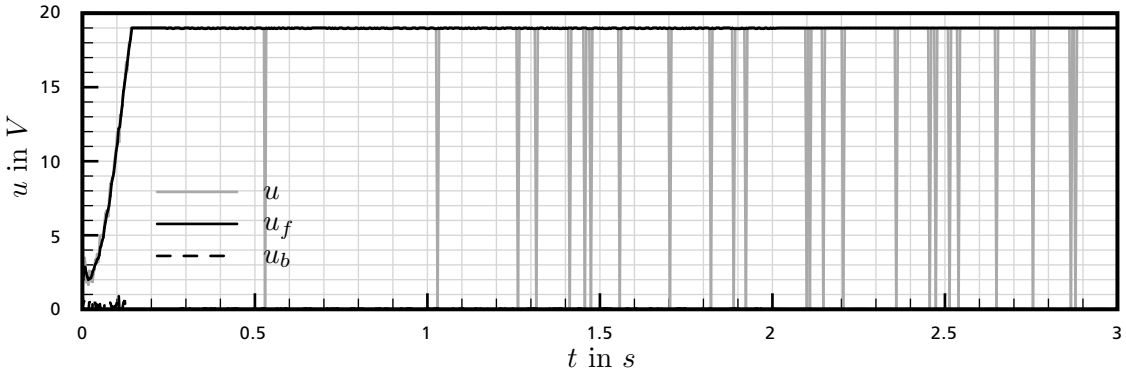

(d) Progressions of the control signals with $\omega_d = 15\ \frac{rad}{s}$ and $\alpha_d = 100\ \frac{rad}{s^2}$.

Figure 5.10.: Performance of the model predictive speed control of the DD-28 servo actuator.

In combination with an anti-windup scheme, the control method provides a nonlinear control law that can be applied on linear and nonlinear controlled systems with existing input constraints. The high adjustability makes for a flexible control system with an extensive operating range [23, 27].

The basic idea of loop-shaping control is to shape the transfer characteristics of the open-loop system by adjusting the frequency response of the feedback controller in order to satisfy defined design requirements. This design approach utilizes the possibility to transform the design requirements for the closed-loop system to complying characteristic values of the frequency response. With the linear or linearized transfer function of the controlled system H_g and the linear transfer function of the feedback controller H_k, the closed-loop output transfer function H_c is given by

$$H_c(s) = \frac{H_k(s)\, H_g(s)}{1 + H_k(s)\, H_g(s)}. \tag{5.65}$$

The open-loop transfer function H_o corresponds to the gain of the closed-loop transfer function H_c and is defined by

$$H_o(s) = H_k(s)\, H_g(s). \tag{5.66}$$

The denominator of the closed-loop transfer function H_c determines the stability and dynamic response characteristics of the feedback control. Because of the close relation between the open-loop transfer function H_o and the closed-loop denominator, the design of the feedback control can be focused on the open-loop transfer function H_o. The design requirements for the feedback control comprise demands in performance, stability and robustness. These demands can be linked to characteristic values of the open-loop frequency response represented by the Bode plot. The angular cross-over frequency ω_c that is also referred as system bandwidth denotes the angular frequency where the gain of the open-loop system $|H_o|$ crosses the 0 decibel axis in angular frequency. The system bandwidth is a measure for the dynamic response of the feedback control that is able to attenuate disturbances with angular frequencies up to the cross-over frequency ω_z. For providing high performance and fast disturbance compensation, the system bandwidth is to be maximized to increase the control rate. The phase margin Φ_m is a criterion for the stability of the feedback control and is specified by the absolute value of the phase $\angle(H_o)$ at the cross-over frequency ω_c read as

$$\Phi_m = 180^\circ - |\angle(H_o(\omega_z))|. \tag{5.67}$$

The control system is stable, if the phase margin Φ_m is positive. The smaller the phase margin Φ_m the more the feedback control will tend to overshoot or oscillate due to step disturbances. In order to assure a control action without overshooting the desired value, the phase margin Φ_m has to be greater that 70°. The gain margin G_m is a measure for the robustness of the feedback control and is defined by the negative gain of the open-loop system $|H_o|$ at a phase of -180° read as

$$G_m = -|H_o|(\omega_\pi) \quad \text{with} \quad \angle(H_o(\omega_\pi)) = -180^\circ. \tag{5.68}$$

The gain margin G_m gives the factor by which the control gain can be increased before the system turns unstable. For a stable and robust control action, the gain margin G_m is to be greater that 12 decibel. Figure 5.11 shows a Bode plot of an open-loop system with the specified characteristic values of the frequency response [23, 27]. The steady-state response is characterized by the dynamic response at low angular frequencies. The control system needs to provide an integral term in order to eliminate steady-state control error resulting from steps in the desired value or disturbance. The integral term has to be located before the entry point of the disturbance to ensure steady-state accuracy [27].

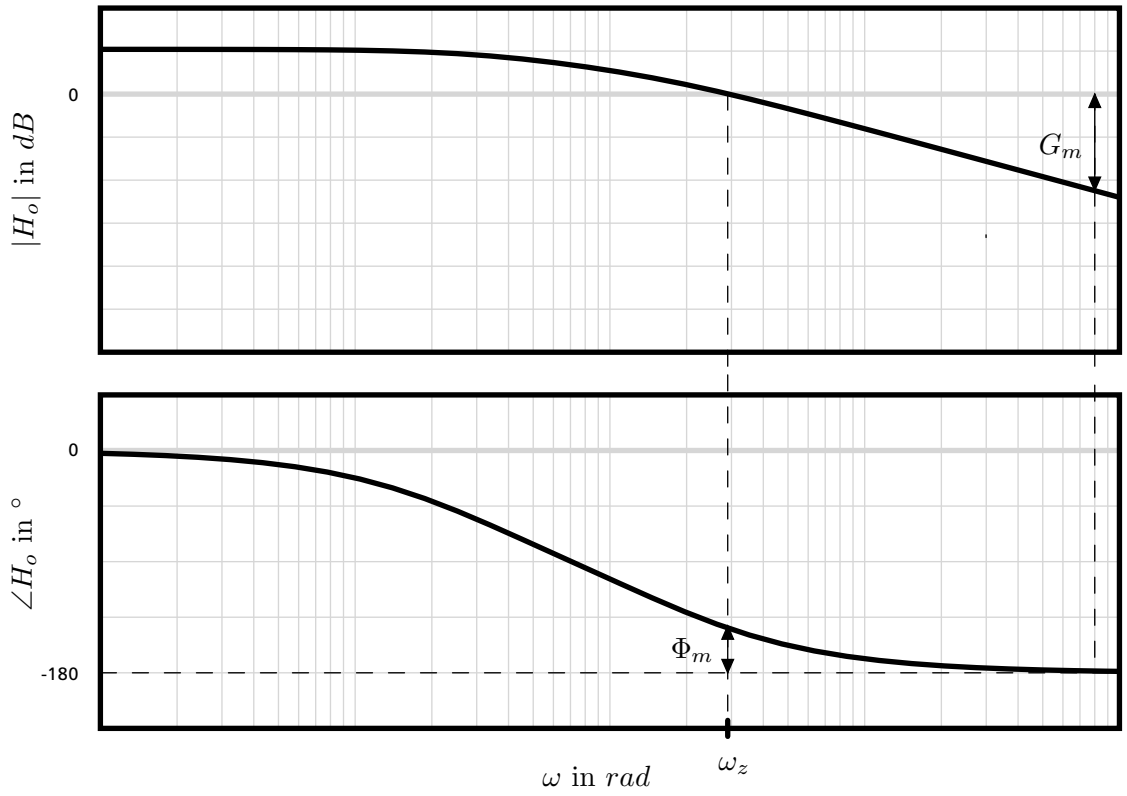

Figure 5.11.: Characteristic values of loop-shaping control.

In loop-shaping control, the desired control action is achieved by shaping the transfer characteristics of the open-loop system. This is done by adjusting the linear transfer function of the feedback controller H_k that corresponds to a rational function. In the control design process, the zeros and poles of the controller transfer function H_k are strategically placed to compensate undesired characteristics of the controlled system or to set desired characteristics of the feedback control. While a pole generates a negative gain slope of -20 decibel per decade and lowers the phase by 90 degrees, a zero produces a positive gain slope of 20 decibel per decade and increases the phase by 90 degrees. A single pole placed at the origin gives the integral term that is required for steady-state accuracy. For the compensation of undesired characteristics of the controlled system, lead and lag compensators are used. Both compensators are zero-pole pairs that are used to shift poles or zeros of the controlled system and manipulate the progression of the phase. A lead compensator with the transfer function H_i specified by

$$H_i(s) = \frac{T_1\, s + 1}{T_2\, s + 1} \quad \text{with} \quad T_1 = \frac{1}{\omega_1} > T_2 = \frac{1}{\omega_2} \tag{5.69}$$

increases the phase between the angular frequencies ω_1 and ω_2 and reduces the gain for low frequencies. This characteristic resembles a delayed differential term with enhancing the phase margin Φ_m and lowering control variable overshoot. A lag compensator with the transfer function H_d defined by

$$H_d(s) = \frac{T_1\, s + 1}{T_2\, s + 1} \quad \text{with} \quad T_1 = \frac{1}{\omega_1} < T_2 = \frac{1}{\omega_2} \tag{5.70}$$

has an integral characteristic and decreases the phase between the angular frequencies ω_1 and ω_2. This property results in an increased gain at low angular frequencies with improved steady-state accuracy. By applying a reasonable combination of poles, zeros and lead or lag compensators, the open-loop

frequency response can be matched to the desired design requirements. For ensuring a causal control system, the number of poles has to be equal to or greater than the number of zeros. As a consequence of these properties, loop-shaping control is not restricted to a specific controller structure and outperforms conventional proportional–integral–derivative controllers in adaptability and scope of operation [27].

In controlled systems with existing input signal saturation, the integral term that provides steady-state accuracy can affect the performance and stability of the control system. If the control signal exceeds the saturation of the input signal, the feedback is effectively suspended and the residual control error is continuously integrated over time. This causes internal controller states to wind up with possibly transcending acceptable limits. After leaving the input signal saturation, the aggregated state values need to be unwound before the feedback controller returns to desired operation. The resulting delayed control action can provoke control variable overshoot up to instability. In order to avoid this adverse effect on the control system, the linear feedback controller has to be extended by a nonlinear anti-windup scheme. The anti-windup scheme prevents internal controller states from winding up and restrains the development of control variable oscillation. The extended control system has a nonlinear control law that provides a stable control action and adequate performance in the case of input signal saturation [2].

5.5.2.1 Tracking Control Structure

For providing an effective loop-shaping control for trajectory tracking, the loop-shaped feedback control is augmented by an external feedforward control. This feedforward control provides a compensation of known disturbances and a pilot control for desired motion values, while the feedback control eliminates uncompensated control errors. Steady-state accuracy and repeatability of the control system is guaranteed by an integral term in the feedback control law that necessitates the application of an anti-windup scheme. By utilizing the instantaneous control action of a feedforward control and the error compensation of a feedback control, this tracking control approach ensures high performance along with offset-free tracking for a controlled system with input signal saturation.

The additional anti-windup scheme modifies the control law and stability characteristics of the control system. For open-loop unstable linear systems, stability of anti-windup control is restricted to a local region in state space. Recent methodical anti-windup approaches address the maximization of this local

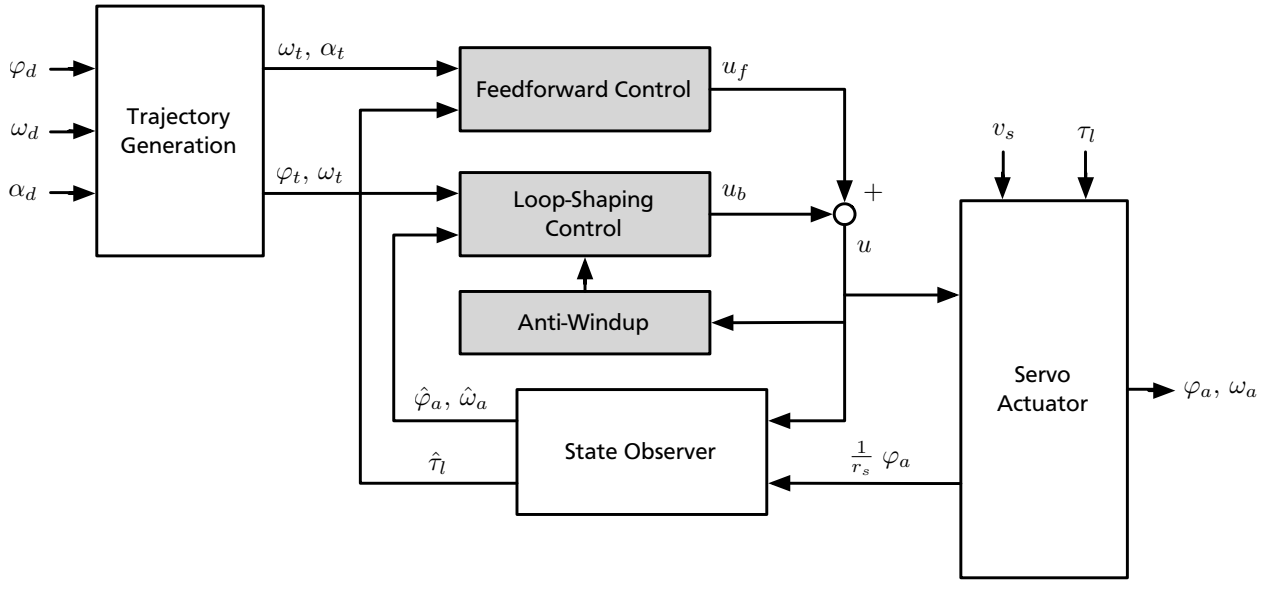

Figure 5.12.: Structure of the loop-shaping control for trajectory tracking.

stability region with preserving performance characteristics. The presented anti-windup approaches are sensitive to the initialization and do not allow for variable input signal saturation [16, 55]. For this reason, a conditional anti-windup approach that is widely used in practical implementations is applied in the tracking control. The feedback control law is conditionally modified by deactivating the integral term in the event of a saturated input signal and reactivating the integral term after the input signal saturation is left. This procedure prevents saturation-related development of control variable oscillation and ensures steady-state accuracy in unsaturated operation. A general stability region is difficult to define, because of the conditional character of the anti-windup approach. This restriction necessitates the validation of stability by simulation and empirical testing.

The introduced loop-shaping control for trajectory tracking is applied in the design of the angular position and speed control of both servo actuator types. The desired trajectory is provided by the trajectory generation and the disturbance is estimated by the state observer. Due to the intended implementation on the digital processing unit of the electronic setup, the tracking control is designed by using digital control methods. Figure 5.12 shows a functional diagram of the loop-shaping control structure for trajectory tracking. For the design and simulation of the loop-shaping control, the numerical computing environment MATLAB/SIMULINK developed by MathWorks is used.

5.5.2.2 Angular Position Control

The design of the loop-shaping control for angular position tracking is based on a linear and time-invariant transfer function of the servo actuators. The input is given by the armature voltage of the servo motor v_m and the output is the angular position of the servo actuator φ_a. With the Laplace-transformed input variable V_m and output variable Φ_a and by setting the initial values to zero, the Laplace-transformed continuous-time transfer function of the controlled system is defined by

$$H_{p,c}(s) = \frac{\Phi_a(s)}{V_m(s)} = \frac{\frac{r_g\, k_\tau}{R_m\, \Theta_a}}{s\left(s + \frac{r_g^2\, k_\tau}{k_\omega\, R_m\, \Theta_a}\right)}. \tag{5.71}$$

By inserting the parameters of the DD-28 and DD-64 servo actuators specified in Appendix A, the corresponding continuous-time transfer functions result in

$$H_{p,c,28}(s) = \frac{70}{s\,(s+134)}, \qquad H_{p,c,64}(s) = \frac{52}{s\,(s+138)}.$$

Both servo actuator types feature an IT_1 characteristic with a pole at the origin and a pole at 134 radians per second for the DD-28 servo actuator or 138 radians per second for the DD-64 servo actuator. The pole at the origin indicates that the controlled system is critically stable with an infinitely growing angular position φ_a for any nonzero constant armature voltage v_m.

In order to consider the discrete-time implementation of the tracking control on the digital processing unit, the continuous-time transfer function is transformed to the appertaining discrete-time transfer function. The discrete-time representation regards the transfer characteristic resulting from the discrete sampling of measurement values and the processing of the control algorithm with the sampling time T_s. The discrete-time transfer function is determined by applying the Z-transformation with a zero-order hold on the continuous-time transfer function. For ensuring an adequate dynamic response relative to the dynamics of the controlled system, the tracking control of both servo actuator types operates with a sampling time T_s of 1 millisecond. The corresponding discrete-time transfer functions are given by

$$H_{p,d,28}(z) = \frac{34\cdot 10^{-6}\, z + 32\cdot 10^{-6}}{z^2 - 1.9\, z + 0.9}, \qquad H_{p,d,64}(z) = \frac{25\cdot 10^{-6}\, z + 24\cdot 10^{-6}}{z^2 - 1.9\, z + 0.9}.$$

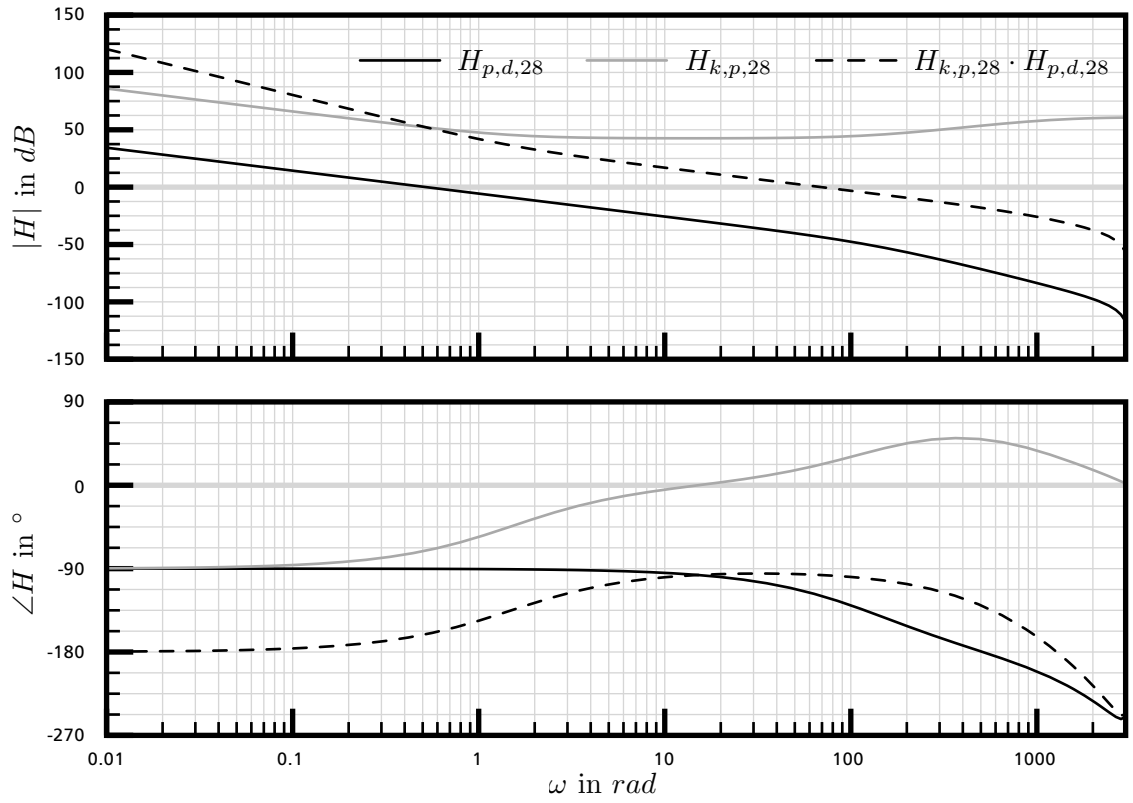

Figure 5.13.: Bode plot of the DD-28 servo actuator for angular position tracking.

A detailed derivation of the continuous-time and discrete-time transfer functions can be found in Appendix C.

Exemplary, the design process of the loop-shaping control for angular position tracking is performed for the DD-28 servo actuator. The design parameters for the DD-64 servo actuator follow from similar considerations. Figure 5.13 presents the frequency response of the controlled system $H_{p,d,28}$. For low angular frequencies, the pole at the origin dominates the progression of the gain resulting in a negative slope of about -20 decibel per decade. At an angular frequency of 134 radians per second, the gain has a break point and the phase drops with about 90 degrees per second. The cross-over frequency $\tilde{\omega}_{z,p,28}$ is given by 0.5 radians per second indicating a low system bandwidth and dynamic response to disturbances. In order to provide improved performance characteristics and assure offset-free tracking, the transfer function of the feedback controller $H_{k,p,28}$ is designed to enhance the system bandwidth by shifting the break point of the gain and eliminate residual control error by introducing an integral term. The resulting gain margin $G_{m,p,28}$ is to be greater that 12 decibel and the phase margin $\Phi_{m,p,28}$ needs to exceed 70 degrees. These design requirements are met by applying a pole, a zero and a lead compensator.

The disturbances of the servo actuator are mainly caused by load and friction torque. The integral term of the controlled system is located behind the entry point of this type of disturbance and is not able to remove residual control error. For this reason, a preceding integral term is integrated into the feedback controller by placing the pole at the origin. The resulting drop of the phase is rejected with the zero placed at 1.5 radians per second. The lead compensator is used to move the break point to a higher angular frequency to increase the system bandwidth. The zero of the lead compensator cancels out the pole of the controlled system and is placed at 134 radians per second. The pole of the lead compensator defines the shifted break point and is placed at 1200 radians per second. The control gain further

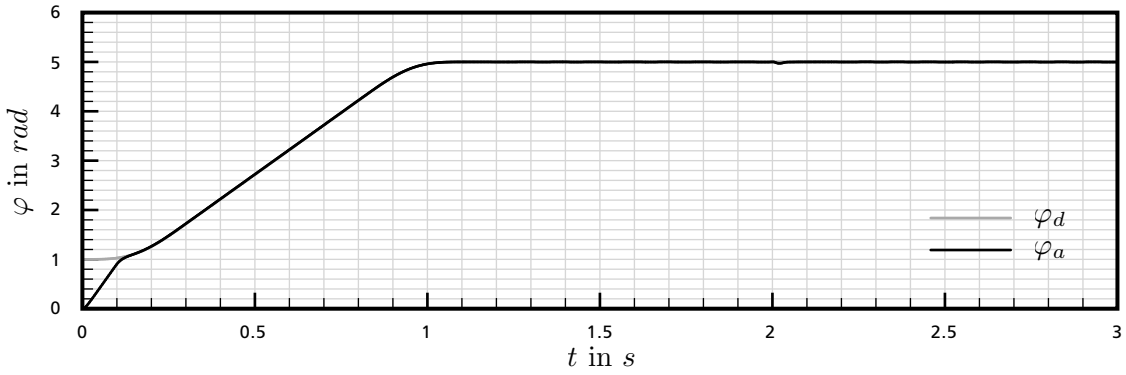

(a) Progression of the angular position with $\varphi_d = 5\ rad$, $\omega_d = 5\ \frac{rad}{s}$ and $\alpha_d = 30\ \frac{rad}{s^2}$.

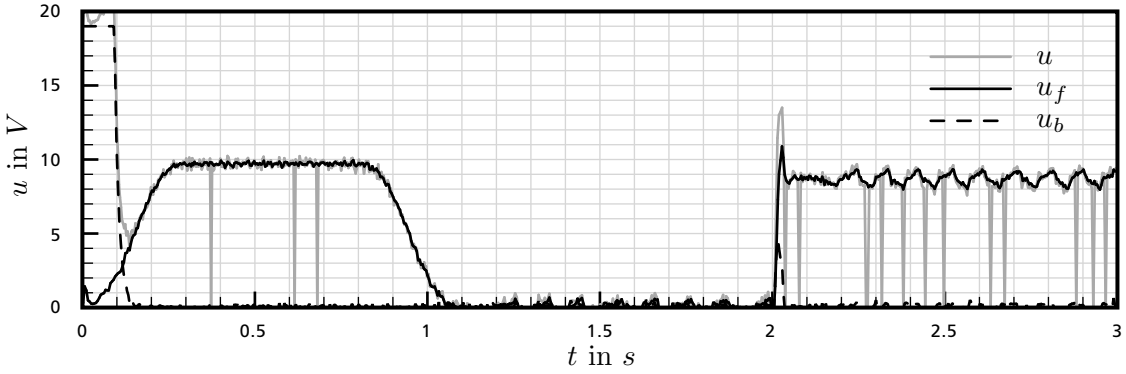

(b) Progressions of the control signals with $\varphi_d = 5\ rad$, $\omega_d = 5\ \frac{rad}{s}$ and $\alpha_d = 30\ \frac{rad}{s^2}$.

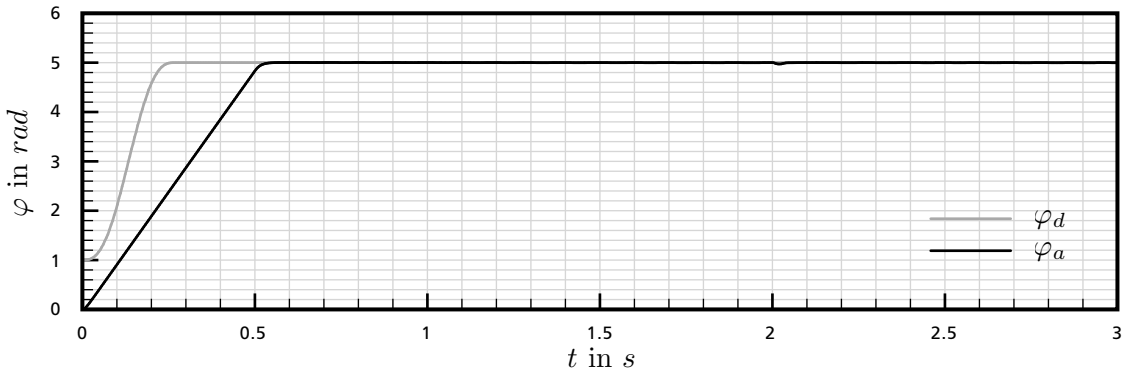

(c) Progression of the angular position with $\varphi_d = 5\ rad$, $\omega_d = 15\ \frac{rad}{s}$ and $\alpha_d = 100\ \frac{rad}{s^2}$.

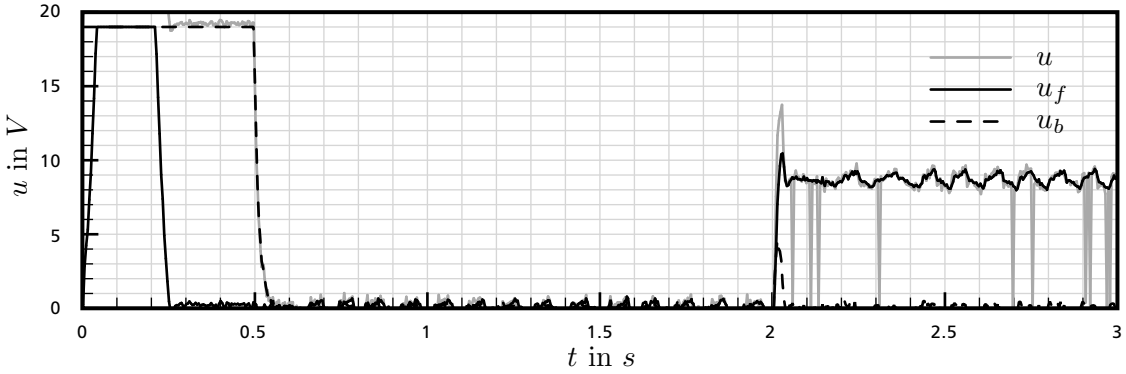

(d) Progressions of the control signals with $\varphi_d = 5\ rad$, $\omega_d = 15\ \frac{rad}{s}$ and $\alpha_d = 100\ \frac{rad}{s^2}$.

Figure 5.14.: Performance of the loop-shaping position control of the DD-28 servo actuator.

increases the dynamic response and is set to 744.3. With these specifications, the transfer function of the feedback controller $H_{k,p,28}$ results in

$$H_{k,p,28}(z) = 744.3 \, \frac{\left(z - e^{-1.5T_s}\right) \, \left(z - e^{-134T_s}\right)}{\left(z - 1\right) \, \left(z - e^{-1200T_s}\right)}. \tag{5.72}$$

The open-loop system has a gain margin $G_{m,p,28}$ of 29.3 decibel and a phase margin $\Phi_{m,p,28}$ of 87.1 degrees. The cross-over frequency $\omega_{z,p,28}$ is shifted to 69.6 radians per second. The frequency responses of the feedback controller and the open-loop system are plotted in Figure 5.13. The transfer function of the applied anti-windup scheme $\bar{H}_{k,p,28}$ is obtained by removing the pole at the origin and the balancing zero at 1.5 radians per second. Changes on the characteristic values are perceived to be marginal. The transfer function with activated anti-windup scheme $\bar{H}_{k,p,28}$ is given by

$$\bar{H}_{k,p,28}(z) = 744.3 \, \frac{\left(z - e^{-134T_s}\right)}{\left(z - e^{-1200T_s}\right)}. \tag{5.73}$$

The loop-shaping control for angular position tracking of both servo actuator types is designed with emphasis on an expeditious dynamic response and compensation of residual control error. In order to evaluate the control action, the loop-shaping control of the DD-28 servo actuator is simulated with an extensive nonlinear model. Figure 5.14 presents the progressions of the angular position and the saturated control signals for two different desired angular speeds and accelerations. The simulations engender unsaturated and saturated operation of the servo actuator. For demonstration, the initial deviation of the angular position is set to a relatively high value of 1 radian. The armature voltage has a constant value of 19 volts. After 2 seconds, a load torque of 2 newton meters is applied on the simulated servo actuator. In unsaturated operation, the initial deviation is compensated with taking advantage of the full input signal range and the desired trajectory is tracked without any offset. In saturated operation, the control system acts similar to a two-step control and reaches the desired angular position in nearly optimal time without any overshoot. The applied load torque is immediately rejected by the feedforward control and the resulting deviation of the angular position is promptly corrected by the feedback control. The overall performance of the control action is characterized by an optimal trajectory tracking and a reactive disturbance compensation with high steady-stated accuracy. All applied design parameters and the resulting transfer functions of the feedback controllers are listed in Appendix E.

5.5.2.3 Angular Speed Control

The design of the loop-shaping control for angular speed tracking is based on a linear and time-invariant transfer function of the servo actuators. The input is given by the armature voltage of the servo motor v_m and the output is the angular speed of the servo actuator ω_a. With the Laplace-transformed input variable V_m and output variable Ω_a and by setting the initial values to zero, the Laplace-transformed continuous-time transfer function of the controlled system is defined by

$$H_{s,c}(s) = \frac{\Omega_a(s)}{V_m(s)} = \frac{\frac{r_g \, k_\tau}{R_m \, \Theta_a}}{s + \frac{r_g^2 \, k_\tau}{k_\omega \, R_m \, \Theta_a}}. \tag{5.74}$$

By inserting the parameters of the DD-28 and DD-64 servo actuators specified in Appendix A, the corresponding continuous-time transfer functions result in

$$H_{s,c,28}(s) = \frac{70}{s + 134} \qquad\qquad H_{s,c,64}(s) = \frac{52}{s + 138}.$$

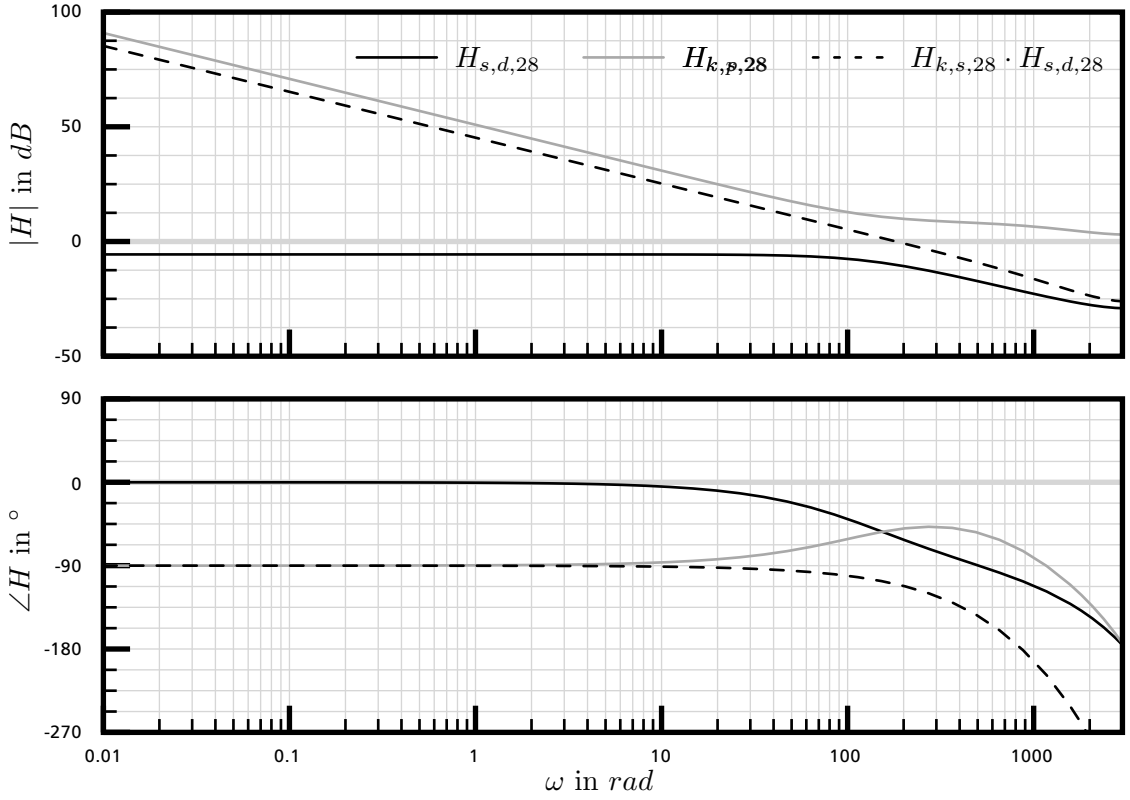

Figure 5.15.: Bode plot of the DD-28 servo actuator for angular speed tracking.

Both servo actuator types feature a PT_1 characteristic with a pole at 134 radians per second for the DD-28 servo actuator or 138 radians per second for the DD-64 servo actuator. The system is stable and responds with a constant angular speed ω_a for any constant armature voltage v_m.

In order to consider the discrete-time implementation of the tracking control on the digital processing unit, the continuous-time transfer function is transformed to the appertaining discrete-time transfer function. The discrete-time representation regards the transfer characteristic resulting from the discrete sampling of measurement values and the processing of the control algorithm with the sampling time T_s. The discrete-time transfer function is determined by applying the Z-transformation with a zero-order hold on the continuous-time transfer function. For ensuring an adequate dynamic response relative to the dynamics of the controlled system, the tracking control of both servo actuator types operates with a sampling time T_s of 1 millisecond. The corresponding discrete-time transfer functions are given by

$$H_{s,d,28}(z) = \frac{66 \cdot 10^{-3}}{z - 875 \cdot 10^{-3}}, \qquad H_{s,d,64}(z) = \frac{49 \cdot 10^{-3}}{z - 871 \cdot 10^{-3}}.$$

A detailed derivation of the continuous-time and discrete-time transfer functions can be found in Appendix C.

Exemplary, the design process of the loop-shaping control for angular speed tracking is performed for the DD-28 servo actuator. The design parameters for the DD-64 servo actuator follow from similar considerations. Figure 5.15 plots the frequency response of the controlled system $H_{s,d,28}$. The progression of the gain is constant at low angular frequencies and below the 0 decibel axis. For that reason, there is no cross-over frequency $\tilde{\omega}_{z,s,28}$ and the phase margin of the controlled system $\tilde{\Phi}_{m,s,28}$ is infinite. This condition meets the small gain theorem and the closed-loop system stays stable, even if the polarity of the feedback is changed [27]. The low gain is prejudicial for the dynamic response and affects the

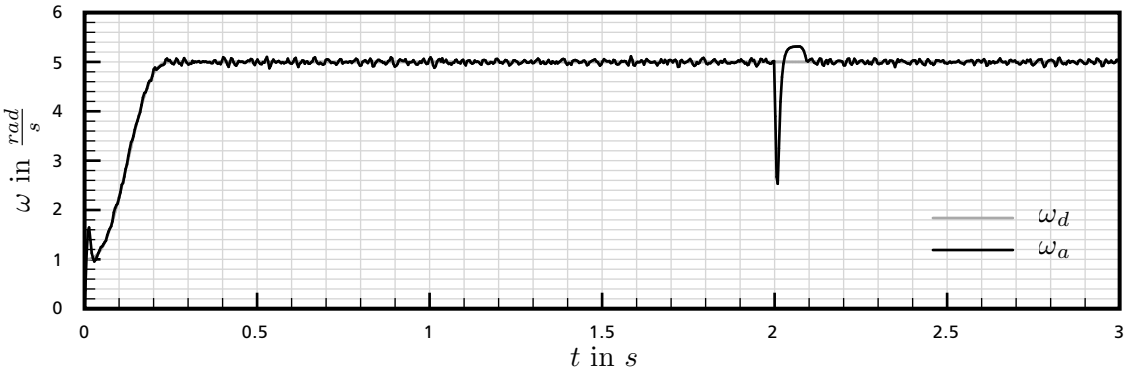

(a) Progression of the angular speed with $\omega_d = 5\ \frac{rad}{s}$ and $\alpha_d = 30\ \frac{rad}{s^2}$.

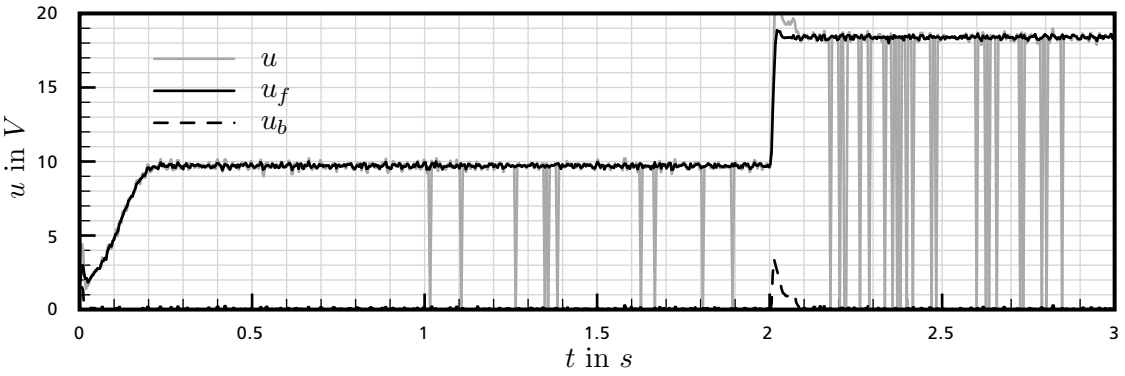

(b) Progressions of the control signals with $\omega_d = 5\ \frac{rad}{s}$ and $\alpha_d = 30\ \frac{rad}{s^2}$.

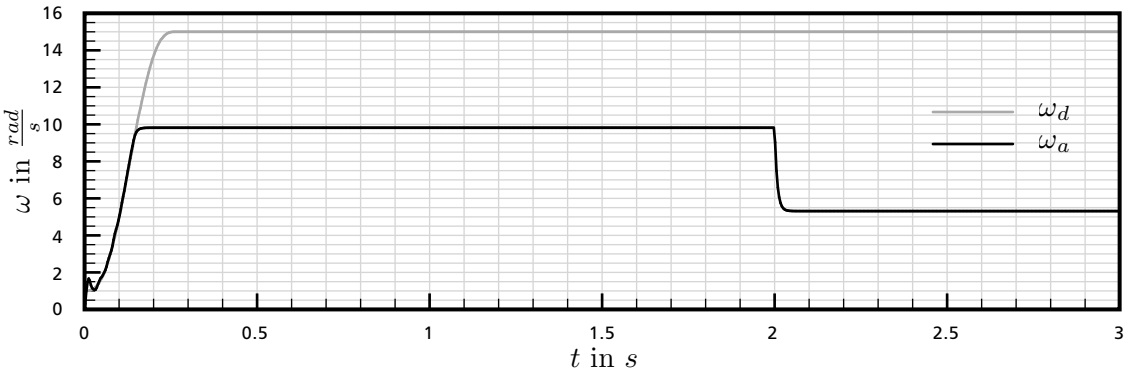

(c) Progression of the angular speed with $\omega_d = 15\ \frac{rad}{s}$ and $\alpha_d = 100\ \frac{rad}{s^2}$.

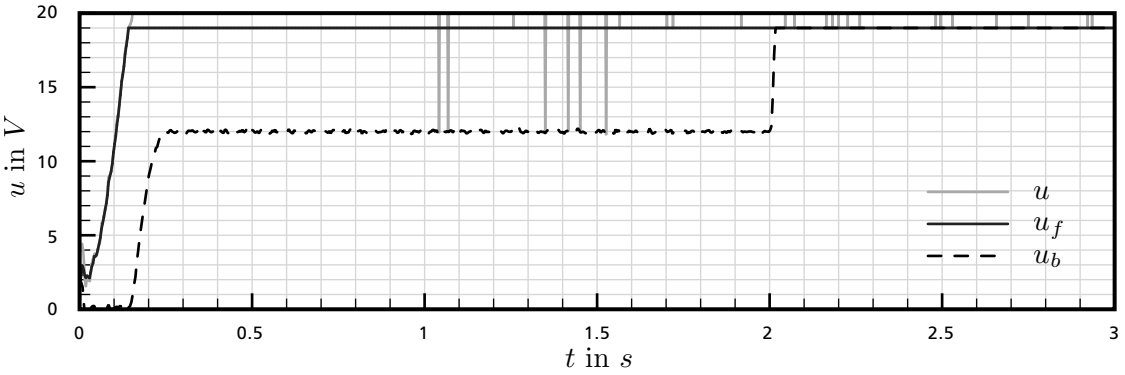

(d) Progressions of the control signals with $\omega_d = 15\ \frac{rad}{s}$ and $\alpha_d = 100\ \frac{rad}{s^2}$.

Figure 5.16.: Performance of the loop-shaping speed control of the DD-28 servo actuator.

performance and steady-state accuracy of the closed-loop system. At an angular frequency of 134 radians per second, the gain has a break point and the phase drops with about 90 degrees per decade. In order to provide improved performance characteristics and assure offset-free tracking, the transfer function of the feedback controller $H_{k,s,28}$ is designed to increase the gain and ensure an appropriate system bandwidth by shifting the break point of the gain. Residual control error is eliminated by introducing an integral term. The resulting gain margin $G_{m,s,28}$ is to be greater that 12 decibel and the phase margin $\Phi_{m,s,28}$ needs to exceed 70 degrees. These design requirements are met by applying a pole and a lead compensator.

The controlled system does not provide an integral term and is not able to remove residual deviations of the control variable caused by disturbances. This characteristic requires an integral term in the feedback controller that is obtained by placing the pole at the origin. For increasing the dynamic response, the control gain is set to 1.9 and the lead compensator is used to move the break point to a higher angular frequency. The zero of the lead compensator cancels out the pole of the controlled system and is placed at 134 radians per second. The pole of the lead compensator defines the shifted break point and is placed at 1200 radians per second. With these specifications, the transfer function of the feedback controller $H_{k,s,28}$ results in

$$H_{k,s,28}(z) = 1.9 \, \frac{\left(z - e^{-134T_s}\right)}{\left(z-1\right)\,\left(z - e^{-1200T_s}\right)}. \tag{5.75}$$

The open-loop system has a gain margin $G_{m,s,28}$ of 14.7 decibel and a phase margin $\Phi_{m,s,28}$ of 70.1 degrees. The cross-over frequency $\omega_{z,p,28}$ has a value of 181.9 radians per second. The frequency responses of the feedback controller and the open-loop system are presented in Figure 5.15. The transfer function of the applied anti-windup scheme $\bar{H}_{k,s,28}$ is determined by removing the pole at the origin. This modification results in a gain margin $\bar{G}_{m,s,28}$ of 20.1 decibel and an infinite phase margin $\bar{\Phi}_{m,s,28}$ in saturated operation. The transfer function with activated anti-windup scheme $\bar{H}_{k,s,28}$ is given by

$$\bar{H}_{k,s,28}(z) = 1.9 \, \frac{\left(z - e^{-134T_s}\right)}{\left(z - e^{-1200T_s}\right)}. \tag{5.76}$$

The loop-shaping control for angular speed tracking of both servo actuator types is designed with emphasis on an expeditious dynamic response and compensation of residual control error. In order to evaluate the control action, the loop-shaping control of the DD-28 servo actuator is simulated with an extensive nonlinear model. Figure 5.16 presents the progressions of the angular speed and the saturated control signals for two different desired angular speeds and accelerations. The simulations engender unsaturated and saturated operation of the servo actuator. For demonstration, the initial deviation of the angular speed is set to a relatively high value of 1 radian per second. The armature voltage has a constant value of 19 volts. After 2 seconds, a load torque of 2 newton meters is applied on the simulated servo actuator. In unsaturated operation, the initial deviation is compensated quickly by the feedforward control with a noticeable overshoot, while the desired trajectory is tracked without any offset. The applied load torque is rejected by the feedforward and feedback control. The compound control signal of both control types exceeds the input signal saturation and activates the anti-windup scheme. Resulting from the modification of the control law and the increased input signal, the feedback control generates an control variable overshoot. This effect shows the uncertain performance of the applied conditional anti-windup scheme. In saturated operation, the full input signal range is utilized and the actual angular speed is maximized at the specified armature voltage. The applied load torque causes an reduction of the actual angular speed that cannot be compensated due to input signal saturation. Because of the residual noise signal of the estimated angular speed, the control action is superimposed by a minor interference. The overall performance of the control action is characterized by an excellent trajectory tracking and a fast disturbance compensation with present overshoot. All applied design parameters and the resulting transfer functions of the feedback controllers are listed in Appendix E.

5.5.3 Evaluation

The introduced control approaches of angular position and speed control comprise a novel model predictive control for arbitrary trajectory tracking and a loop-shaping control with an conditional anti-windup scheme. Both control approaches apply a combined feedforward and feedback control to ensure high performance along with offset-free tracking for controlled systems with input signal saturation.

The presented model predictive control for angular position and speed tracking optimizes a quadratic performance index over the arbitrary desired trajectory with respect to input and state constraints. The applied terminal set and terminal constraint guarantee exponential stability over an extensive operating range. By considering the variable input constraint, an excellent utilization of the full input signal range is assured for maximizing the control rate. The explicit definition of the control law reduces the computational complexity by increasing the consumption of memory space. The generated explicit solution of the optimization problem forms an advanced and effective control system for the specific control problem. Any subsequent modifications of the process parameters or desired control action require a complete recomputation and revised implementation of the control algorithm.

The presented loop-shaping control approach for angular position and speed tracking provides an expeditious control action with an attuned transfer characteristic and a conditional anti-windup scheme for considering input signal saturation. The attained phase and gain margins are dimensioned for a reactive dynamic response without any overshoot of the control variable and a robust stability considering parameter variations. With the enhanced system bandwidth, the control system is able to reject fast changing disturbances in unsaturated operation, while the applied anti-windup scheme prevents the development of control variable oscillation in the event of input signal saturation. The undefined stability region of the anti-windup scheme is an element of uncertainty and has to be verified in practical application. The low computational complexity of the control law allows a further reduction of the sampling time to improve the transfer characteristics of the control system. For adjusting the control action to changed process parameters or performance requirements, characteristic control parameters can be modified subsequently without adapting the implementation of the control algorithm.

In the simulation of the control action in saturated an unsaturated operation, both control approaches demonstrate an excellent trajectory tracking with high steady-state accuracy. The model predictive control features a fast rejection of initial deviations and disturbances. In angular position control, the desired trajectory is tracked without any offset, while the compensation of the initial deviation in angular speed control causes a slight overshoot. The loop-shaping control provides an immediate control action with eliminating the control error in nearly optimal time. The angular position control supports an offset-free trajectory tracking, while the angular speed control is impaired by a noticeable overshoot when compensating the initial deviation and the disturbance. The overshoot of both control approaches in angular speed control results from a delayed estimation of the actual angular speed by the state observer. This effect is increased by the high control rates and the conditional anti-windup scheme of the loop-shaping control. The emerging deviation of the control variable is eliminated quickly and does not affect the overall performance of the control systems.

Both control approaches comply with the defined requirements for the control design and are suitable for an application in the DD-28 and DD-64 servo actuators. The model predictive control approach ensures a stable operation with consistent performance, but has a high memory consumption and is inflexible regarding subsequent modifications. The loop-shaping control approach provides a flexible and comprehensible control law with an expeditious control action and low demands in computing power, but has an uncertain stability region. For a final verification of the simulation results and an analysis of the uncertain stability characteristic of the loop-shaping control approach, both control approaches needs to be implemented and tested on the actual servo actuators.

6 Conclusion

The upcoming chapter summarizes the results and findings of this thesis and points to further development and improvements in control design.

6.1 Results

In the course of this thesis, improved electronics and advanced control for the RX-28 and RX-64 servo actuators of the Dynamixel series produced by Robotis were developed and evaluated. By applying the designed electronic setup and control concept, the enhanced DD-28 and DD-64 servo actuators become universal and capable drives for robotic applications with an increased performance and durability.

The initial analysis of the original RX-28 and RX-64 servo actuators revealed the deficiencies of the implemented electronic setup and control concept. The vulnerability of the original electronic setup was traced to the limited angular operating range and durability of the position senor, the low computing power of the processing unit and the inefficiency of the voltage regulator. The survey of the original control concept exposed the varying accuracy and restricted adjustability of the angular position feedback control as well as the constricted applicability of the angular speed feedforward control.

In the design process of the enhanced electronic setup, the deficient components were replaced considering the specifications, dimensions and interfaces of the original servo actuators. The applied position sensor provides a wearless operation and quadruples the theoretical resolution of the angular position measurement. These properties increase the durability of the servo actuator and ensure an accurate determination of the actual angular position and speed. For the implementation of an advanced control and firmware concept, the used processing unit offers high computing power and additional memory space. The symbol rate of the communication interface was enhanced in order to provide a fast and a reliable networked operation of multiple servo actuators. The applied switched-mode voltage regulator supports an extended supply voltage range and decreases the overall power consumption with reducing the thermal load of adjacent components.

In the design process of the enhanced control concept, a tracking control with a highly adjustable desired trajectory was introduced for the individual control of the angular position and speed. The applied trajectory generation allows to modify the desired trajectory for customizing the actuator motion and controlling the acceleration and deceleration characteristics. Based on the measured actual angular position, a model-based state observer estimates the actual angular speed, load torque and armature current. For the implementation of the tracking control, a novel model predictive control approach was introduced and compared to a competitive loop-shaping control with a conditional anti-windup scheme. Both control approaches regard the saturation of the input signal and apply a combined feedforward and feedback control to ensure high performance along with offset-free tracking.

The introduced model predictive control approach is a universal and efficient tracking control strategy for variably constrained systems. The modified finite optimization problem ensures optimal performance and exponential stability. By including the future progression of the desired trajectory into the constrained state space of the optimization problem, offset-free tracking is guaranteed for any type of trajectory. This characteristic generalizes offset-free tracking in model predictive control for the case of arbitrary motion.

The designed control systems were simulated using an extensive model of the servo actuators and evaluated by the characteristics of the control action. According to the simulation results of unsaturated and

saturated operation, both control systems provide an excellent trajectory tracking with high steady-state accuracy. In angular speed control, the compensation of initial deviations and disturbances results in a present overshoot caused by a delayed estimation of the actual angular speed by the state observer. This overshoot is eliminated quickly and does not affect the overall performance of the control systems. For a final verification of the simulation results, both control systems needs to be implemented and tested on the actual DD-28 and DD-64 servo actuators.

6.2 Outlook

With the introduced electronic setup and control concept, the enhanced DD-28 and DD-64 servo actuators become universal drives with an advanced angular position and speed control. The extended configuration of the servo actuators provides an effective and flexible environment for further development and improvements in control design. The subsequent development of the control concept can be subdivided into a verification and readjustment of the developed control systems and an extension with further enhancements.

The control concept was developed and simulated by applying a sophisticated mathematical model of the servo actuators. This design procedure considers a quite accurate but not exact representation of the actual controlled system. For a final verification of the simulation results, the control concept needs to be implemented and tested in practical application and under controlled conditions.

An important test objective is the actual stability and overshoot characteristic of the loop-shaping control with conditional anti-windup scheme in saturated operation. To verify the simulation results, the actual steady-state accuracy and repeatability of both control approaches need to be tested over a wide range of disturbance conditions. The obtained test results are to be used to improve the correspondence of the process model and actual controlled system. The improved model allows to validate and readjust the control parameters of the control approaches resulting in an enhanced control action. Further test objectives cover the influence of parameter variations and the temperature dependency of the operating performance and control action.

The introduced control concept provides an adjustable angular position and speed control and an comprehensive set of operating data. The extended configuration of the servo actuators allows to integrate further enhancements to expand the field of application and improve the performance characteristics.

A possible extension of the control system is the implementation of torque control by applying the estimated load torque of the state observer. The control of torque allows robotic applications to interact with surrounded objects and respect actual contact forces. The prevention of exceeding contact forces enables the operation and manipulation of objects in sensitive and fragile configurations. This ability permits the adaptation to various environments and extends the range of application to complex positioning and manipulation problems.

A possible extension of the safety measures is the augmentation of the state observer by a temperature model of the servo motor. By taking the thermodynamic characteristics into consideration, the estimated armature temperature gives a better overview on the actual operating condition than the indirect measurement of the temperature sensors. The progression of the estimated armature temperature indicates an exceedance of the specified operating temperature in better time and can be used to take countermeasures at an early stage. This procedure prevents enduring damages and increases the durability of the servo actuator.

A Servo Actuator Parameters

The parameters of the DD-28 and DD-64 servo actuators combine the electrical and mechanical parameters of the servos motors, the gearboxes and the angular position sensors that are used in the modeling of the servo actuator in Appendix C. The friction parameters and the gearbox backlash are approximated values based on empirical analysis. A description of the estimation method of the friction parameters and the derivation of the friction model is presented in Appendix D. The calculation of the gearbox inertia and gearbox ratio parameters can be found in Appendix B.

Table A.1.: Parameters of DD-28 and DD-64 servo actuators [9, 33, 34].

	Symbol	Unit	**DD-28** (Robotis/SIM)	**DD-64** (Robotis/SIM)
Servo motor speed constant	k_ω	$\frac{rad}{Vs}$	100.7	74.9
Servo motor torque constant	k_τ	$\frac{mNm}{A}$	9.9	13.4
Armature inertia	Θ_m	kgm^2	$86.4 \cdot 10^{-9}$	$217.0 \cdot 10^{-9}$
Armature inductance	L_m	mH	0.2	0.2
Armature resistance	R_m	Ω	8.3	6.3
Gearbox inertia	Θ_g	kgm^2	$79.6 \cdot 10^{-6}$	$154.9 \cdot 10^{-6}$
Gearbox ratio	r_g		192.6	199.6
Gearbox backlash	φ_b	$mrad$	5.0	5.0
Sensor resolution	r_s	rad	$2\,\pi \cdot 2^{-12}$	$2\,\pi \cdot 2^{-12}$
Sensor noise variance	σ_n^2	$mrad^2$	0.3	0.3
Static friction constant	k_s	mNm	78.1	186.8
Kinetic friction constant	k_k	mNm	13.0	31.1
Viscous friction constant	k_v	$mNms$	4.1	9.9

B Gearbox Parameters

The gearboxes of the DD-28 and DD-64 servo actuators consist of two single and four double spur gears made of steel, brass or aluminum. The gears are approximated as solid cylinders with the diameter d_g and the height h_g. In order to take drill holes, gear notches, the attached magnet mounting and the magnet of the angular position sensor into account, rectified dimensions are derived from the overall dimensions. The dimensions, inertia and number of teeth of the individual gears are listed in the tables B.1 and B.2.

Table B.1.: Gear specifications of DD-28 servo actuators.

#	Teeth	Material	$\mathbf{d_{g,overall}}$ in mm	$\mathbf{d_{g,rectified}}$ in mm	$\mathbf{h_{g,overall}}$ in mm	$\mathbf{h_{g,rectified}}$ in mm	$\boldsymbol{\Theta_i}$ in kgm^2
1	13	steel	5.0	4.0	3.0	3.0	$5.93 \cdot 10^{-10}$
2	12 / 31	brass	4.5 / 10.0	3.5 / 9.0	2.4 / 1.2	2.4 / 1.2	$6.79 \cdot 10^{-9}$
3	13 / 40	brass	5.0 / 12.7	4.0 / 11.7	2.6 / 1.2	2.6 / 1.2	$19.09 \cdot 10^{-9}$
4	12 / 39	steel	5.8 / 12.7	4.8 / 11.7	2.8 / 1.7	2.8 / 1.7	$25.76 \cdot 10^{-9}$
5	13 / 28	steel	6.4 / 12.3	5.4 / 11.3	5.2 / 1.9	5.2 / 1.9	$27.35 \cdot 10^{-9}$
6	45	aluminum	19.4 / 6.0	18.4 / 6.0	4.0 / 13.4	3.0 / 15.4	$96.44 \cdot 10^{-9}$

Table B.2.: Gear specifications of DD-64 servo actuators.

#	Teeth	Material	$\mathbf{d_{g,overall}}$ in mm	$\mathbf{d_{g,rectified}}$ in mm	$\mathbf{h_{g,overall}}$ in mm	$\mathbf{h_{g,rectified}}$ in mm	$\boldsymbol{\Theta_i}$ in kgm^2
1	13	steel	5.0	4.0	3.0	3.0	$5.93 \cdot 10^{-10}$
2	13 / 48	steel	4.8 / 15.4	3.8 / 14.4	2.5 / 1.3	2.5 / 1.3	$43.6 \cdot 10^{-9}$
3	13 / 50	steel	6.4 / 11.0	5.4 / 10.0	2.5 / 1.6	2.5 / 1.6	$14.0 \cdot 10^{-9}$
4	13 / 35	steel	7.8 / 11.7	6.8 / 11.2	2.8 / 1.9	2.8 / 1.9	$20.52 \cdot 10^{-9}$
5	14 / 25	steel	8.5 / 14.3	7.5 / 13.3	5.2 / 2.0	5.2 / 2.0	$61.06 \cdot 10^{-9}$
6	38	aluminum	20.8 / 9.0	19.8 / 9.0	5.0 / 15.0	3.5 / 17.0	$172.16 \cdot 10^{-9}$

The inertia of the individual gears Θ_i is calculated by applying the mass densities ρ_{steel} of 7870 kilogram cubic meters, ρ_{brass} of 8400 kilogram cubic meters and $\rho_{aluminum}$ of 2700 kilogram cubic meters [4] and the rectified dimensions

$$\Theta_{i,single} = \frac{1}{32}\,\pi\,\rho\,h\,d^4 \tag{B.1}$$

$$\Theta_{i,double} = \frac{1}{32}\,\pi\,\rho\,(h_1\,d_1^4 + h_2\,d_2^4) \tag{B.2}$$

The gearbox ratio r_g is composed of the product of the subordinate gear ratios of the engaged single and double gears. With the specified numbers of teeth, the subordinate gear ratios of the DD-28 type $r_{ij,28}$ result in

$$r_{12,28} = \frac{31}{13} \tag{B.3}$$

$$r_{23,28} = \frac{40}{12} \tag{B.4}$$

$$r_{34,28} = \frac{39}{13} \tag{B.5}$$

$$r_{45,28} = \frac{28}{12} \tag{B.6}$$

$$r_{56,28} = \frac{45}{13} \tag{B.7}$$

$$r_{46,28} = r_{45,28}\,r_{56,28} = 8.1 \tag{B.8}$$

$$r_{36,28} = r_{34,28}\,r_{45,28}\,r_{56,28} = 24.2 \tag{B.9}$$

$$r_{26,28} = r_{23,28}\,r_{34,28}\,r_{45,28}\,r_{56,28} = 80.8 \tag{B.10}$$

The gearbox ratio of the DD-28 type $r_{g,28}$ results from the subordinate gear ratios $r_{ij,28}$ and is given by

$$r_{g,28} = r_{16,28} = r_{12,28}\,r_{23,28}\,r_{34,28}\,r_{45,28}\,r_{56,28} = 192.6 \tag{B.11}$$

With the specified numbers of teeth, the subordinate gear ratios of the DD-64 type $r_{ij,64}$ result in

$$r_{12,64} = \frac{48}{13} \tag{B.12}$$

$$r_{23,64} = \frac{50}{13} \tag{B.13}$$

$$r_{34,64} = \frac{35}{13} \tag{B.14}$$

$$r_{45,64} = \frac{25}{13} \tag{B.15}$$

$$r_{56,64} = \frac{38}{14} \tag{B.16}$$

$$r_{46,64} = r_{45,64}\, r_{56,64} = 5.2 \tag{B.17}$$

$$r_{36,64} = r_{34,64}\, r_{45,64}\, r_{56,64} = 14.1 \tag{B.18}$$

$$r_{26,64} = r_{23,64}\, r_{34,64}\, r_{45,64}\, r_{56,64} = 54.1 \tag{B.19}$$

The gearbox ratio of the DD-64 type $r_{g,64}$ results from the subordinate gear ratios $r_{ij,64}$ and is given by

$$r_{g,64} = r_{16,64} = r_{12,64}\, r_{23,64}\, r_{34,64}\, r_{45,64}\, r_{56,64} = 199.6 \tag{B.20}$$

The gearbox inertia Θ_g is obtained by summing up the inertias of the gears weighted with the subordinate gear ratios. The gearbox inertias of both servo actuator types $\Theta_{g,28}$ and $\Theta_{g,64}$ result in

$$\begin{aligned}\Theta_{g,28} &= \Theta_{1,28}\, r_{16,28}^2 + \Theta_{2,28}\, r_{26,28}^2 + \Theta_{3,28}\, r_{36,28}^2 + \Theta_{4,28}\, r_{46,28}^2 + \Theta_{5,28}\, r_{56,28}^2 + \Theta_{6,28} \\ &= 79.6 \cdot 10^{-6}\ kgm^2\end{aligned} \tag{B.21}$$

$$\begin{aligned}\Theta_{g,64} &= \Theta_{1,64}\, r_{16,64}^2 + \Theta_{2,64}\, r_{26,64}^2 + \Theta_{3,64}\, r_{36,64}^2 + \Theta_{4,64}\, r_{46,64}^2 + \Theta_{5,64}\, r_{56,64}^2 + \Theta_{6,64} \\ &= 154.9 \cdot 10^{-6}\ kgm^2\end{aligned} \tag{B.22}$$

C Servo Actuator Model

The modeling of the DD-28 and DD-64 servo actuators provides a mathematical description of the controlled system that is used for the design and simulation of the control system in Chapter 5. In order to consider different requirements in structure and complexity, separate process models for the simulation, state observer and control design are introduced. The extensive model applied in the simulation process is a comprehensive representation of the controlled system including nonlinearities and disturbances. The reduced models used in the control and state observer design neglect disturbances and are derived by assuming a linear transfer characteristic of the controlled system with time-invariant parameters. For enabling the differentiated modeling, the modeling process is divided into the derivation of a linear model and a set of nonlinear model extensions.

The controlled system of both servo actuator types consists of the electronic and mechanical setup of the drive section. The control voltage actuates the servo motor driver that is powered by the power supply and provides the armature voltage of the servo motor. In this process, the absolute value of the armature voltage is restricted by the supply voltage resulting in a saturation of the input signal. The servo motor converts the provided armature voltage into an angular motion that is transformed by the gearbox. Caused by the clearance of the individual gears, the gearbox has a backlash that affects the progression of the controlled variable. The position sensor measures the actual angular position by applying a quantization in time and value on the measurand. Figure C.1 shows a functional diagram of the controlled system with the related system variables.

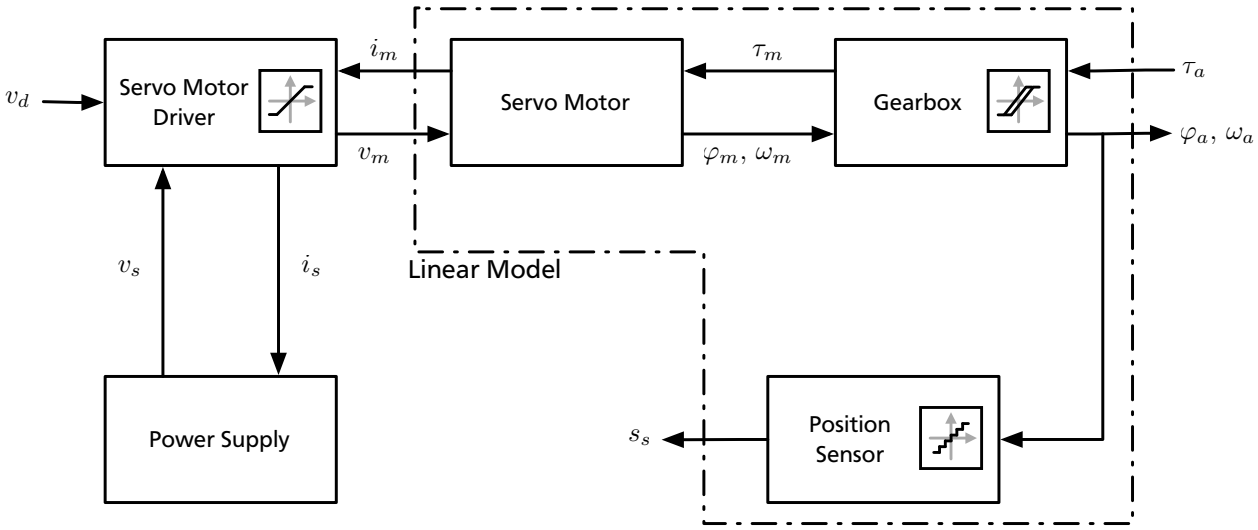

Figure C.1.: Functional diagram of the controlled system.

C.1 Linear Model of the Controlled System

The linear model of the controlled system describes the linear characteristic of the servo motor, gearbox and position sensor. The input variable is given by the armature voltage of the servo motor and results in the angular motion of the servo actuator given by the output variable that is measured by the position sensor. For simplifying the modeling process, the gears and shafts of the drive train are assumed to be rigid and the influence of temperature on the electronic and mechanical configuration is neglected. Figure C.2 presents the structure of the linear model.

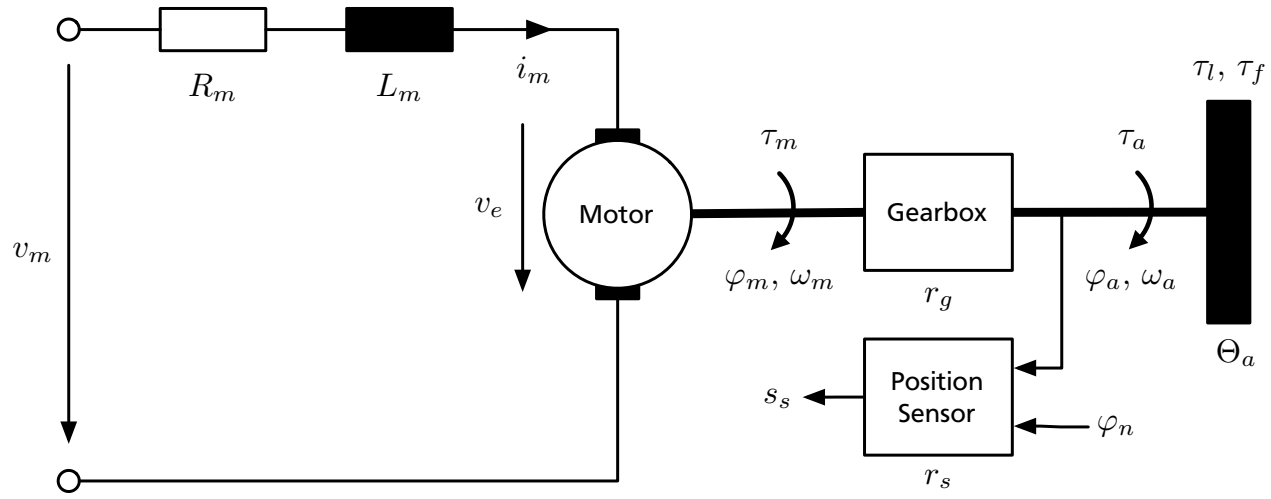

Figure C.2.: Structure of the linear model.

By applying the mesh rule on the armature of the servo motor with the armature resistance R_m, the armature inductance L_m, the back electromotive force v_e and the armature current i_m, the armature voltage v_m is determined by

$$v_m(t) = R_m\, i_m(t) + L_m\, \dot{i}_m(t) + v_e(t). \tag{C.1}$$

The back electromotive force v_e is the induced voltage resulting from the angular speed of the servo motor ω_m weighted with the reciprocal of the speed constant k_ω read as

$$v_e(t) = \frac{1}{k_\omega}\, \omega_m(t). \tag{C.2}$$

The produced torque of the servo motor τ_m corresponds to the armature current i_m multiplied with the torque constant k_τ read as

$$\tau_m(t) = k_\tau\, i_m(t). \tag{C.3}$$

The gearbox transforms the angular speed ω_m and torque τ_m of the servo motor with the gearbox ratio r_g into the angular speed ω_a and torque τ_a of the servo actuator read as

$$\omega_a(t) = \frac{1}{r_g}\, \omega_m(t), \tag{C.4}$$

$$\tau_a(t) = r_g\, \tau_m(t). \tag{C.5}$$

By rearranging (C.1) and inserting (C.2) and (C.4), the derivative of the armature current of the servo motor i_m is given by

$$\dot{i}_m(t) = \frac{v_m(t) - R_m\, i_m(t) - \frac{r_g}{k_\omega}\, \omega_a(t)}{L_m}. \tag{C.6}$$

The inertia of the servo actuator Θ_a referred to the output shaft is determined by the inertia of the gearbox Θ_g and the transformed inertia of the servo motor $\Theta_m\, r_g^2$ read as

$$\Theta_a = \Theta_m\, r_g^2 + \Theta_g. \tag{C.7}$$

The torque of inertia in combination with the applied load torque τ_l and the friction torque τ_f yields the torque of the servo actuator τ_a read as

$$\tau_a(t) = \Theta_a\, \dot{\omega}_a(t) + \tau_f(t) + \tau_l(t). \tag{C.8}$$

where the friction torque τ_f is defined in Appendix D. By rearranging the equalization of (C.5) with (C.8) and inserting (C.3), the derivative of the angular speed of the servo actuator ω_a results in

$$\dot{\omega}_a(t) = \frac{r_g\, k_\tau\, i_m(t) - \tau_f(t) - \tau_l(t)}{\Theta_a}. \tag{C.9}$$

The derivative of the angular position of the servo motor φ_m and the servo actuator φ_a are given by the appertaining angular speeds ω_m read as

$$\dot{\varphi}_m(t) = \omega_m(t), \tag{C.10}$$

and ω_a read as

$$\dot{\varphi}_a(t) = \omega_a(t). \tag{C.11}$$

The actual angular position of the servo actuator φ_a is measured by the position sensor. The measurement signal s_s results from the resolution of the position sensor r_s and is interfered by a noise signal φ_n that is assumed to be zero-mean, white and normal distributed with the constant variance σ_n^2 read as

$$s_s(t) = \frac{1}{r_s}\,(\varphi_a(t) + \varphi_n(t) \tag{C.12}$$

where

$$P\{\varphi_n(t)\} \sim \mathcal{N}(0, \sigma_n^2). \tag{C.13}$$

With the Laplace-transformed variables of the angular position Φ_a and angular speed Ω_a of the servo actuator, the armature voltage V_m and armature current I_m of the servo motor as well as the load torque T_l and the friction torque T_f and by setting the initial values to zero, the Laplace-transformations of (C.6), (C.9) and (C.11) are given by

$$\mathscr{L}\left\{\dot{i}_m(t)\right\} = I_m(s)\, s = \frac{V_m(s) - R_m\, I_m(s) - \frac{r_g}{k_\omega}\, \Omega_a(s)}{L_m}, \tag{C.14}$$

$$\mathscr{L}\left\{\dot{\omega}_a(t)\right\} = \Omega_a(s)\, s = \frac{r_g\, k_\tau\, I_m(s) - T_f(s) - T_l(s)}{\Theta_a}, \tag{C.15}$$

$$\mathscr{L}\left\{\dot{\varphi}_a(t)\right\} = \Phi_a(s)\, s = \Omega_a(s). \tag{C.16}$$

C.2 Nonlinear Model Extensions

The nonlinear model extensions define significant nonlinearities of the controlled system that augment the given linear model. The nonlinearities are caused by specific transfer properties of the servo motor driver, gearbox and position sensor.

C.2.1 Nonlinear Saturation of the Servo Motor Driver

The servo motor driver is powered by the power supply with the time-variant supply voltage v_s and provides the armature voltage of the servo motor v_m dependent on the reference control voltage v_d. With the absolute maximum value of the control voltage $v_{d,m}$ of 3.3 volts, the relation between the control voltage v_d and the armature voltage v_m is given by

$$v_m(t) = \frac{v_s(t)}{v_{d,m}}\, v_d(t) = \frac{v_s(t)}{3.3\ V}\, v_d(t). \tag{C.17}$$

Caused by the restricted supply voltage v_s, the armature voltage v_m saturates with a time-variant saturation limit. The nonlinear saturation function sat$[\cdot]$ of the servo motor driver is defined by

$$\text{sat}[v_m(t)] = \begin{cases} v_s(t) & \text{for } v_m(t) \geq v_s(t), \\ v_m(t) & \text{for } -v_s(t) < v_m(t) < v_s(t), \\ -v_s(t) & \text{for } v_m(t) \leq -v_s(t). \end{cases} \tag{C.18}$$

C.2.2 Nonlinear Backlash of the Gearbox

The gearbox consists of six spur gears and transforms the angular motion of the servo actuator. The clearance of the individual gears originates a lost in motion when the direction is reversed. This backlash effect is modeled as a dead zone around the actual angular position φ_a and is defined as the nonlinear backlash function back$[\cdot]$ with the backlash φ_b read as

$$\text{back}[\varphi_a(t)] = \begin{cases} \varphi_a(t) - \varphi_b & \text{for } \dot{\varphi}_a(t) > 0 \text{ and } \text{back}[\varphi_a(t)] = \varphi_a(t) - \varphi_b, \\ \varphi_a(t) + \varphi_b & \text{for } \dot{\varphi}_a(t) < 0 \text{ and } \text{back}[\varphi_a(t)] = \varphi_a(t) + \varphi_b, \\ \varphi_a(t-) & \text{otherwise} \end{cases} \tag{C.19}$$

where $\varphi(t-)$ means no change in the the angular position value [3].

C.2.3 Nonlinear Quantization of the Position Sensor

The position sensor measures the actual angular position of the servo actuator by applying a quantization in time and value on the measurement signal. The quantization in time samples the measurement signal s_s with the sampling time T_s and results in a sequence of weighted rectangle functions [22]. The weight is given by the quantization in value that utilizes the nonlinear nearest integer function $\lfloor \cdot \rceil$ returning the

nearest integer to the argument. The nonlinear quantization function quan[·] of the position sensor is defined by

$$\text{quan}[s_s(t)] = \sum_{k=0}^{\infty} \lfloor s_s(t) \rceil \; (\sigma(t - kT_s) - \sigma(t - (k+1)T_s)) \tag{C.20}$$

where $\sigma(t)$ corresponds to the Heaviside step function.

C.3 Simulation Model

The simulation model regards the entire linear time-invariant model of the controlled system including the armature current i_m of the servo motor and the angular position φ_a and angular speed ω_a of the servo actuator. The considered disturbances are the load torque τ_l, the friction torque τ_f and the noise signal φ_n. The simulation model is established by applying (C.6), (C.9), (C.11) and (C.12). With the input vector $\boldsymbol{u}_n$, the state vector $\boldsymbol{x}_n$ and the output vector $\boldsymbol{y}_n$ specified by

$$\boldsymbol{u}_n(t) = \begin{bmatrix} v_m(t) & \tau_l(t) & \tau_f(t) & \varphi_n(t) \end{bmatrix}^T, \tag{C.21a}$$

$$\boldsymbol{x}_n(t) = \begin{bmatrix} i_m(t) & \varphi_a(t) & \omega_a(t) \end{bmatrix}^T, \tag{C.21b}$$

$$\boldsymbol{y}_n(t) = \begin{bmatrix} i_m(t) & \varphi_a(t) & \omega_a(t) & s_s(t) \end{bmatrix}^T, \tag{C.21c}$$

the continuous-time state space model used in the simulation process is given by

$$\dot{\boldsymbol{x}}_n(t) = \boldsymbol{A}_{n,c}\, \boldsymbol{x}_n(t) + \boldsymbol{B}_{n,c}\, \boldsymbol{u}_n(t)$$

$$= \begin{bmatrix} -\frac{R_m}{L_m} & 0 & -\frac{r_g}{k_\omega L_m} \\ 0 & 0 & 1 \\ \frac{r_g\, k_\tau}{\Theta_a} & 0 & 0 \end{bmatrix} \boldsymbol{x}_n(t) + \begin{bmatrix} \frac{1}{L_m} & 0 & 0 & 0 \\ 0 & 0 & 0 & 0 \\ 0 & -\frac{1}{\Theta_a} & -\frac{1}{\Theta_a} & 0 \end{bmatrix} \boldsymbol{u}_n(t), \tag{C.22a}$$

$$\boldsymbol{y}_n(t) = \boldsymbol{C}_{n,c}\, \boldsymbol{x}_n(t) + \boldsymbol{D}_{n,c}\, \boldsymbol{u}_n(t)$$

$$= \begin{bmatrix} 1 & 0 & 0 \\ 0 & 1 & 0 \\ 0 & 0 & 1 \\ 0 & \frac{1}{r_s} & 0 \end{bmatrix} \boldsymbol{x}_n(t) + \begin{bmatrix} 0 & 0 & 0 & 0 \\ 0 & 0 & 0 & 0 \\ 0 & 0 & 0 & 0 \\ 0 & 0 & 0 & \frac{1}{r_s} \end{bmatrix} \boldsymbol{u}_n(t). \tag{C.22b}$$

By inserting the parameters of the DD-28 and DD-64 servo actuators specified in Appendix A, the matrices of the corresponding continuous-time simulation models result in

$$\boldsymbol{A}_{n,c,28} = \begin{bmatrix} -41500 & 0 & -9563 \\ 0 & 0 & 1 \\ 581 & 0 & 0 \end{bmatrix}, \quad \boldsymbol{B}_{n,c,28} = \begin{bmatrix} 5000 & 0 & 0 & 0 \\ 0 & 0 & 0 & 0 \\ 0 & -304 & -304 & 0 \end{bmatrix},$$

$$\boldsymbol{C}_{n,c,28} = \begin{bmatrix} 1 & 0 & 0 \\ 0 & 1 & 0 \\ 0 & 0 & 1 \\ 0 & 652 & 0 \end{bmatrix}, \quad \boldsymbol{D}_{n,c,28} = \begin{bmatrix} 0 & 0 & 0 & 0 \\ 0 & 0 & 0 & 0 \\ 0 & 0 & 0 & 0 \\ 0 & 0 & 0 & 652 \end{bmatrix},$$

$$\boldsymbol{A}_{n,c,64} = \begin{bmatrix} -31500 & 0 & -13324 \\ 0 & 0 & 1 \\ 304 & 0 & 0 \end{bmatrix}, \quad \boldsymbol{B}_{n,c,64} = \begin{bmatrix} 5000 & 0 & 0 & 0 \\ 0 & 0 & 0 & 0 \\ 0 & -114 & -114 & 0 \end{bmatrix},$$

$$\boldsymbol{C}_{n,c,64} = \begin{bmatrix} 1 & 0 & 0 \\ 0 & 1 & 0 \\ 0 & 0 & 1 \\ 0 & 652 & 0 \end{bmatrix}, \quad \boldsymbol{D}_{n,c,64} = \begin{bmatrix} 0 & 0 & 0 & 0 \\ 0 & 0 & 0 & 0 \\ 0 & 0 & 0 & 0 \\ 0 & 0 & 0 & 652 \end{bmatrix}.$$

In addition to the defined linear state space models, the nonlinear saturation function sat$[\upsilon_m(t)]$, backlash function back$[\varphi_a(t)]$ and quantization function quan$[s_s(t)]$ are considered in the simulation process.

C.4 State Observer Model

In order to simplify the design and implementation process, the state observer model regards a reduced linear time-invariant model of the controlled system including the angular position φ_a, angular speed ω_a and load torque τ_l of the servo actuator. Compared to speed changes in the mechanical subsystem of the servo motor, transitions of the armature current i_m resulting from a changing armature voltage υ_m are presumed to be instantaneous. Based on this assumption, the influence of the armature inductance L_m is supposed to be insignificant resulting in

$$L_m = 0\ H. \tag{C.23}$$

For this reason, the armature current i_m of the servo motor is not contained in the specified state observer model, but can be approximated with the known armature voltage υ_m and the angular speed of the servo actuator ω_a by rearranging (C.6) and canceling the armature inductance L_m yielding

$$i_m(t) = \frac{\upsilon_m(t) - \frac{r_g}{k_\omega}\,\omega_a(t)}{R_m}. \tag{C.24}$$

The disturbance caused by the friction torque τ_f is assumed to be small and is neglected in the state observer model resulting in

$$\tau_f(t) = 0\ Nm. \tag{C.25}$$

The load torque τ_l is presumed to have a constant value with a vanishing time derivative read as

$$\dot{\tau}_l = 0 \; \frac{Nm}{s}. \tag{C.26}$$

To regard stochastic noise effects that influence the actuator state and measurement values, the state observer model is extended by a generalized process and measurement noise. The process noise $\boldsymbol{a}_n$ includes system parameter uncertainties and disturbances, while the measurement noise b_n contains uncertainties, disturbances and quantization noise of the sensor elements. Both noise signals are assumed to be independent, zero-mean, white and normal distributed with the constant, symmetric covariances $\boldsymbol{Q}_n$ and R_n read as

$$P\{a_n(t)\} \sim \mathcal{N}(0, \boldsymbol{Q}_n), \tag{C.27}$$

$$P\{b_n(t)\} \sim \mathcal{N}(0, R_n). \tag{C.28}$$

This definition comprises the normal distributed noise signal of the position sensor φ_n that is covered by the introduced measurement noise. The input variable of the state observer model is the armature voltage of the servo motor v_m. In order to ensure a correct estimation by the state observer, the nonlinear saturation of the input signal needs to be considered in the state observer model. In combination with the specified simplifications (C.23) to (C.26), the state observer model is established by inserting (C.6) and applying (C.9), (C.11) and (C.12). With the input variable u_o, the state vector $\boldsymbol{x}_o$ and the output variable y_o specified by

$$u_o(t) = \mathrm{sat}[v_m(t)], \tag{C.29a}$$

$$\boldsymbol{x}_o(t) = \begin{bmatrix} \varphi_a(t) & \omega_a(t) & \tau_l \end{bmatrix}^T, \tag{C.29b}$$

$$y_o(t) = \frac{1}{r_s} \, \varphi_a(t), \tag{C.29c}$$

the continuous-time state space model used in the state observer design is given by

$$\begin{aligned} \dot{\boldsymbol{x}}_o(t) &= \boldsymbol{A}_{o,c} \, \boldsymbol{x}_o(t) + \boldsymbol{B}_{o,c} \, u(t) + \boldsymbol{a}_n(t), \\ &= \begin{bmatrix} 0 & 1 & 0 \\ 0 & -\frac{r_g^2 \, k_\tau}{k_\omega \, R_m \, \Omega_a} & -\frac{1}{\Theta_a} \\ 0 & 0 & 0 \end{bmatrix} \boldsymbol{x}_o(t) + \begin{bmatrix} 0 \\ \frac{r_g \, k_\tau}{R_m \, \Theta_a} \\ 0 \end{bmatrix} u_o(t) + \boldsymbol{a}_n(t), \end{aligned} \tag{C.30a}$$

$$\begin{aligned} y_o(t) &= \boldsymbol{C}_{o,c} \, \boldsymbol{x}_o(t) + \boldsymbol{D}_{o,c} \, u_o(t) + b_n(t) \\ &= \begin{bmatrix} \frac{1}{r_s} & 0 & 0 \end{bmatrix} \boldsymbol{x}_o(t) + b_n(t). \end{aligned} \tag{C.30b}$$

By inserting the parameters of the DD-28 and DD-64 servo actuators specified in Appendix A, the matrices of the corresponding continuous-time state observer models result in

$$\boldsymbol{A}_{o,c,28} = \begin{bmatrix} 0 & 1 & 0 \\ 0 & -134 & -304 \\ 0 & 0 & 0 \end{bmatrix}, \qquad \boldsymbol{B}_{o,c,28} = \begin{bmatrix} 0 \\ 70 \\ 0 \end{bmatrix},$$

$$\boldsymbol{C}_{o,c,28} = \begin{bmatrix} 652 & 0 & 0 \end{bmatrix}, \qquad \boldsymbol{D}_{o,c,28} = \begin{bmatrix} 0 \end{bmatrix},$$

$$\boldsymbol{A}_{o,c,64} = \begin{bmatrix} 0 & 1 & 0 \\ 0 & -138 & -114 \\ 0 & 0 & 0 \end{bmatrix}, \qquad \boldsymbol{B}_{o,c,64} = \begin{bmatrix} 0 \\ 52 \\ 0 \end{bmatrix},$$

$$\boldsymbol{C}_{o,c,64} = \begin{bmatrix} 652 & 0 & 0 \end{bmatrix}, \qquad \boldsymbol{D}_{o,c,64} = \begin{bmatrix} 0 \end{bmatrix}.$$

In order to consider the discrete implementation of the developed state observer on the digital processing unit, the continuous-time state observer model is transformed to appertaining discrete-time representation. This discrete-time state observer model regards the transfer characteristic resulting from the discrete sampling of measurement values and the processing of the state observer algorithm with the sampling time T_s. The discrete-time state space model is derived from the Z-transformation of the continuous-time state space model [28]. With the substitutions

$$a_1 = -\frac{r_g^2\, k_\tau}{k_\omega\, R_m\, \Theta_a}, \qquad a_2 = -\frac{1}{\Theta_a}, \qquad b = \frac{r_g\, k_\tau}{R_m\, \Theta_a}$$

and the process noise vector $\boldsymbol{a}_n$ and the measurement noise variable b_n as well as the input variable u_o, the state vector $\boldsymbol{x}_o$ and the output variable y_o specified by

$$u_o(k) = \mathrm{sat}[v_m(k)], \tag{C.31a}$$

$$\boldsymbol{x}_o(k) = \begin{bmatrix} \varphi_a(k) & \omega_a(k) & \tau_l \end{bmatrix}^T, \tag{C.31b}$$

$$y_o(k) = \frac{1}{r_s}\, \varphi_a(k), \tag{C.31c}$$

the discrete-time state space model used in the state observer design is given by

$$\boldsymbol{x}_o(k) = \boldsymbol{A}_{o,d}\, \boldsymbol{x}_o(k-1) + \boldsymbol{B}_{o,d}\, u_o(k) + \boldsymbol{a}_n(k-1), \tag{C.32a}$$

$$y_o(k) = \boldsymbol{C}_{o,d}\, \boldsymbol{x}_o(k-1) + \boldsymbol{D}_{o,d}\, u_o(k) + b_n(k) \tag{C.32b}$$

where

$$\boldsymbol{A}_{o,d} = e^{\boldsymbol{A}_{o,c} T_s} = \begin{bmatrix} 1 & \frac{1}{a_1}\left(e^{a_1 T_s} - 1\right) & \frac{a_2}{a_1^2}\left(e^{a_1 T_s} - a_1\, T_s - 1\right) \\ 0 & e^{a_1 T_s} & \frac{a_2}{a_1}\left(e^{a_1 T_s} - 1\right) \\ 0 & 0 & 1 \end{bmatrix}, \tag{C.33a}$$

$$\boldsymbol{B}_{o,d} = \int_0^{T_s} e^{\boldsymbol{A}_{o,c}\,\tau}\,\boldsymbol{B}_{o,c}\,\mathrm{d}t = \begin{bmatrix} \frac{b}{a_1^2}\left(e^{a_1 T_s} - a_1\,T_s - 1\right) \\ \frac{b}{a_1}\left(e^{a_1 T_s} - 1\right) \\ 0 \end{bmatrix}, \tag{C.33b}$$

$$\boldsymbol{C}_{o,d} = \boldsymbol{C}_{o,c}, \tag{C.33c}$$

$$\boldsymbol{D}_{o,d} = \boldsymbol{D}_{o,c}. \tag{C.33d}$$

By inserting the parameters of the DD-28 and DD-64 servo actuators specified in Appendix A and a sampling time T_s of 0.5 milliseconds, the matrices of the corresponding discrete-time state observer models result in

$$\boldsymbol{A}_{o,d,28} = \begin{bmatrix} 1 & 484 \cdot 10^{-6} & -37 \cdot 10^{-6} \\ 0 & 935 \cdot 10^{-3} & -147 \cdot 10^{-3} \\ 0 & 0 & 1 \end{bmatrix}, \qquad \boldsymbol{B}_{o,d,28} = \begin{bmatrix} 9 \cdot 10^{-6} \\ 34 \cdot 10^{-3} \\ 0 \end{bmatrix},$$

$$\boldsymbol{C}_{o,d,28} = \begin{bmatrix} 652 & 0 & 0 \end{bmatrix}, \qquad \boldsymbol{D}_{o,d,28} = \begin{bmatrix} 0 \end{bmatrix},$$

$$\boldsymbol{A}_{o,d,64} = \begin{bmatrix} 1 & 483 \cdot 10^{-6} & -14 \cdot 10^{-6} \\ 0 & 933 \cdot 10^{-3} & -55 \cdot 10^{-3} \\ 0 & 0 & 1 \end{bmatrix}, \qquad \boldsymbol{B}_{o,d,64} = \begin{bmatrix} 6 \cdot 10^{-6} \\ 25 \cdot 10^{-3} \\ 0 \end{bmatrix},$$

$$\boldsymbol{C}_{o,d,64} = \begin{bmatrix} 652 & 0 & 0 \end{bmatrix}, \qquad \boldsymbol{D}_{o,d,64} = \begin{bmatrix} 0 \end{bmatrix}.$$

For applying the discrete-time state observer models in the development of an state observer of the controlled system, the observability of the models has to be guaranteed. The observability is ensured, if the rank of the observability matrix $\boldsymbol{M}_o$ specified by

$$\boldsymbol{M}_o = \begin{bmatrix} \boldsymbol{C}_d & \boldsymbol{C}_d\,\boldsymbol{A}_d & \boldsymbol{C}_d\,\boldsymbol{A}_d^2 \end{bmatrix}^T \tag{C.34}$$

equals to the order of the model [28]. This condition holds for the discrete-time state observer models of both servo actuator types.

C.5 Control Model

In order to simplify the design and implementation process, the control model regards a reduced linear time-invariant model of the controlled system. The control model in angular position control includes the angular position φ_a and the angular speed ω_a of the servo actuator. In angular speed control, the control model is reduced to the angular speed ω_a of the servo actuator. Compared to speed changes in the mechanical subsystem of the servo motor, transitions of the armature current i_m resulting from a

changing armature voltage v_m are presumed to be instantaneous. Based on this assumption, the influence of the armature inductance L_m is supposed to be insignificant resulting in

$$L_m = 0\ H. \tag{C.35}$$

The load torque τ_l is considered as an additive disturbance, while the friction torque τ_f and the noise signal φ_n are assumed to be small and are neglected in the control model yielding

$$\tau_f(t) = 0\ Nm, \tag{C.36}$$

$$\varphi_n(t) = 0\ rad. \tag{C.37}$$

C.5.1 Position Control Model

With the specified simplifications (C.35) to (C.37) and by applying (C.14) to (C.16), the continuous-time transfer function of the controlled system used in position control is defined by

$$H_{p,c}(s) = \frac{\Phi_a(s)}{V_m(s)} = \frac{\frac{r_g\, k_\tau}{R_m\, \Theta_a}}{s^2 + \frac{r_g^2\, k_\tau}{k_\omega\, R_m\, \Theta_a}\, s}. \tag{C.38}$$

By inserting the parameters of the DD-28 and DD-64 servo actuators specified in Appendix A, the corresponding continuous-time transfer functions result in

$$H_{p,c,28}(s) = \frac{70}{s^2 + 134\, s}, \qquad H_{p,c,64}(s) = \frac{52}{s^2 + 138\, s}.$$

The position control model is established by inserting (C.6) and applying (C.9) and (C.11). With the input variable u_p, the state vector $\boldsymbol{x}_p$, the output variable y_p and the disturbance variable d_p specified by

$$u_p(t) = v_m(t), \tag{C.39a}$$

$$\boldsymbol{x}_p(t) = \begin{bmatrix} \varphi_a(t) & \omega_a(t) \end{bmatrix}^T, \tag{C.39b}$$

$$y_p(t) = \varphi_a(t), \tag{C.39c}$$

$$d_p(t) = \tau_l(t), \tag{C.39d}$$

the continuous-time state space model used in the position control design is given by

$$\begin{aligned} \dot{\boldsymbol{x}}_p(t) &= \boldsymbol{A}_{p,c}\, \boldsymbol{x}_p(t) + \boldsymbol{B}_{p,c}\, u_p(t) + \boldsymbol{V}_{p,c}\, d_p(t) \\ &= \begin{bmatrix} 0 & 1 \\ 0 & -\frac{r_g^2\, k_\tau}{k_\omega\, R_m\, \Omega_a} \end{bmatrix} \boldsymbol{x}_p(t) + \begin{bmatrix} 0 \\ \frac{r_g\, k_\tau}{R_m\, \Theta_a} \end{bmatrix} u_p(t) + \begin{bmatrix} 0 \\ -\frac{1}{\Theta_a} \end{bmatrix} d_p(t), \end{aligned} \tag{C.40a}$$

$$y_p(t) = \boldsymbol{C}_{p,c}\,\boldsymbol{x}_p(t) + \boldsymbol{D}_{p,c}\,u_p(t)$$

$$= \begin{bmatrix} 1 & 0 \end{bmatrix} \boldsymbol{x}_p(t). \tag{C.40b}$$

By inserting the parameters of the DD-28 and DD-64 servo actuators specified in Appendix A, the matrices of the corresponding continuous-time position control models result in

$$\boldsymbol{A}_{p,c,28} = \begin{bmatrix} 0 & 1 \\ 0 & -134 \end{bmatrix}, \qquad \boldsymbol{B}_{p,c,28} = \begin{bmatrix} 0 \\ 70 \end{bmatrix}, \qquad \boldsymbol{V}_{p,c,28} = \begin{bmatrix} 0 \\ -304 \end{bmatrix},$$

$$\boldsymbol{C}_{p,c,28} = \begin{bmatrix} 1 & 0 \end{bmatrix}, \qquad \boldsymbol{D}_{p,c,28} = \begin{bmatrix} 0 \end{bmatrix},$$

$$\boldsymbol{A}_{p,c,64} = \begin{bmatrix} 0 & 1 \\ 0 & -138 \end{bmatrix}, \qquad \boldsymbol{B}_{p,c,64} = \begin{bmatrix} 0 \\ 52 \end{bmatrix}, \qquad \boldsymbol{V}_{p,c,64} = \begin{bmatrix} 0 \\ -114 \end{bmatrix},$$

$$\boldsymbol{C}_{p,c,64} = \begin{bmatrix} 1 & 0 \end{bmatrix}, \qquad \boldsymbol{D}_{p,c,64} = \begin{bmatrix} 0 \end{bmatrix}.$$

In order to consider the discrete implementation of the developed position control on the digital processing unit, the continuous-time transfer function and state space model are transformed to appertaining discrete-time representations. These discrete-time models regard the transfer characteristic resulting from the discrete sampling of measurement values and the processing of the control algorithm with the sampling time T_s. The discrete-time transfer function is determined by applying the Z-transformation with a zero-order hold on the continuous-time transfer function. With the substitutions

$$a = -\frac{r_g^2\,k_\tau}{k_\omega\,R_m\,\Theta_a}, \qquad b = \frac{r_g\,k_\tau}{R_m\,\Theta_a}, \qquad c = -\frac{1}{\Theta_a},$$

the discrete-time transfer function used in the development of the position control is given by

$$H_{p,d}(z) = \frac{\Phi_a(z)}{V_m(z)} = \mathscr{Z}\left\{H_{p,c}(s)\,\frac{1-e^{Ts}}{s}\right\}$$

$$= \frac{\frac{b}{a}\left(\frac{1}{a}\left(e^{aT_s}-1\right)-T_s\right)z + \frac{b}{a}\left(\frac{1}{a}-\left(\frac{1}{a}-T_s\right)e^{aT_s}\right)}{z^2-\left(e^{aT_s}+1\right)z+e^{aT_s}}. \tag{C.41}$$

By inserting the parameters of the DD-28 and DD-64 servo actuators specified in Appendix A and a sampling time T_s of 1 millisecond, the corresponding discrete-time transfer functions result in

$$H_{p,d,28}(z) = \frac{34\cdot10^{-6}\,z + 32\cdot10^{-6}}{z^2 - 1.9\,z + 0.9}, \qquad H_{p,d,64}(z) = \frac{25\cdot10^{-6}\,z + 24\cdot10^{-6}}{z^2 - 1.9\,z + 0.9}.$$

The discrete-time state space model is derived from the Z-transformation of the continuous-time state space model [28]. With the input variable u_p, the state vector $\boldsymbol{x}_p$, the output variable y_p and the disturbance variable d_p specified by

$$u_p(k) = v_m(k), \tag{C.42a}$$

$$\boldsymbol{x}_p(k) = \begin{bmatrix} \varphi_a(k) & \omega_a(k) \end{bmatrix}^T, \tag{C.42b}$$

$$y_p(k) = \varphi_a(k), \tag{C.42c}$$

$$d_p(k) = \tau_l(k), \tag{C.42d}$$

the discrete-time state space model used in the development of the position control is given by

$$\boldsymbol{x}_p(k+1) = \boldsymbol{A}_{p,d}\, \boldsymbol{x}_p(k) + \boldsymbol{B}_{p,d}\, u_p(k) + \boldsymbol{V}_{p,d}\, d_p(k), \tag{C.43a}$$

$$y_p(k) = \boldsymbol{C}_{p,d}\, \boldsymbol{x}_p(k) + \boldsymbol{D}_{p,d}\, u_p(k) \tag{C.43b}$$

where

$$\boldsymbol{A}_{p,d} = e^{\boldsymbol{A}_{p,c} T_s} = \begin{bmatrix} 1 & \frac{1}{a}\left(e^{a T_s} - 1\right) \\ 0 & e^{a T_s} \end{bmatrix}, \tag{C.44a}$$

$$\boldsymbol{B}_{p,d} = \int_0^{T_s} e^{\boldsymbol{A}_{p,c}\tau}\, \boldsymbol{B}_{p,c}\, \mathrm{d}t = \begin{bmatrix} \frac{b}{a^2}\left(e^{a T_s} - a\, T_s - 1\right) \\ \frac{b}{a}\left(e^{a T_s} - 1\right) \end{bmatrix}, \tag{C.44b}$$

$$\boldsymbol{V}_{p,d} = \int_0^{T_s} e^{\boldsymbol{A}_{p,c}\tau}\, \boldsymbol{V}_{p,c}\, \mathrm{d}t = \begin{bmatrix} \frac{c}{a^2}\left(e^{a T_s} - a\, T_s - 1\right) \\ \frac{c}{a}\left(e^{a T_s} - 1\right) \end{bmatrix}, \tag{C.44c}$$

$$\boldsymbol{C}_{p,d} = \boldsymbol{C}_{p,c}, \tag{C.44d}$$

$$\boldsymbol{D}_{p,d} = \boldsymbol{D}_{p,c}. \tag{C.44e}$$

By inserting the parameters of the DD-28 and DD-64 servo actuators specified in Appendix A and a sampling time T_s of 1 millisecond, the matrices of the corresponding discrete-time position control models result in

$$\boldsymbol{A}_{p,d,28} = \begin{bmatrix} 1 & 936 \cdot 10^{-6} \\ 0 & 875 \cdot 10^{-3} \end{bmatrix}, \quad \boldsymbol{B}_{p,d,28} = \begin{bmatrix} 33 \cdot 10^{-6} \\ 66 \cdot 10^{-3} \end{bmatrix}, \quad \boldsymbol{V}_{p,d,28} = \begin{bmatrix} -37 \cdot 10^{-6} \\ -147 \cdot 10^{-3} \end{bmatrix},$$

$$\boldsymbol{C}_{p,d,28} = \begin{bmatrix} 1 & 0 \end{bmatrix}, \quad \boldsymbol{D}_{p,d,28} = \begin{bmatrix} 0 \end{bmatrix},$$

$$\boldsymbol{A}_{p,d,64} = \begin{bmatrix} 1 & 934 \cdot 10^{-6} \\ 0 & 871 \cdot 10^{-3} \end{bmatrix}, \quad \boldsymbol{B}_{p,d,64} = \begin{bmatrix} 25 \cdot 10^{-6} \\ 49 \cdot 10^{-3} \end{bmatrix}, \quad \boldsymbol{V}_{p,d,64} = \begin{bmatrix} -14 \cdot 10^{-6} \\ -55 \cdot 10^{-3} \end{bmatrix},$$

$$\boldsymbol{C}_{p,d,64} = \begin{bmatrix} 1 & 0 \end{bmatrix}, \quad \boldsymbol{D}_{p,d,64} = \begin{bmatrix} 0 \end{bmatrix}.$$

For applying the discrete-time position control models in the development of a control concept, the controllability of the models has to be guaranteed. With neglecting the additive disturbance d_p, the controllability is ensured, if the rank of the controllability matrix $\boldsymbol{M}_{c,p}$ specified by

$$\boldsymbol{M}_{c,p} = \begin{bmatrix} \boldsymbol{B}_{p,d} & \boldsymbol{A}_{p,d}\,\boldsymbol{B}_{p,d} \end{bmatrix} \tag{C.45}$$

equals to the order of the model [28]. This condition holds for the discrete-time position control models of both servo actuator types.

C.5.2 Speed Control Model

With the specified simplifications (C.35) to (C.37) and by applying (C.14) and (C.15), the continuous-time transfer function of the controlled system used in speed control is defined by

$$H_{s,c}(s) = \frac{\Omega_a(s)}{V_m(s)} = \frac{\frac{r_g\,k_\tau}{R_m\,\Theta_a}}{s + \frac{r_g^2\,k_\tau}{k_\omega\,R_m\,\Theta_a}}. \tag{C.46}$$

By inserting the parameters of the DD-28 and DD-64 servo actuators specified in Appendix A, the corresponding continuous-time transfer functions result in

$$H_{s,c,28}(s) = \frac{70}{s+134}, \qquad H_{s,c,64}(s) = \frac{52}{s+138}.$$

The speed control model is established by inserting (C.6) into (C.9). With the input variable u_s, the state variable x_s, the output variable y_s and the disturbance variable d_s specified by

$$u_s(t) = v_m(t), \tag{C.47a}$$

$$x_s(t) = \omega_a(t), \tag{C.47b}$$

$$y_s(t) = \omega_a(t), \tag{C.47c}$$

$$d_s(t) = \tau_l(t), \tag{C.47d}$$

the continuous-time state space model used in the speed control design is given by

$$\begin{aligned} \dot{x}_s(t) &= A_{s,c}\,x_s(t) + B_{s,c}\,u_s(t) + V_{s,c}\,d_s(t) \\ &= -\frac{r_g^2\,k_\tau}{k_\omega\,R_m\,\Omega_a}\,x_s(t) + \frac{r_g\,k_\tau}{R_m\,\Theta_a}\,u_s(t) + -\frac{1}{\Theta_a}\,d_s(t), \end{aligned} \tag{C.48a}$$

$$\begin{aligned} y_s(t) &= C_{s,c}\,x_s(t) + D_{s,c}\,u_s(t) \\ &= x_s(t). \end{aligned} \tag{C.48b}$$

By inserting the parameters of the DD-28 and DD-64 servo actuators specified in Appendix A, the values of the corresponding continuous-time speed control models result in

$$A_{s,c,28} = -134, \qquad B_{s,c,28} = 70, \qquad V_{s,c,28} = -304,$$

$$C_{s,c,28} = 1, \qquad D_{s,c,28} = 0,$$

$$A_{s,c,64} = -138, \qquad B_{s,c,64} = 52, \qquad V_{s,c,64} = -114,$$

$$C_{s,c,64} = 1, \qquad D_{s,c,64} = 0.$$

In order to consider the discrete implementation of the developed speed control on the digital processing unit, the continuous-time transfer function and state space model are transformed to appertaining discrete-time representations. These discrete-time models regard the transfer characteristic resulting from the discrete sampling of measurement values and the processing of the control algorithm with the sampling time T_s. The discrete-time transfer function is determined by applying the Z-transformation with a zero-order hold on the continuous-time transfer function. With the substitutions

$$a = -\frac{r_g^2\, k_\tau}{k_\omega\, R_m\, \Theta_a}, \qquad b = \frac{r_g\, k_\tau}{R_m\, \Theta_a}, \qquad c = -\frac{1}{\Theta_a},$$

the discrete-time transfer function used in the development of the speed control is given by

$$H_{s,d}(z) = \mathscr{Z}\left\{ H_{s,c}(s)\, \frac{1 - e^{T_s s}}{s} \right\} = \frac{\Omega_a(z)}{V_m(z)} = \frac{\frac{b}{a}\, e^{aT_s} - \frac{b}{a}}{z - e^{aT_s}}. \tag{C.49}$$

By inserting the parameters of the DD-28 and DD-64 servo actuators specified in Appendix A and a sampling time T_s of 1 millisecond, the corresponding discrete-time transfer functions result in

$$H_{s,d,28}(z) = \frac{66 \cdot 10^{-3}}{z - 875 \cdot 10^{-3}}, \qquad H_{s,d,64}(z) = \frac{49 \cdot 10^{-3}}{z - 871 \cdot 10^{-3}}.$$

The discrete-time state space model is derived from the transformation of the continuous-time state space model [28]. With the input variable u_s, the state variable x_s, the output variable y_s and the disturbance variable d_s specified by

$$u_s(k) = v_m(k), \tag{C.50a}$$

$$x_s(k) = \omega_a(k), \tag{C.50b}$$

$$y_s(k) = \omega_a(k), \tag{C.50c}$$

$$d_s(k) = \tau_l(k), \tag{C.50d}$$

the discrete-time state space model used in the development of the speed control is given by

$$x_s(k+1) = A_{s,d}\, x_s(k) + B_{s,d}\, u_s(k) + V_{s,d}\, d_s(k), \tag{C.51a}$$

$$y_s(k) = C_{s,d}\, x_s(k) + D_{s,d}\, u_s(k) \tag{C.51b}$$

where

$$A_{s,d} = e^{A_{s,c} T_s} = e^{a T_s}, \tag{C.52a}$$

$$B_{s,d} = \int_0^{T_s} e^{A_{s,c}\tau}\, B_{s,c}\, \mathrm{d}t = \frac{b}{a}\left(e^{a T_s} - 1\right), \tag{C.52b}$$

$$B_{s,d} = \int_0^{T_s} e^{A_{s,c}\tau}\, V_{s,c}\, \mathrm{d}t = \frac{c}{a}\left(e^{a T_s} - 1\right), \tag{C.52c}$$

$$C_{s,d} = C_{s,c}, \tag{C.52d}$$

$$D_{s,d} = D_{s,c}. \tag{C.52e}$$

By inserting the parameters of the DD-28 and DD-64 servo actuators specified in Appendix A and a sampling time T_s of 1 millisecond, the values of the corresponding discrete-time speed control models result in

$$A_{s,d,28} = 875 \cdot 10^{-3}, \qquad B_{s,d,28} = 66 \cdot 10^{-3}, \qquad V_{s,d,28} = -147 \cdot 10^{-3},$$

$$C_{s,d,28} = 1, \qquad D_{s,d,28} = 0,$$

$$A_{s,d,64} = 871 \cdot 10^{-3}, \qquad B_{s,d,64} = 49 \cdot 10^{-3}, \qquad V_{s,d,64} = -55 \cdot 10^{-3},$$

$$C_{s,d,64} = 1, \qquad D_{s,d,64} = 0.$$

For applying the discrete-time speed control models in the development of a control concept, the controllability of the models has to be guaranteed. With neglecting the additive disturbance d_p, the controllability is ensured, if the rank of the controllability matrix $M_{c,s}$ specified by

$$M_{c,s} = B_{s,d} \tag{C.53}$$

equals to the order of the model [28]. This condition holds for the discrete-time speed control models of both servo actuator types.

D Friction Model

The friction model of the DD-28 and DD-64 servo actuators regards static, kinetic and viscous friction of the servo motor, the gearbox and the bearings. Static friction describes the initial breakaway torque that is required to initiate a rotational motion from idle state caused by static cohesion. The servo actuator does not move until the servo actuator torque τ_a and the load torque τ_l exceed the static friction constant k_s. Kinetic friction is a constant torque that counteracts the rotational motion resulting from the conversion of kinetic energy into heat between two relative moving surfaces. The kinetic friction constant k_k is a constant load torque applied on the turning servo actuator. Viscous friction is caused by molecules rubbing against each other in a lubricating film and depends on the angular speed. The viscous friction constant k_v weighted with the angular speed of the servo actuator ω_a is a variable-speed load torque applied on the servo actuator in motion [4]. Figure D.1 illustrates the defined friction model. The total friction torque τ_f of the idle and moving servo actuator results in

$$\tau_f(t) = \begin{cases} \min[\tau_a(t) + \tau_l(t),\ k_s \operatorname{sign}[\tau_a(t) + \tau_l(t)]] & \text{for } \omega_a(t) = 0, \\ k_k \operatorname{sign}[\omega_a(t)] + k_v\ \omega_a(t) & \text{for } \omega_a(t) \neq 0. \end{cases} \tag{D.1}$$

The static friction constant is equal to the threshold torque of the servo actuator $\tau_{a,t}$, that is experimentally determined with the application of the servo actuator model introduced in Appendix C. The corresponding threshold armature voltage of the servo motor $v_{m,t}$ is measured by slowly increasing the armature voltage until the idle and unloaded servo actuator starts to move. In idle and steady operation, that is ensured by the slow increase of the armature voltage, the angular speed $\omega_{m,t}$ and the derivative of the armature current $i_{m,t}$ of the servo motor are zero. By applying the mesh rule on the armature of the servo motor with the armature resistance R_m, the armature inductance L_m, the gearbox ratio r_g and the speed constant k_ω, the static friction constant k_s is given by

$$k_s = \tau_{a,t} = r_g\ k_\tau\ i_{m,t} = r_g\ k_\tau\ \frac{v_{m,t}}{R_m} \tag{D.2}$$

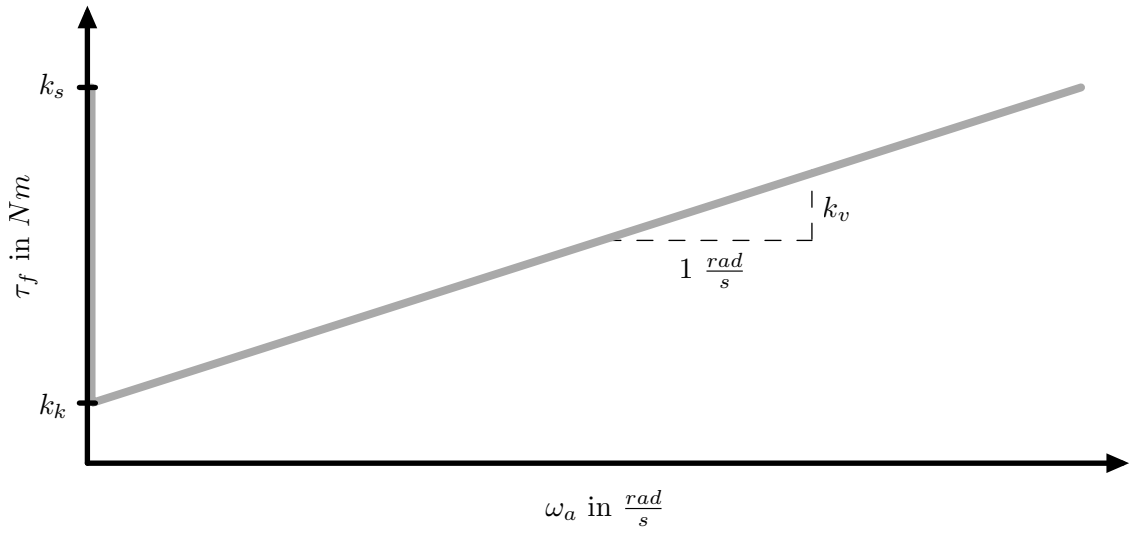

Figure D.1.: Characteristic of the friction model.

where

$$v_{m,t} = R_m\, i_{m,t} + L_m\, \dot{i}_{m,t} + \frac{r_g}{k_\omega}\, \omega_{m,t} \quad \text{with } \omega_{m,t} = 0 \text{ and } \dot{i}_{m,t} = 0, \tag{D.3}$$

$$i_{m,t} = \frac{v_{m,t}}{R_m}. \tag{D.4}$$

With inserting the measured threshold armature voltages $v_{m,t,28}$ and $v_{m,t,64}$ and the parameters of the DD-28 and DD-64 servo actuators specified in Appendix A, the static friction constants of both servo actuator types $k_{s,28}$ and $k_{s,64}$ are equal to

$$k_{s,28} \approx r_{g,28}\, k_{\tau,28}\, \frac{0.34\ V}{R_{m,28}} = 192.6 \cdot 9.9\ \tfrac{mNm}{A} \cdot \frac{0.34\ V}{8.3\Omega} = 78.1\ mNm, \tag{D.5}$$

$$k_{s,64} \approx r_{g,64}\, k_{\tau,64}\, \frac{0.44\ V}{R_{m,64}} = 199.6 \cdot 13.4\ \tfrac{mNm}{A} \cdot \frac{0.34\ V}{6.3\Omega} = 186.8\ mNm, \tag{D.6}$$

where

$$v_{m,t,28} \approx 0.34\ V, \tag{D.7}$$

$$v_{m,t,64} \approx 0.44\ V. \tag{D.8}$$

The kinetic friction constant k_k and the viscous friction constant k_v are derived from the static friction constant k_s by an approximately estimated multiplier. The kinetic friction constant $k_{k,28}$ and the viscous friction constant $k_{v,28}$ of the DD-28 type result in

$$k_{k,28} \approx \frac{1}{6}\, k_{s,28} = 13.0\ mNm, \tag{D.9}$$

$$k_{v,28} \approx \frac{1}{6\pi\ \frac{1}{s}}\, k_{s,28} = 4.1\ mNms. \tag{D.10}$$

The kinetic friction constant $k_{k,64}$ and the viscous friction constant $k_{v,64}$ of the DD-64 type are given by

$$k_{k,64} \approx \frac{1}{6}\, k_{s,64} = 31.1\ mNm, \tag{D.11}$$

$$k_{v,64} \approx \frac{1}{6\pi\ \frac{1}{s}}\, k_{s,64} = 9.9\ mNms. \tag{D.12}$$

E Control Design Parameters

The control design parameters comprise all applied characteristic values and computed results of the state observer and control design for the DD-28 and DD-64 servo actuators. The control design process is described in Chapter 5.

E.1 State Observer

$$\boldsymbol{Q}_{n,28} = \begin{bmatrix} 0.001 & 0 & 0 \\ 0 & 0.001 & 0 \\ 0 & 0 & 100 \end{bmatrix} \qquad R_{n,28} = 10^5$$

$$\boldsymbol{P}_{e,28} = \begin{bmatrix} 49.3 \cdot 10^{-3} & 8.3 & -5.3 \\ 3.3 & 2.5 \cdot 10^3 & -1.9 \cdot 10^3 \\ -5.3 & -1.9 \cdot 10^3 & 1.9 \cdot 10^3 \end{bmatrix} \qquad \boldsymbol{K}_{o,28} = \begin{bmatrix} 0.3 \cdot 10^{-3} \\ 46.0 \cdot 10^{-3} \\ -28.8 \cdot 10^{-3} \end{bmatrix}$$

$$\boldsymbol{Q}_{n,64} = \begin{bmatrix} 0.001 & 0 & 0 \\ 0 & 0.001 & 0 \\ 0 & 0 & 100 \end{bmatrix} \qquad R_{n,64} = 10^5$$

$$\boldsymbol{P}_{e,64} = \begin{bmatrix} 34.3 \cdot 10^{-3} & 3.6 & -5.2 \\ 3.6 & 0.8 \cdot 10^3 & -1.4 \cdot 10^3 \\ -5.2 & -1.4 \cdot 10^3 & 2.8 \cdot 10^3 \end{bmatrix} \qquad \boldsymbol{K}_{o,64} = \begin{bmatrix} 0.2 \cdot 10^{-3} \\ 20.9 \cdot 10^{-3} \\ -29.5 \cdot 10^{-3} \end{bmatrix}$$

E.2 Feedforward Control

$$K_{f,\omega;28} = 1.9 \qquad K_{f,\alpha,28} = 14.3 \cdot 10^{-3} \qquad K_{f,\tau,28} = 4.3$$

$$K_{f,\omega;64} = 2.7 \qquad K_{f,\alpha,64} = 20.8 \cdot 10^{-3} \qquad K_{f,\tau,64} = 2.4$$

E.3 Feedback Control

E.3.1 Model Predictive Control for Angular Position Tracking

$$\boldsymbol{P}_{c,p,28} = \begin{bmatrix} 10^5 & 0 \\ 0 & 5 \end{bmatrix} \qquad \boldsymbol{Q}_{c,p,28} = \begin{bmatrix} 75052.2 & 451.3 \\ 451.3 & 6.9 \end{bmatrix}$$

$$R_{c,p,28} = 0.01 \qquad N_{c,p,28} = 2$$

$$\boldsymbol{x}_{m,p,28} = \begin{bmatrix} 4000 & 40 & 4000 & 40 & 10^5 & 4000 & 40 & 10^5 & 4000 & 40 & 10^5 & 20 & 40 \end{bmatrix}^T$$

$$\boldsymbol{P}_{c,p,64} = \begin{bmatrix} 10^5 & 0 \\ 0 & 5 \end{bmatrix} \qquad \boldsymbol{Q}_{c,p,64} = \begin{bmatrix} 97565.4 & 658.6 \\ 658.6 & 8.9 \end{bmatrix}$$

$$R_{c,p,64} = 0.01 \qquad N_{c,p,64} = 2$$

$$\boldsymbol{x}_{m,p,64} = \begin{bmatrix} 4000 & 40 & 4000 & 40 & 10^5 & 4000 & 40 & 10^5 & 4000 & 40 & 10^5 & 20 & 40 \end{bmatrix}^T$$

E.3.2 Model Predictive Control for Angular Speed Tracking

$$P_{c,s,28} = 10^5 \qquad Q_{c,s,28} = 1147.9$$

$$R_{c,s,28} = 0.01 \qquad N_{c,s,28} = 2$$

$$\boldsymbol{x}_{m,s,28} = \begin{bmatrix} 40 & 40 & 10^5 & 40 & 10^5 & 40 & 10^5 & 20 & 40 \end{bmatrix}^T$$

$$P_{c,s,28} = 10^5 \qquad Q_{c,s,28} = 1274.9$$

$$R_{c,s,28} = 0.01 \qquad N_{c,s,28} = 2$$

$$\boldsymbol{x}_{m,s,28} = \begin{bmatrix} 40 & 40 & 10^5 & 40 & 10^5 & 40 & 10^5 & 20 & 40 \end{bmatrix}^T$$

E.3.3 Loop-Shaping Control for Angular Position Tracking

$$\omega_{z,p,28} = 69.6\ \frac{rad}{s} \qquad G_{m,p,28} = 29.3\ dB \qquad \Phi_{m,p,28} = 83.1^{\circ}$$

$$H_{k,p,28}(z) = 744.3\ \frac{\left(z - e^{-1.5T_s}\right)\ \left(z - e^{-134T_s}\right)}{(z-1)\ \left(z - e^{-1200T_s}\right)} \qquad \bar{H}_{k,p,28}(z) = 744.3\ \frac{\left(z - e^{-134T_s}\right)}{\left(z - e^{-1200T_s}\right)}$$

$$\omega_{z,p,64} = 69.9\ \frac{rad}{s} \qquad G_{m,p,64} = 29.3\ dB \qquad \Phi_{m,p,64} = 83.1^{\circ}$$

$$H_{k,p,64}(z) = 1088.1\ \frac{\left(z - e^{-1.5T_s}\right)\ \left(z - e^{-138T_s}\right)}{(z-1)\ \left(z - e^{-1200T_s}\right)} \qquad \bar{H}_{k,p,64}(z) = 1088.1\ \frac{\left(z - e^{-138T_s}\right)}{\left(z - e^{-1200T_s}\right)}$$

E.3.4 Loop-Shaping Control for Angular Speed Tracking

$$\omega_{z,s,28} = 181.9\ \frac{rad}{s} \qquad G_{m,s,28} = 14.7\ dB \qquad \Phi_{m,s,28} = 70.1^{\circ}$$

$$H_{k,s,28}(z) = 1.9\ \frac{\left(z - e^{-134T_s}\right)}{(z-1)\ \left(z - e^{-1200T_s}\right)} \qquad \bar{H}_{k,s,28}(z) = 1.9\ \frac{\left(z - e^{-134T_s}\right)}{\left(z - e^{-1200T_s}\right)}$$

$$\omega_{z,s,64} = 185.9\ \frac{rad}{s} \qquad G_{m,s,64} = 14.5\ dB \qquad \Phi_{m,s,64} = 69.5^{\circ}$$

$$H_{k,s,64}(z) = 2.9\ \frac{\left(z - e^{-138T_s}\right)}{(z-1)\ \left(z - e^{-1200T_s}\right)} \qquad \bar{H}_{k,s,64}(z) = 2.9\ \frac{\left(z - e^{-138T_s}\right)}{\left(z - e^{-1200T_s}\right)}$$

F Circuit Diagrams

The circuit diagrams and circuit layouts of the DD-28 and DD-64 servo actuators are designed in regard to the specifications of the electronic design listed in Chapter 4. All printed circuit boards are made of double-sided copper clad epoxy laminate with the grade designation FR-4 and a thickness of 1 millimeter. The circuit diagrams of the original RX-28 and RX-64 servo actuators are derived from analyzing the corresponding original circuit boards.

F.1 DD-28 Servo Actuator

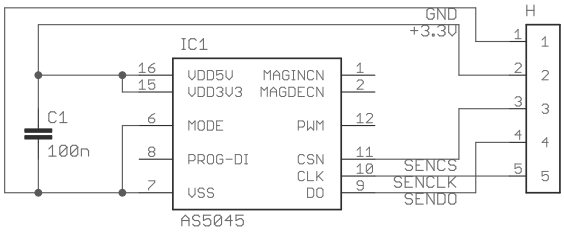

Figure F.1.: Sensor circuit diagram of the DD-28 servo actuator.

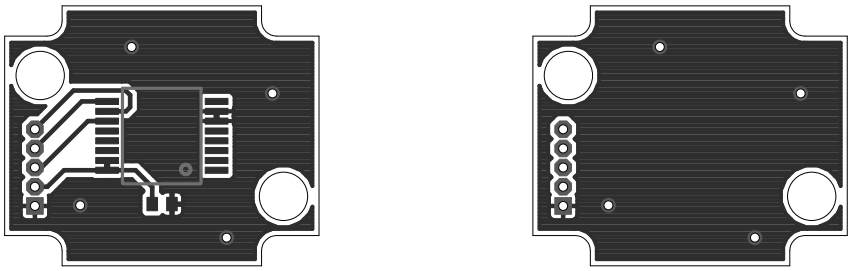

(a) Top side in double magnification. **(b)** Bottom side in double magnification.

Figure F.2.: Sensor circuit board of the DD-28 servo actuator.

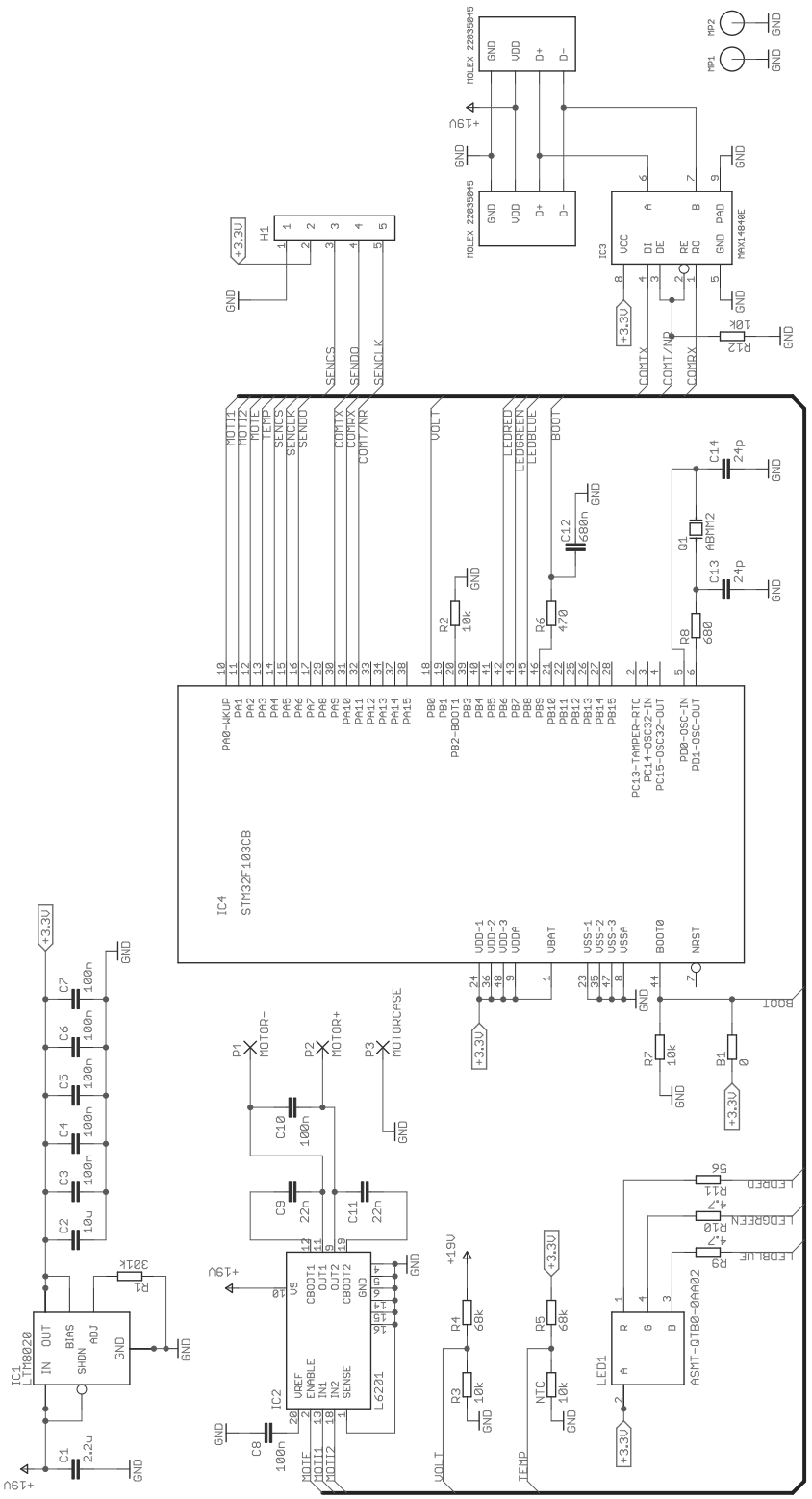

Figure F.3.: Main circuit diagram of the DD-28 servo actuator.

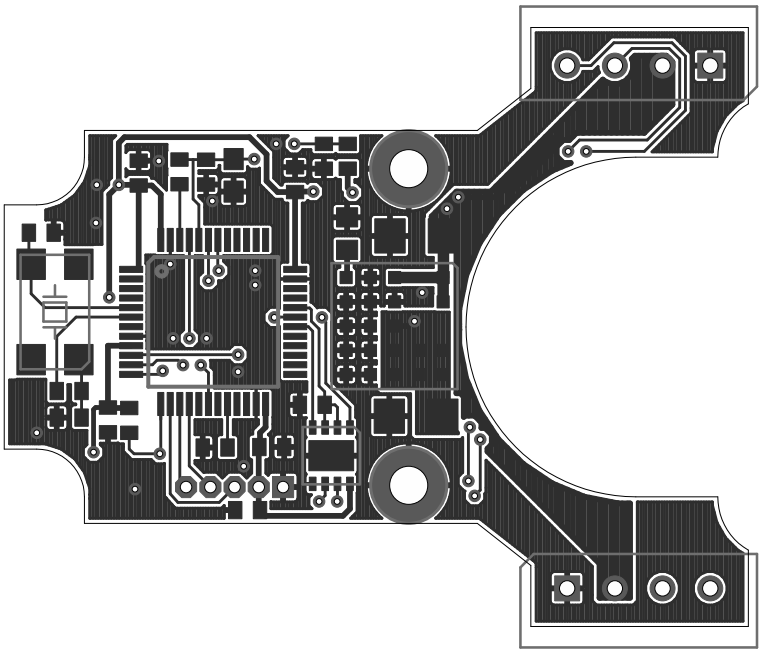

(a) Top side in fourfold magnification.

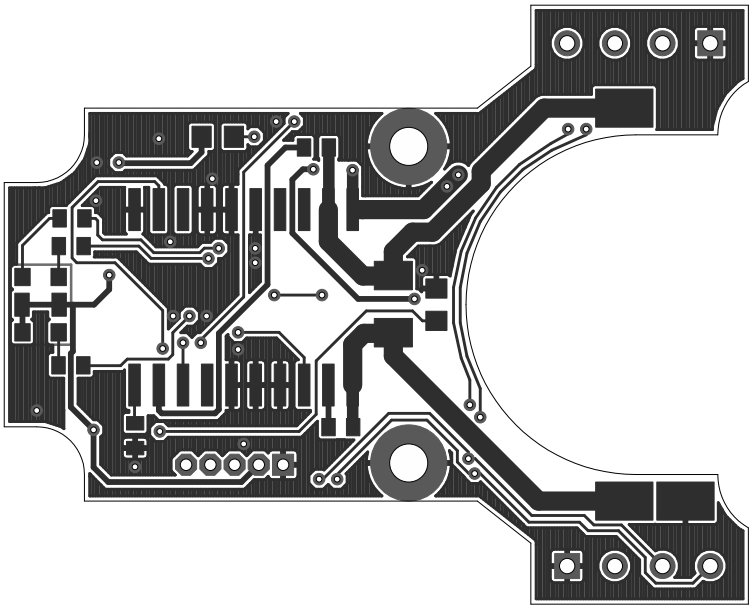

(b) Bottom side in fourfold magnification.

Figure F.4.: Main circuit board of the DD-28 servo actuator.

F.2 DD-64 Servo Actuator

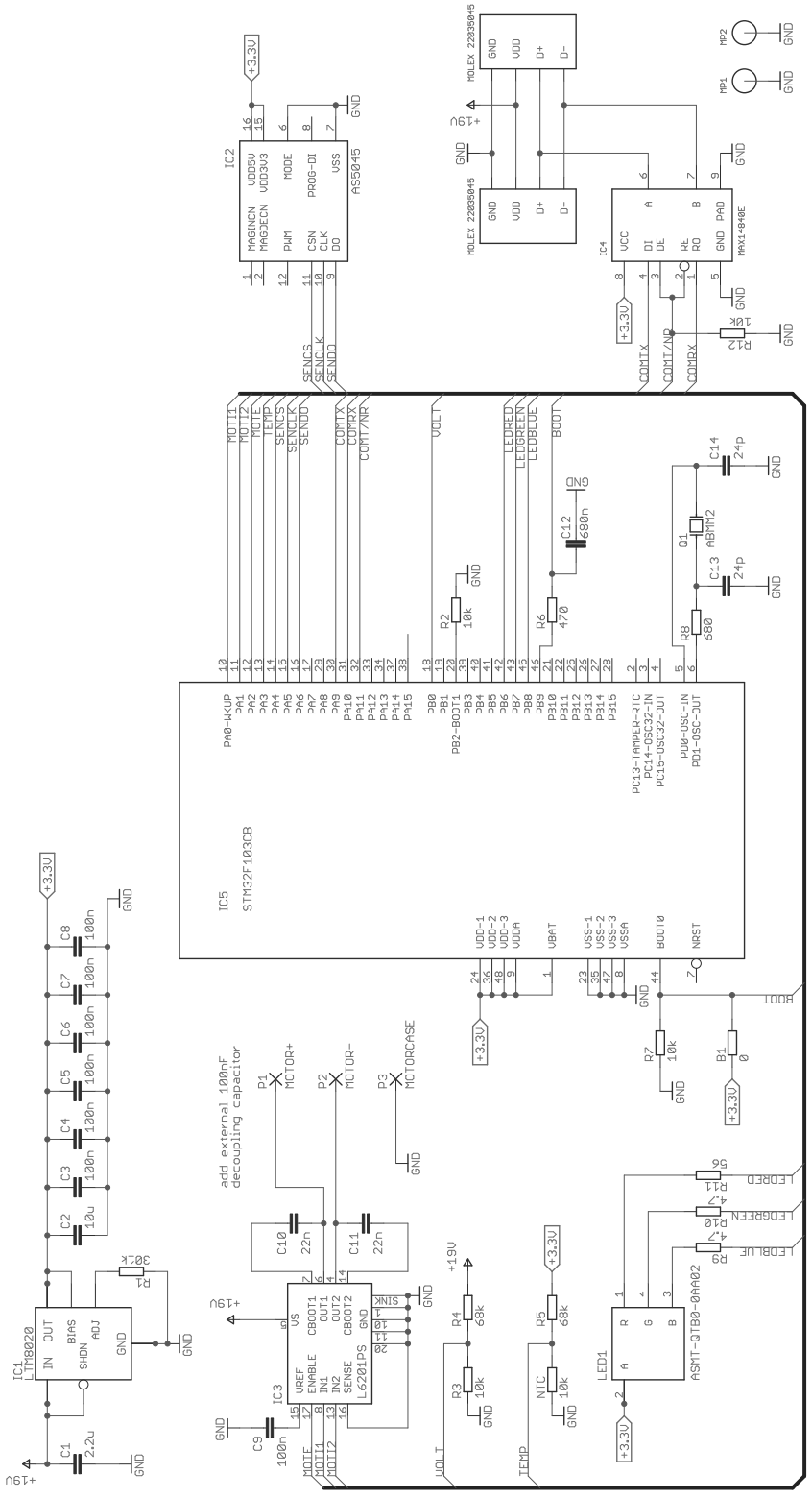

Figure F.5.: Circuit diagram of the DD-64 servo actuator.

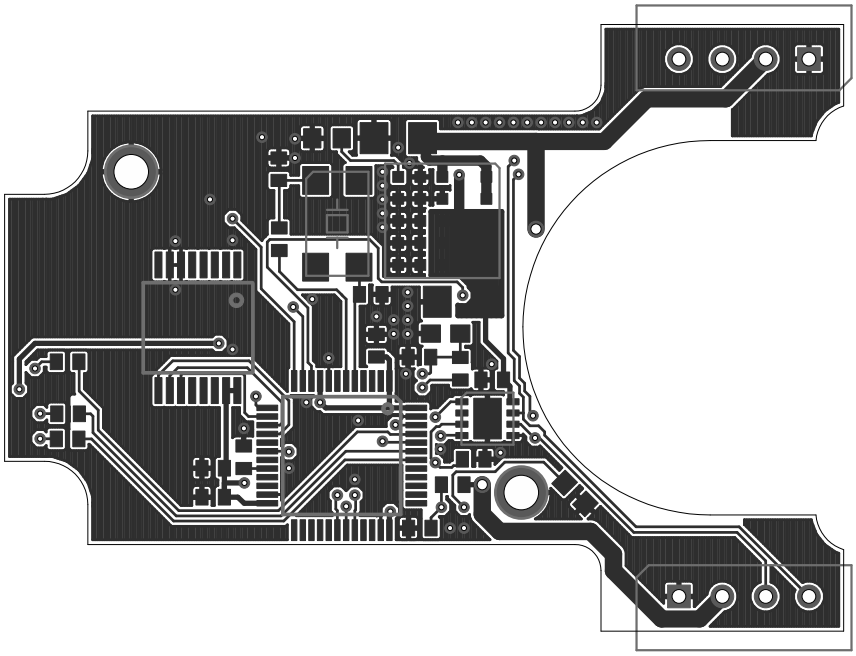

(a) Top side in fourfold magnification.

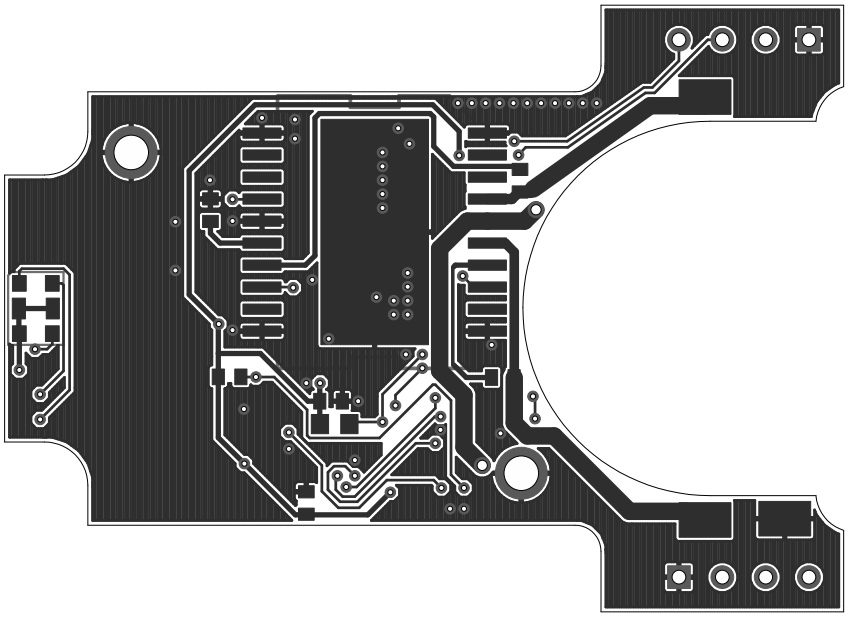

(b) Bottom side in fourfold magnification.

Figure F.6.: Circuit board of the DD-64 servo actuator.

F.3 RX-28 Servo Actuator

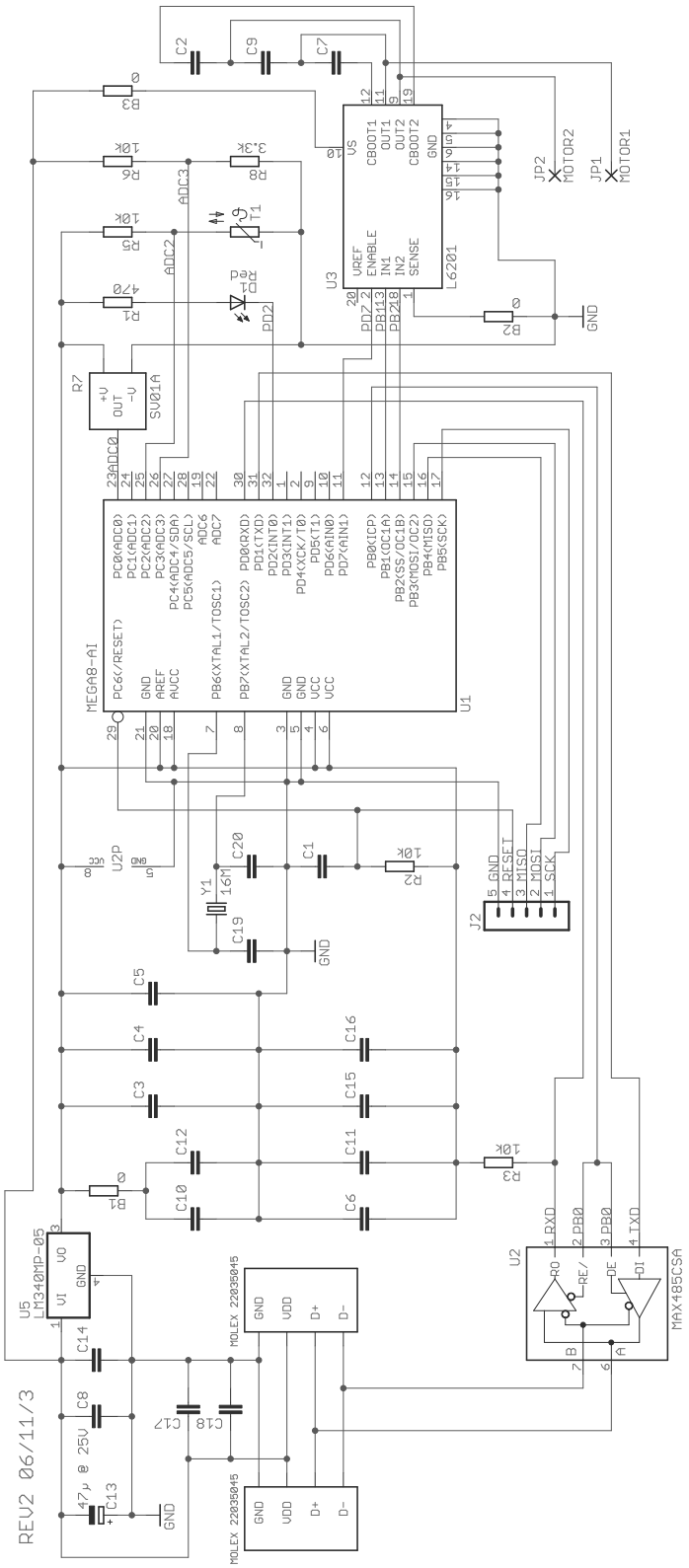

Figure F.7.: Circuit diagram of the RX-28 servo actuator.

F.4 RX-64 Servo Actuator

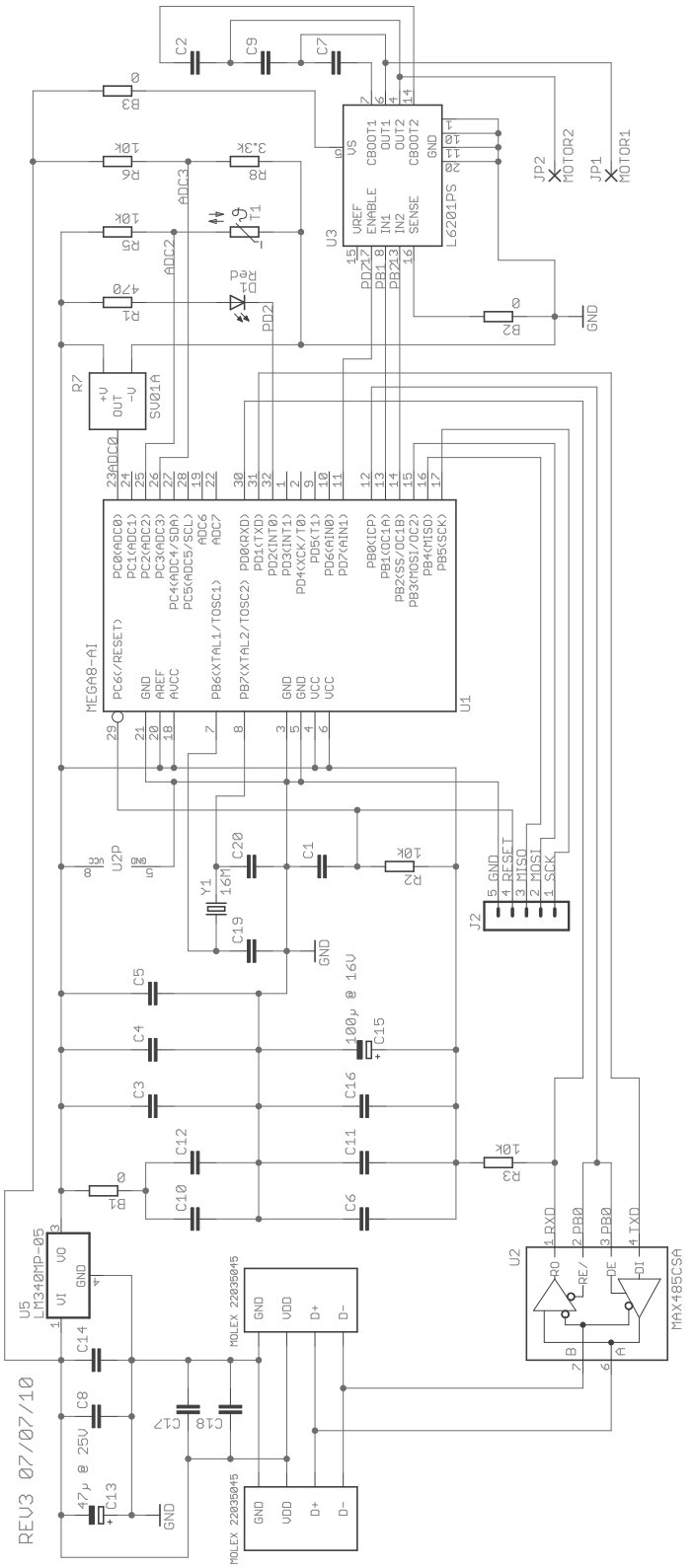

Figure F.8.: Circuit diagram of the RX-64 servo actuator.

G Technical Drawings

The magnet mountings of the DD-28 and DD-64 servo actuators provide a mechanical link between the output shaft of the servo actuator and a diametral magnet for angular position measurement. The diametral magnet has a size of 6 millimeters in diameter and 2.5 millimeters in height. A detailed description of the position sensor setup can be found in Chapter 4. All parts are produced in an automated manufacturing process and made of selective-laser-sintered polyamide.

G.1 DD-28 Servo Actuator

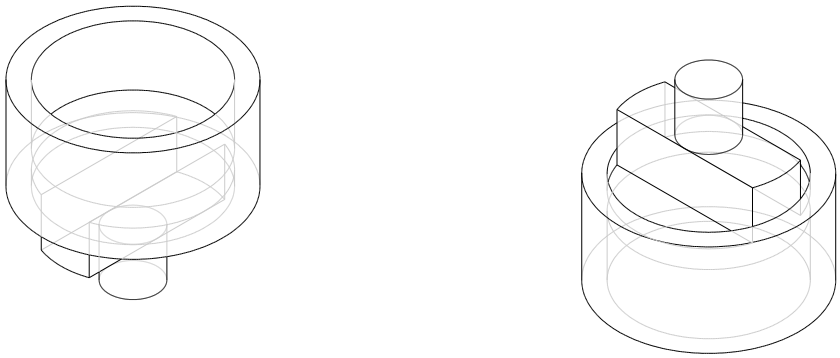

Figure G.1.: Wire frame model of the DD-28 magnet mount.

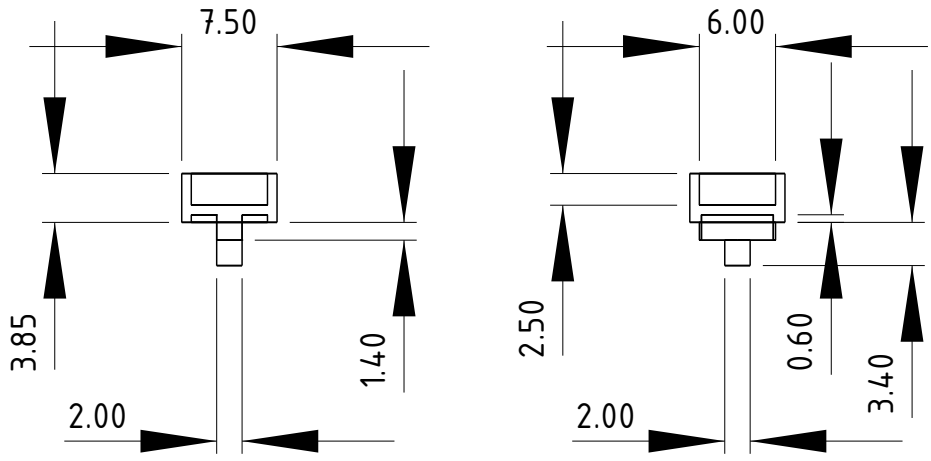

Figure G.2.: Dimensions of the DD-28 magnet mount.

G.2 DD-64 Servo Actuator

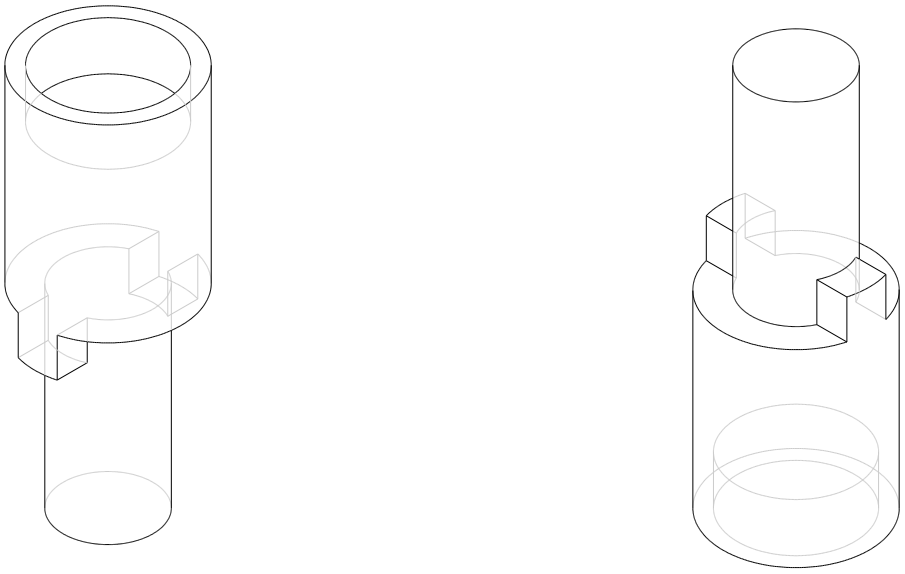

Figure G.3.: Wire frame model of the DD-64 magnet mount.

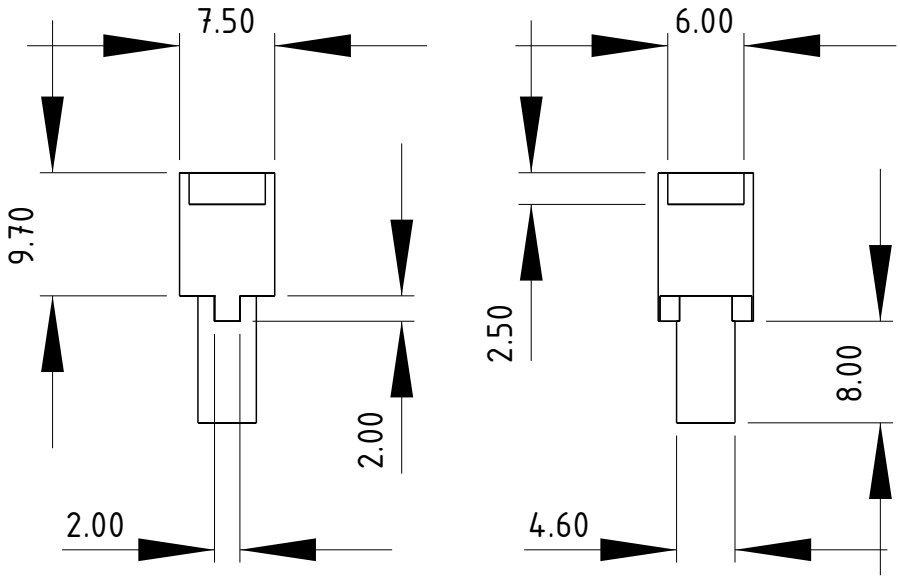

Figure G.4.: Dimensions of the DD-64 magnet mount.

Bibliography

[1] 01 Mechatronics LP. SuperModified Website. http://www.01mech.com/supermodified, 2010.

[2] J. Adamy. *Nichtlineare Regelungen*. Springer, 1. edition, 2009.

[3] N. J. Ahmad and F. Khorrami. Adaptive control of systems with backlash hysteresis at the input. *American Control Conference.*, 1999.

[4] Akademischer Verein Hütte e.V. *Hütte - Das Ingenieurwissen*. Springer, 33. edition, 2007.

[5] M. Andriluka, M. Friedmann, S. Kohlbrecher, J. Meyer, K. Petersen, C. Reinl, P. Schauß, P. Schnitzspan, A. Strobel, D. Thomas, and O. von Stryk. RoboCupRescue 2009 - Robot League Team - Darmstadt Rescue Robot Team. Technical report, Simulation, Systems Optimization and Robotics Group, Technische Universität Darmstadt, 2009.

[6] ARM Ltd. ARM Website. http://www.arm.com/, 2010.

[7] Atmel Corp. *ATmega8 Series Datasheet*, 2008.

[8] Atollic AB. Atollic Website. http://www.atollic.com/, 2010.

[9] austriamicrosystems AG. *AS5045 Datasheet*, 2010.

[10] austriamicrosystems AG. *AS5055 Datasheet*, 2010.

[11] Avago Technologies Ltd. *ASMT-QTB0 Datasheet*, 2007.

[12] AVX Corp. *NTC Thermistor NB21 Datasheet*, 2006.

[13] A. Bemporad, M. Morati, V. Dua, and E. N. Pistikopoulous. The explicite linear quadratic regulator for constraint systems. *Automatica 38.*, 2002.

[14] K. Binner. Team Photographs of Darmstadt Dribblers, 2010.

[15] B. Carter. OpenServo Website. http://www.openservo.com/, 2010.

[16] J. M. G. da Silva and S. Tarbouriech. Anti-windup Design with Guaranteed Regions of Stability: An LMI-based Approach. *Conference on Decision and Control.*, 2003.

[17] M. Friedmann, K. Petersen, S. Petters, K. Radkhah, D. Scholz, D. Thomas, and O. von Stryk. Darmstadt Dribblers - Team Description for Humanoid KidSize League of RoboCup 2009. Technical report, Simulation, Systems Optimization and Robotics Group, Technische Universität Darmstadt, 2009.

[18] O. Föllinger. *Regelungstechnik: Einführung in die Methoden und ihre Anwendung*. Hüthig, 8. edition, 1994.

[19] Hobbico Inc. Futaba Website. http://www.futaba-rc.com/, 2010.

[20] R. Isermann. *Identifikation Dynamischer Systeme 1: Grundlegende Methoden*. Springer, 2. edition, 1992.

[21] S. Kohlbrecher. Team Photographs of Darmstadt Hector, 2010.

[22] U. Konigorski. *Digitale Regelung mechatronscher Systeme I und II*. Lecture notes, 2009.

[23] G. Kopasakis. Feedback Control Systems Loop-Shaping Design with Practical Considerations. *NASA STI Program.*, 2007.

[24] M. Kvasnica, P. Grieder, and M. Baotić. Multi-Parametric Toolbox. http://control.ee.ethz.ch/ mpt/, 2004.

[25] M. Liechty. Servo Database Website. http://www.servodatabase.com/, 2010.

[26] Linear Technology Corp. *LTM8020 Datasheet*, 2007.

[27] J. Lunze. *Regelungstechnik 1: Systemtheoretische Grundlagen, Analyse und Entwurf einschleifiger Regelungen*. Springer, 7. edition, 2008.

[28] J. Lunze. *Regelungstechnik 2: Mehrgrößensysteme, Digitale Regelung*. Springer, 5. edition, 2008.

[29] J. Löfberg. YALMIP: A Toolbox for Modeling and Optimization in MATLAB. http://users.isy.liu.se/johanl/yalmip, 2004.

[30] U. Maeder and M. Morati. Offset-free reference tracking with model predictive control. *Automatica 46.*, 2010.

[31] Maxim Integrated Products Inc. *MAX48X Series Datasheet*, 2003.

[32] Maxim Integrated Products Inc. *MAX1484XE Series Datasheet*, 2010.

[33] Maxon Motor AG. *RE-max 17 Datasheet*, 2009.

[34] Maxon Motor AG. *RE-max 21 Datasheet*, 2009.

[35] Maxon Motor AG. Maxon Motor Website. http://www.maxonmotor.com/, 2010.

[36] D. Q. Mayne, J. B. Rawlings, C. V. Rao, and P. O. M. Scokaert. Constrained model predictive control: Stability and optimality. *Automatica 36.*, 2000.

[37] MTG Europe e.K. Power Magnet Shop Website. http://www.powermagnetshop.de/, 2010.

[38] Murata Manufacturing Co., Ltd. *SV01A103AEA01 Datasheet*, 2009.

[39] National Semiconductor Corp. *LM340/LM78XX Series Datasheet*, 2006.

[40] RoboCup Federation. RoboCup Website. http://www.robocup.org/, 2010.

[41] Robotis Co., Ltd. *Dynamixel RX-64: User's Manual*, 2006.

[42] Robotis Co., Ltd. *Dynamixel RX-28: User's Manual*, 2007.

[43] Robotis Co., Ltd. Robotis Website. http://www.robotis.com/, 2010.

[44] E. Schuitema, M. Wisse, T. Ramakers, and P. Jonker. The design of LEO: a 2D bipedal walking robot for online autonomous reinforcement learning. *IEEE/RSJ International Conference on Intelligent Robots and Systems*, 2010.

[45] Simulation, Systems Optimization and Robotics Group. Simulation, Systems Optimization and Robotics Group Website. http://www.sim.tu-datmstadt.de, 2010.

[46] M. W. Spong, S. Hutchinson, and M. Vidyasagar. *Robot Modeling and Control*. John Wiley & Sons, 1. edition, 2005.

[47] S. S. Stevens. On the Psychophysical Law. *Psychological Review.*, 1957.

[48] STMicroelectronics N.V. *L620X Series Datasheet*, 1997.

[49] STMicroelectronics N.V. *EEPROM Emulation in STM32F10xx Microcontrollers*, 2009.

[50] STMicroelectronics N.V. *STM32F103xB Series Datasheet*, 2009.

[51] STMicroelectronics N.V. *STM32F103xx Series Reference Manual*, 2009.

[52] STMicroelectronics N.V. STMicroelectronics Website. http://www.st.com/, 2010.

[53] STMicroelectronics N.V. *USART Protocol Used in the STM32 Bootloader*, 2010.

[54] E. Tira-Thompson. Digital Servo Calibration and Modeling. Technical report, Robotics Institute, Carnegie Mellon University, 2009.

[55] M. C. Turner, G. Herrmann, and I. Postlethwaite. Anti-windup Compensation using a Decoupling Architecture. *Lecture Notes in Control and Information Sciences.*, 2007.

[56] Volz Servos GmbH & Co KG. Volz Website. http://www.volz-servos.com/, 2010.

[57] G. Welch and G. Bishop. An Introduction to the Kalman Filter. *SIGGRAPH course pack.*, 2001.